A&A 425, 263–270 (2004)
DOI: 10.1051/0004-6361:20041011

Astronomy & Astrophysics

A spectroscopic atlas of the HgMn star HD 175640 (B9 V) $\lambda\lambda$ 3040–10 000 Å⋆,⋆⋆,⋆⋆⋆

F. Castelli[1,2] and S. Hubrig[3]

[1] Istituto di Astrofisica Spaziale e Fisica Cosmica, CNR, via del Fosso del Cavaliere, 00133 Roma, Italy
[2] Osservatorio Astronomico di Trieste, via GB Tiepolo 11, Trieste, Italy
e-mail: castelli@ts.astro.it
[3] European Southern Observatory, Casilla 19001, Santiago 19, Chile
e-mail: shubrig@eso.org

Received 2 April 2004 / Accepted 27 May 2004

Abstract. We present a high resolution spectral atlas of the HgMn star HD 175640 covering the 3040−10 000 Å region. UVES spectra observed with 90 000−110 000 resolving power and signal to noise ratio ranging from 200 to 400 are compared with a synthetic spectrum computed with the SYNTHE code (Kurucz 1993b). The model atmosphere is an ATLAS12 model (Kurucz 1997) with parameters $T_{\rm eff}$ = 12 000 K, log g = 3.95, ξ = 0 km s^{-1}. The stellar individual abundances in ATLAS12 were derived from an iterative procedure. The starting atomic line lists downloaded from the Kurucz website have been improved and extended by examining different sources in the literature and by comparing the computed profiles with the observed spectrum. The high quality of the data allowed us to study the isotopic and hyperfine structure for several lines of Mn II, Ga II, Ba II, Pt II, Hg I, and Hg II. Numerous weak emission lines from Cr II and Ti II have been identified in the red part of the spectrum, starting at $\approx\lambda$ 5847 Å. Two emission lines of C I (mult. 10, mult. 9) have been observed for the first time. All Cr II and Ti II emission lines originate from the high excitation states ($\chi_{\rm low} \gtrsim 89\,000$ cm^{-1} for Cr II and $\chi_{\rm low} \gtrsim 62\,000$ cm^{-1} for Ti II) with large transition probabilities (log $gf > -1.00$). The synthetic spectrum superimposed on the observed spectrum as well as the adopted improved atomic line lists are available at the CDS and http://wwwuser.oat.ts.astro.it/castelli/stars.html. An extended discussion on each identified ion and related atomic data is available both on the quoted website and in an electronic Appendix to the paper.

Key words. stars: abundances – line: identification – atomic data – stars: atmospheres – stars: chemically peculiar – stars: individual: HD 175640 (B9V)

1. Introduction

HD 175640 (HR 7143) is to a large extent representative of the HgMn stars, which constitute a well defined subgroup of chemically peculiar (CP) stars of late B spectral types in the temperature range 10 000–14 000 K. The most distinctive features are extreme atmospheric overabundances of Hg (up to 6 dex) and of Mn (up to 3 dex).

In the present study we undertook a detailed spectroscopic analysis of UVES spectra of HD 175640 in the whole region 3040–10 000 Å. The high quality of the UV-Visual Echelle Spectrograph UVES at the 8 m UT2 telescope, its high resolution (R = 90 000–110 000) and high signal-to-noise ratio (200–400), the large wavelength coverage, the low $v \sin i$ (2.5 km s^{-1}) of HD 175640 and its nature as a single star, led us to compute a synthetic spectrum for the whole observed interval. We used Kurucz codes and Kurucz line lists that we modified and implemented as explained in Sect. 4. The final results, which are available at the CDS and in our website[1], are the plots of the superimposed observed and synthetic spectra supplied with the line identifications as well as the modified Kurucz line lists that we adopted for the computations. An extended discussion of each ion analyzed during the preparation of the atlas is available in the electronic Appendix A of the paper.

The atlas of HD 175640 increases the number of those already published in a similar form. They are the o Peg atlas in the region $\lambda\lambda$3826−4882 Å (Gulliver et al. 2004) and the Deneb atlas in the region $\lambda\lambda$3825−5212 Å (Albayrak et al. 2003). In analogy with the two atlases quoted above the present one should also provide useful guidance for studies of other stars with similar spectral type. We wish to point out the much larger wavelength coverage (3040−10 000 Å) of our atlas.

Compiling the atlas has required an abundance analysis for the 48 ions listed in Table 1 to which 9 more ions with

⋆ Based on observations obtained at the European Southern Observatory, Paranal, Chile (ESO program No. 67.D-0579).
⋆⋆ Appendices is only available in electronic form at http://www.edpsciences.org
⋆⋆⋆ Atlas is available in electronic form at the CDS via anonymous ftp to cdsarc.u-strasbg.fr (130.79.128.5) or via http://cdsweb.u-strasbg.fr/cgi-bin/qcat?J/A+A/425/263

[1] http://wwwuser.oat.ts.astro.it/castelli/stars.html

Table 1. Abundances $\log(N_{\rm elem}/N_{\rm tot})$ for HD 175640.

	HD 175640		Sun		
	measured	adopted		[Element]	λ region
H		−0.008163	−0.036023		
He I	−1.73	−1.73	−1.11	[−0.62]	Vis
Be II	−10.64	−10.64	−10.64	[0.00]	UV
C I	−4.11 ± 0.23	−4.00	−3.52	[−0.59]	Vis
C II	−4.05 ± 0.16	−4.00	−3.52	[−0.53]	Vis
N I	≤−5.78	−5.78	−4.12	<[−1.66]	Vis
O I	−3.18 ± 0.11	−3.18	−3.21	[+0.03]	Vis
Ne I	−4.35	−4.35	−3.96	[−0.39]	Vis
Na I	−5.47:	−5.47	−5.71	[+0.24]	Vis
Mg I	−4.64 ± 0.06	−4.69	−4.46	[−0.18]	Vis
Mg II	−4.71 ± 0.07	−4.69	−4.46	[−0.25]	Vis
Al I	<−7.50	−7.50	−5.57	<[−1.93]	Vis
Si II	−4.72 ± 0.08	−4.71	−4.49	[−0.23]	Vis
Si III	−4.58 ± 0.04	−4.71	−4.49	[−0.09]	Vis
P II	−6.28 ± 0.08	−6.28	−6.59	[+0.31]	Vis
S II	−5.12 ± 0.03	−5.12	−4.71	[−0.41]	Vis
Ca I	−5.26	−5.54	−5.68	[+0.42]	Vis
Ca II	−5.67 ± 0.25	−5.54	−5.68	[+0.01]	UV(−5.83 ± 0.06); Vis(−5.62 ± 0.26)
Sc II	−9.08 ± 0.15	−9.08	−8.87	[−0.21]	UV(−8.89 ± 0.03); Vis(−9.21 ± 0.08)
Ti II	−5.67 ± 0.11	−5.67	−7.02	[+1.35]	UV(−5.59 ± 0.09); Vis(−5.72 ± 0.08)
V II	≤−9.04	−9.04	−8.04	<[−1.00]	UV
Cr I	−5.22 ± 0.09	−5.36	−6.37	[+1.15]	UV(−5.18 ± 0.05); Vis(−5.24 ± 0.06)
Cr II	−5.41 ± 0.07	−5.36	−6.37	[+0.96]	UV(−5.34 ± 0.06); Vis(−5.41 ± 0.07)
Mn I	−4.20 ± 0.08	−4.20	−6.65	[+2.45]	UV(−4.22 ± 0.08); Vis(−4.19 ± 0.08)
Mn II	−4.25 ± 0.04	−4.20	−6.65	[+2.40]	UV
Fe I	−4.78 ± 0.08	−4.83	−4.54	[−0.24]	UV(−4.90 ± 0.06); Vis(−4.75 ± 0.05)
Fe II	−4.84 ± 0.13	−4.83	−4.54	[−0.30]	Vis
Co II	−8.08:	−8.08	−7.12	[−0.96]:	UV
Ni II	−6.09 ± 0.16	−6.09	−5.79	[−0.30]	UV(−6.01 ± 0.13); Vis(−6.14 ± 0.16)
Cu I	−6.52	−6.88	−7.83	[+0.95]	UV
Ga II	−5.43 ± 0.04	−5.43	−9.16	[+3.73]	Vis
Br II	−7.12 ± 0.04	−7.12	−9.41	[+2.29]	Vis
Sr II	−8.41	−8.41	−9.07	[+0.66]	Vis
Y II	−6.66 ± 0.20	−6.66	−9.80	[+3.14]	UV(−6.42 ± 0.06); Vis(−6.79 ± 0.10)
Zr II	−8.67 ± 0.17	−8.67	−9.44	[+0.77]	UV(−8.65 ± 0.18); Vis(−8.78)
Rh II	−8.50:	−8.50	−10.92	[+2.42]:	UV
Pd I	−6.41 ± 0.30	−6.41	−10.35	[+3.94]	UV
Xe II	−5.96 ± 0.20	−5.96	−9.83	[+3.87]	Vis
Ba II	−9.27	−9.27	−9.91	[+0.64]	Vis
Pr III	−9.62:	−9.62	−11.33	[+1.71]:	Vis
Nd III	−9.57 ± 0.08:	−9.60	−10.54	[+0.97]:	Vis
Yb II	−8.10 ± 0.19	−8.10	−10.96	[+2.86]	UV(−7.82); Vis(−8.20 ± 0.10)
Yb III	−7.31 ± 0.01	−8.10	−10.96	[+3.66]	UV
Os II	−10.55:	−10.55	−10.55	[0.0]:	UV
Ir II	−10.65:	−10.65	−10.65	[0.0]:	UV
Pt II	−7.63	−7.63	−10.20	[+2.57]	Vis
Au II	−7.51 ± 0.06	−7.51	−11.03	[+3.52]	Vis
Hg I	−6.19 ± 0.18	−6.30	−10.91	[+4.72]	Vis
Hg II	−6.53 ± 0.23	−6.30	−10.91	[+4.38]	Vis

dubious identifications or with no measurable lines can be added. They are B II, O II, S I, Zn I, Zn II, Ga I, As II, Ce II, and Ce III. Previous abundance determinations based on a few selected lines are those of Sadakane et al. (1985) for Be II, B II;

Dworetsky & Buday (2000) for Ne I; Smith (1993) for Mg, Al, Si; Smith & Dworetsky (1993) and Jomaron et al. (1999) for Cr II, Mn II, Fe II, Co II, Ni II; Sadakane et al. (1988) and Smith (1996) for Cu II, Zn II; Smith (1996) and Dworetsky et al. (1998) for Ga II; Smith (1997) and Dolk et al. (2003) for Hg I, Hg II. We therefore extended the abundance analysis to more elements than those previously examined for this star.

The presence of emission lines was discovered for the first time in this star by Wahlgren & Hubrig (2000) in spectra observed in the intervals 6005–6095 Å and 6105–6190 Å. While most of them were identified as Ti II and Cr II lines, others could not be classified. In this paper we extended the search for the presence of emission lines to a larger wavelength interval than that explored by Wahlgren & Hubrig (2000). The nature of these emission lines remains unclear. A systematic investigation of the emission lines and the production of identification line lists in stars with different stellar parameters such as effective temperature, gravity, chemical composition, magnetic field strength, and rotational velocity would allow us to put tighter constraints on the modelling of the origin of emission lines in the HgMn, He-weak and PGa stars. Because the emission lines may be correlated with abundance stratification (Sigut 2001), UVES spectra also present an excellent opportunity to further investigate the vertical stratification of different chemical elements through the determination of the abundances from lines of the same ions formed on either side of the Balmer jump. For Ca II, Sc II, Ti II, Cr I, Cr II, Mn I, Fe I, Ni II, Y II, Zr II, and Yb II we compared abundances from lines lying shortward and longward of the Balmer discontinuity. Savanov & Hubrig (2003) already discussed the presence of Cr stratification in HD 175640 by analyzing Cr II lines on the wings of Hβ.

2. Observations

The spectrum of HD 175640 was recorded on June 13, 2001 at ESO with the VLT UV-Visual Echelle Spectrograph UVES at UT2. We used the UVES DIC1 and DIC2 standard settings covering the spectral range from 3030 Å to 10 000 Å. The slit width was set to 0.″3 for the red arm, corresponding to a resolving power of $\lambda/\Delta\lambda \approx 1.1 \times 10^5$. For the blue arm, we used a slit width of 0.″4 to achieve a resolving power of $\approx 0.9 \times 10^5$. The spectra were reduced by the UVES pipeline Data Reduction Software (version 1.4.0), which is an evolved version of the ECHELLE context of MIDAS. The manual for the UVES pipeline can be found on the ESO web page[2]. The signal-to-noise ratios of the resulting UVES spectra are very high, ranging from 200 in the near UV to 400 in the visual region.

There are two gaps in the observed range at $\lambda\lambda$ 5759–5835 Å and 8519–8656 Å, which are caused by the physical gap between the two detector chips of the red CCD mosaic. Furthermore, the $\lambda\lambda$ 9074–9098 Å range cannot be used, as the spectrum quality is poor in this interval. The observed spectrum was shifted in wavelength in order to be superimposed on the computed spectrum. The shift ranges from 33.5 km s^{-1} in the ultraviolet to 34.5 km s^{-1} in the red, indicating an uncertainty of about 1.0 km s^{-1} in the wavelength calibration.

When the continuum was drawn in the spectrum reduced with the UVES pipeline, we noticed strong distortions, mostly in the ultraviolet, conspicuous jumps corresponding to the boundaries of the orders, and several spurious absorptions. Therefore we renormalised the unmerged spectra order by order from 3040 Å to 7000 Å. For $\lambda > 7000$ Å, we adopted for the analysis the spectrum reduced with the UVES pipeline owing to the large undulations affecting the order by order spectra. As a consequence there are jumps in the red spectrum which modify the lines lying just where the jump occurs, as for instance Mn II at 8784 Å. There are also jumps at 8776.5 Å and 9316 Å, which could be confused with He I 8776.77 Å and with an emission line, respectively. Another jump occurs at 9038.3 Å.

The continuum was subjectively drawn by connecting the highest points of the spectrum by a straight line. When needed, it was then adjusted in steps of 6 Å intervals with the help of the synthetic spectrum. The continuous level just longward of the Balmer and Paschen discontinuities is highly uncertain. It was also very difficult to drawn it at the position of the Balmer and Paschen lines owing to the jumps and distortions of the échelle spectra. For this reason we did not use hydrogen lines for the analysis.

Equivalent widths were measured in the spectra by direct integration of the line profiles with the trapezium rule. A suitable number of points, which depends on the profile shape and intensity, was adopted for each measurament.

3. The synthetic spectrum

The synthetic spectrum was computed with the SYNTHE code (Kurucz 1993b) and with an opacity sampling ATLAS12 model (Kurucz 1997) computed for the individual abundances of the star.

Stellar parameters have been previously determined by Hubrig et al. (1999) from Strömgren photometry and high resolution spectra in the framework of a spectroscopic search for magnetic fields in HgMn stars. We adopted the same values for the present analysis, namely $T_{\rm eff}$ = 12 000 K, log g = 3.95, microturbulent velocity ξ = 0 km s^{-1} and rotational velocity $v \sin i$ = 2.5 km s^{-1}. Although Hubrig & Castelli (2001) suggested the possible presence of a weak variable magnetic field in this star, we did not consider any Zeeman effect in the computed spectrum. The spectrum was broadened for $v \sin i$ = 2.5 km s^{-1} and for a Gaussian instrumental profile with resolving power 90 000 shortward of the Balmer discontinuity and 110 000 longward of the Balmer discontinuity.

The final synthetic spectrum is the result of an iterative procedure. An opacity distribution function ATLAS9 (Kurucz 1993a) model atmosphere computed with solar abundances for all the elements was used in the SYNTHE code to generate a preliminary synthetic spectrum. The abundances in the synthetic spectrum were then modified to get agreement between observed and computed profiles of selected lines. The individual abundances estimated in that way were then used

[2] http://www.eso.org/observing/dfo/quality/UVES/pipeline/pipe_gen.html

for computing an ATLAS12 model. This model and the measured equivalent widths of unblended lines with critically evaluated log gfs were the input data of the WIDTH code (Kurucz 1993a) which yields abundances from equivalent widths. A final ATLAS12 model computed for the average abundances derived from equivalent widths or, in a few cases, from line profiles, was the final input model used for computing the final synthetic spectrum. The final adopted abundances are listed in Table 1, Col. 3. They are logarithmic abundances relative to the total number of atoms $N_{\rm tot}$. The second column of Table 1 shows the average abundances derived from the measured equivalent widths or from comparison of observed and computed profiles. Column 4 shows the solar abundances from Grevesse & Sauval (1998), where the scale $\log(N_{\rm elem})$ relative to $\log(N_{\rm H}) = 12$ was changed to the scale $\log(N_{\rm elem}/N_{\rm tot})$; Col. 5 gives the over- or underabundance of the ions in HD 175640 relative to the solar abundances. The last column indicates whether lines lying shortward (UV) or longward (Vis) of the Balmer discontinuity (placed at λ = 3647 Å) were used for the abundance determination. When both regions were used, the average abundance from each region is given in parentheses. The aim of this separation is to investigate the presence of vertical abundance stratifications. Each of the 57 ions considered for the analysis is extensively discussed in the Appendix A. Tables of the input and output line data for WIDTH can also be found in Appendix A (Tables A.1–A.3).

Figure 1 compares the $T-\log\tau_{\rm ross}$ relation of the ATLAS9 and ATLAS12 models used for HD 175640. The He underabundance of HD 175640 is the main cause of the different temperature stratifications, in contrast with the statement of Norris (1971) that the helium abundance has little effect on the temperature structure. Abundances from the equivalent widths of Mn I and Mn II lines and of Fe I and Fe II lines did not indicate any need for a model parameter redetermination.

Starting from λ = 5500 Å telluric absorptions were also approximately modelled by using telluric lines of the HITRAN database[3] converted into the SYNTHE format by Kurucz (1998, private communication). The computed telluric spectrum was simply superimposed on the observed and computed spectra without performing any instrumental broadening and convolution with the synthetic spectrum. The atlas is made up of the superimposed plots of the observed spectrum, the computed stellar spectrum supplied with the line identifications, and the computed telluric spectrum.

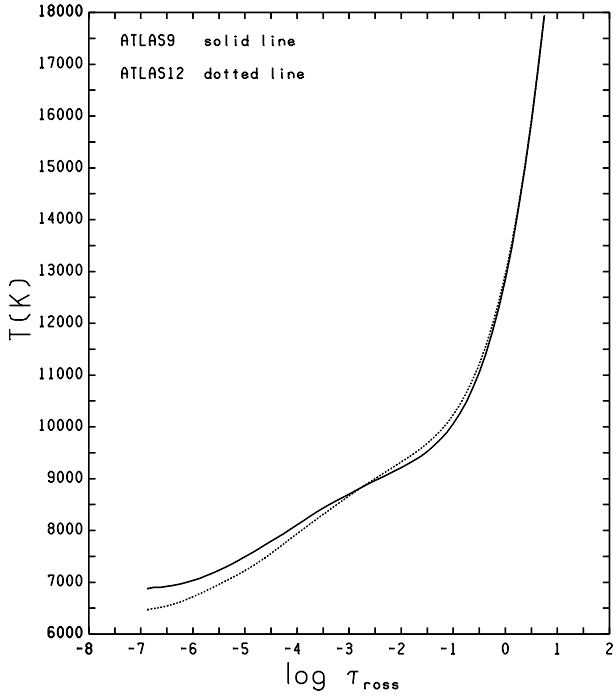

Fig. 1. The $T-\log\tau_{\rm ross}$ relation of an ATLAS9 model computed for solar abundances for all the elements (solid line) is compared with the $T-\log\tau_{\rm ross}$ relation of an ATLAS12 model computed with the individual abundances of HD 175640 (dotted line). Model parameters are $T_{\rm eff}$ = 12 000 K, log g = 3.95, ξ = 0 km s^{-1}.

4. Line data

Atomic line lists from the Kurucz database[4] have provided the basis for the line data. They contain data mostly from the literature for light and heavy elements and computed by Kurucz (1992) for the iron group elements. In this case the critically evaluated transition probabilities from Martin et al. (1988) and Fuhr et al. (1988) were adopted for the lines in common. The files that we downloaded from the Kurucz website differ from those available in Kurucz & Bell (1995) for the Fe I line data.

We implemented the files gf0400.100, gf0500.100, gf0600.100, gf0800.100 and gf1200.100, which cover the range 3040–10 000 Å, by replacing several log gfs with more up-to-date determinations and by adding missing lines, Stark broadening parameters, and hyperfine and isotopic components. In particular, we compared the line data of all the elements identified in HD 175640 on the basis of the Kurucz line lists with the line data from the NIST database[5] and from Wiese et al. (1996) for CNO. Generally, we preferred for our analysis NIST and Wiese et al. (1996) log gfs, although the differences with Kurucz's data are very small for most of the lines. We added several O I lines from Wiese et al. (1996), and a few Br II and several Xe II lines from NIST. We also examined other sources for specific elements like Si II (Lanz & Artru 1985), Ti II (Pickering et al. 2002), Cr II (Sigut & Landstreet 1990), Ga II (Isberg & Litzén 1985; Ryabchikova & Smirnov 1994; Nielsen et al. 2000), Y II (Nilsson et al. 1991), Xe II (Hansen & Persson 1987), Ce III (Biémont et al. 1999), Pr III (Biémont et al. 2001b), Nd III (Zhang et al. 2002), Yb II (Biémont et al. 1998), Yb III (Biémont et al. 2001a), Pt II (Dworetsky et al. 1984), Au II (Rosberg & Wyart 1997), Hg I (Benck et al. 1989) and Hg II (Sansonetti & Reader 2001; Proffitt et al. 1999). Actually, for the Rare Earth Elements we examined the DREAM database[6].

[3] http://cfa-www.harvard.edu/HITRAN
[4] http://kurucz.harvard.edu/linelists/gf100
[5] http://physics.nist.gov/cgi-bin/AtData/lines_form
[6] http://www.umh.ac.be/astro/dream.shtml

Because the Stark effect is an important line broadening mechanism in HD 175640 we also scrutinized the Stark line data. In the Kurucz line lists the damping constants $\gamma_S = 4\pi cw/\lambda^2$ are taken from the literature when available. The Griem (1974) tables are the source for the damping constants of a large number of light element lines, while for all the lines of the iron group elements the damping constants are due to Kurucz's (1992) computations. The γ_S value for $T = 20\,000$ K is that adopted in the line lists. We added Stark damping constants from Lanz et al. (1988) for some Si II lines not considered by Griem (1974). Damping constants not available from the literature are computed inside the SYNTHE code with an approximate formula (Kurucz & Avrett 1981).

Lines of He I are computed separately. Stark profiles are given in tabular form as function of temperature, electron density and ion density for the He I lines at 4026 Å, 4387 Å, 4471 Å and 4922 Å. The Stark profiles for the first two lines were taken from Shamey (1969), those for the last two lines from Barnard et al. (1974) and Barnard et al. (1975), respectively. The Stark profile for the given model atmosphere is computed by interpolating in the tables. For some other He I lines, Stark profiles are obtained by interpolating for temperature the Stark widths and shifts taken from the Griem (1974) tables. For a few He I lines not available in Griem (1974) we added Stark widths and shifts computed by Dimitrijević & Sahal-Bréchot (1990) with a semiempirical approach. Figure 2 compares two synthetic profiles for He I at 4009.26 Å predicted by the HD 175640 model atmosphere. They differ only in the Stark damping constant, which is computed according to the approximation made in the SYNTHE code in one case, and is derived from the Stark widths and shifts computed by Dimitijevic & Sahal-Brèchot (1990) in the other case. This last profile agrees with the observed spectrum which is also plotted in Fig. 2. The large influence of the Stark effect, in spite of the weakness of the line, is evident from the figure.

Thanks to the very high resolution of the UVES spectra, isotopic shifts and hyperfine splittings are well detectable in several profiles, in particular those of Mn II, Ga II and Hg II. As a consequence, we may expect good agreement in their observed and computed profiles only when isotopic and hyperfine structures are taken into account in the computations. But these data are rather scarse in the literature, so that only few lines can be accurately computed. We included in the line list hyperfine components for some lines of Mn II (Holt et al. 1999); isotopic and hyperfine components for some lines of Ga II (Karlsson & Litzén 2000), Pt II (Engleman 1989), Hg I (Dolk et al. 2003), and Hg II (Dolk et al. 2003); isotopic components for Ba II at 4554.03 Å (Becker & Werth 1983; Becker et al. 1968). When the hyperfine components were not directly available in the literature, but only the A and B hyperfine constants were given, we used them in the HYPERFINE code (Kurucz & Bell 1995) for computing the hyperfine wavelengths and the corresponding hyperfine log gfs. Figure 3 shows the extreme hyperfine broadening which affects the Mn II lines at 7353.549 Å and 7415.803 Å. In the figure each observed profile is compared with two synthetic profiles which differ in the hyperfine structure. One profile was computed by considering the hyperfine structure, the other profile was computed without it.

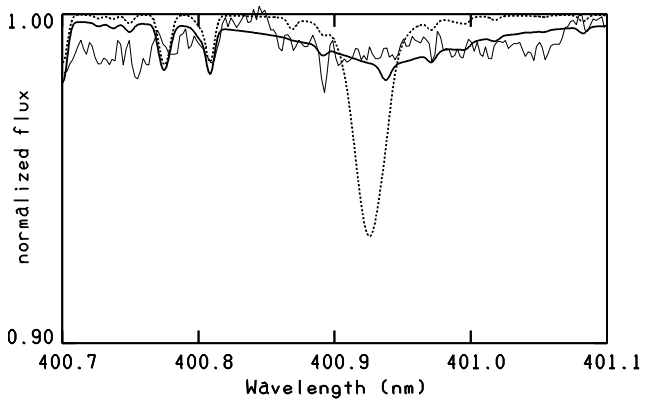

Fig. 2. Two synthetic profiles of He I 400.9257 nm differing only in the Stark damping constants are compared with the observations (full thin line). The thick line shows the profile computed with the Stark widths and shifts from Dimitrijević & Sahal-Bréchot (1990), the dotted line shows the profile computed with the approximate Stark damping constant yielded by the SYNTHE code (Kurucz & Avrett 1981) when it is not available from the literature. We used the model for HD 175640 having parameters $T_{\rm eff} = 12\,000$ K, log $g = 3.95$, microturbulent velocity $\xi = 0$ km s^{-1}. The synthetic profiles are also broadened for $v \sin i = 2.5$ km s^{-1} and for a Gaussian instrumental profile with 110 000 resolving power.

Isotopic and hyperfine components for Mn II, Ga II, Ba II, Hg I, and Hg II are discussed and listed in Appendix A (Tables A.6–A.9).

5. Discussion

The inspection of the atlas of HD 175640 shows a very large number of identified absorptions. The spectrum is crowded with Mn II, Mn I, Ti II and Cr II lines. In addition to H I, other identified species are He I, Be II, C I, C II, O I, O II, Ne I, Na I, Mg I, Mg II, Si II, Si III, P II, S I, S II, Ca I, Ca II, Sc II, Ti II, Cr I, Cr II, Mn I, Mn II, Fe I, Fe II, Co II(?), Ni II, Cu I, Ga I, Ga II, Br II, Sr II, Y II, Zr II, Rh II, Pd I, Xe II, Ba II, Pr III(?),Nd III(?), Yb II, Yb III, Os II(?), Ir II(?), Pt II, Au II, Hg I and Hg II. Here, the question marks indicate doubtful identifications. A previous identification work in the range 3050–6750 Å based on the same spectrum studied by us was performed by Bord et al. (2003)[7] by using the wavelength coincidence statistics (WCS) method. They also identified Pd II which was missed by us (see Appendix A). The Bord et al. (2003) analysis as well as our atlas show that numerous features, in particular for $\lambda > 5000$ Å, could not be identified. A list of unidentified lines in the range 4700–5800 Å is available in Appendix A (Table A.10). This region is approximately the same covered by the table of unanalyzed lines in HR 7775 in Wahlgren et al. (2000). The comparison of the two lists of unidentified lines has given a very small number of coincidences. In HD 175640, several unidentified absorptions coincide with lines of Mn II and Cr II having log gf values too low to yield a predicted profile of intensity similar to the observed one.

[7] http://www.astro.lsa.umich.edu/users/cowley/AAS0503Don/P7143.htm

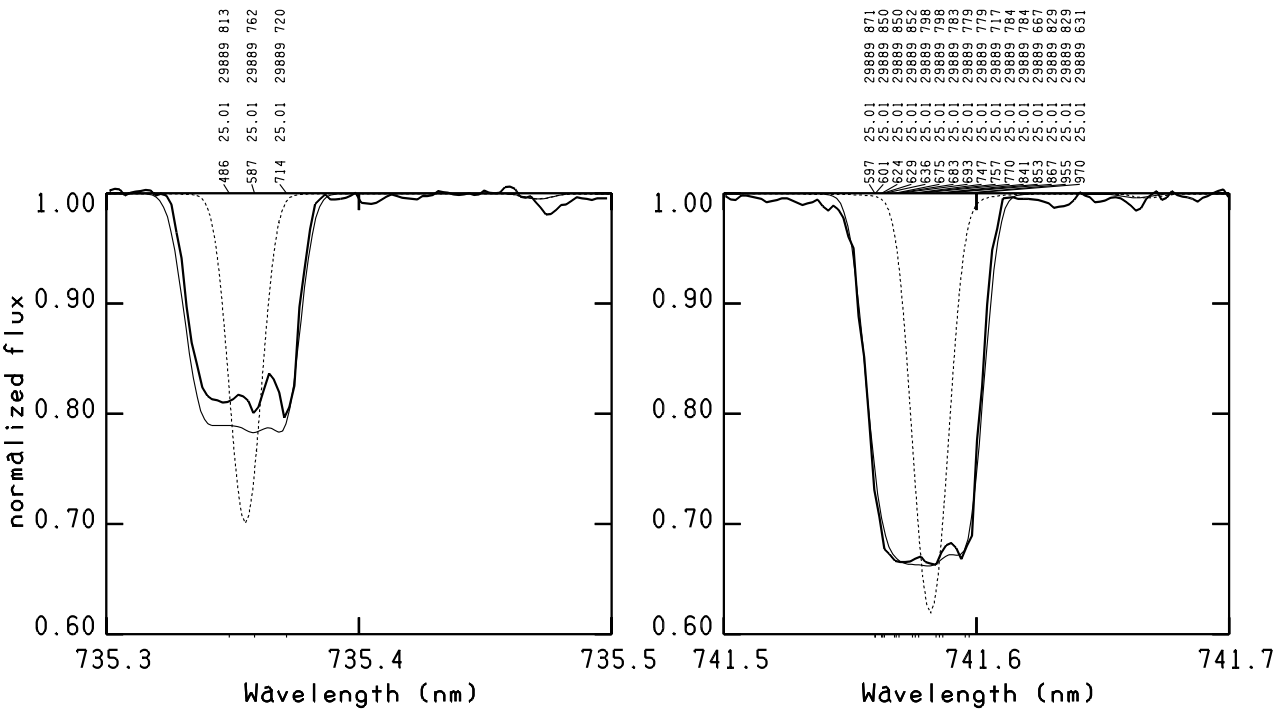

Fig. 3. The observed profiles (thick full lines) of Mn II at $\lambda\lambda$ 735.3549 and 741.5803 nm are compared with synthetic profiles computed once without any hyperfine structure (dotted lines) and once with hyperfine structure (thin full lines). The meaning of the line identification labels like 486 25.01 29889 813 is: 486, last 3 digits of wavelength in nm (735.3486); 25.01, element (25) and charge (01), i.e. Mn II; 29889, lower energy level in cm^{-1}; 813, per mil residual flux of the isolated line before rotation.

Numerous weak emission lines from Cr II and Ti II have been identified in the red part of the spectrum, starting at $\approx\lambda$ 5847 Å. They are all the Ti II lines with the lower excitation potential $\gtrsim$62 000 cm^{-1} and log $gf > -1.0$ and all the Cr II lines with the lower excitation potential $\gtrsim$89 000 cm^{-1} and log $gf > -0.8$. The observed emission lines of Ti II and Cr II are tabulated in Appendix A (Tables A.4 and A.5) together with a few unidentified observed emission lines (Table A.11). Emission lines of C I at 9335.148 Å (mult. 10) and 9405.730 Å (mult. 9) have been observed for the first time. No clear Mn II emission lines were observed in HD 175640.

Considering the observational material at our disposal we notice that it is possible to identify different subgroups of HgMn stars on the basis of which ions appear in emission. 46 Aql (HD 186122) was the first HgMn star where emission lines of Mn II were detected (Sigut et al. 2000). Wahlgren & Hubrig (2000) found additional emission lines originating from the ions Fe II and Cr II. Emission lines of Mn II have further been found in HD 16727 and HD 41040. However, some other HgMn stars (e.g., HD 175640, HD 71066, HD 11073 or HD 178640) show exclusively Cr II and Ti II emission lines. The hypothesis has been made that the presence of emission lines of a particular element is correlated in some way with its abundance (Wahlgren & Hubrig 2000). Sigut (2001) explains the emission lines as due to NLTE effects interlocked with vertical stratified abundances of particular elements. However, there is also a group of HgMn stars which does not exhibit emission lines at all (e.g. HD 49606, HD 77350 or HD 78316). At the moment, the very small sample of HgMn stars with observed emission lines cannot answer the question of what excitation process leads to the weak emission lines. The proper identification and tabulation of emission lines in the spectrum of HD 175640 should help to advance and to test the theoretical explanation of their origin.

We can see in the atlas that unpredicted red components affect the K and H Ca II profiles at 3933 Å and 3968 Å and the Na I profiles at 5890 Å and 5896 Å. Their circumstellar or interstellar origin should be further investigated. An unexpected redshift of 0.2 Å for the Ca II profiles at 8498 Å and 8662 Å was explained by Castelli & Hubrig (2004) by an anomalous isotopic composition of Ca in HD 175640. The only other element in HD 175640 with an anomalous isotopic composition is Hg (Dolk et al. 2003).

Abundances for 49 ions from 40 elements (Table 1) were determined from both equivalent width and line profile analyses. The analysis of each ion is extensively discussed in Appendix A. The abundances for a number of ions (He I, C I-C II, O I, Na I, P II, S II, Ca I-Ca II, Sc II, Ti II, Br II, Sr II, Y II, Zr II, Rh II, Pd I, Xe II, Ba II, Nd III, Yb II-Yb III, Pt II and Au II) are reported here for the first time. The main interest in carrying out the abundance study of HD 175640 comes from the fact that no convincing explanation of the origin of HgMn stars presently exists and that the physical mechanisms producing observed abundance anomalies are not fully understood (e.g., Hubrig & Mathys 1995; Leckrone et al. 1999; Dolk et al. 2003). Abundance determinations from the analysis of stellar spectra play a critical and defining role for testing the several mechanisms that have been proposed to explain the development of the anomalies.

The examination of Table 1 shows that both excesses and deficiencies occur in the atmosphere. Compared to the solar abundance, Hg is the most overabundant element. It exceeds the solar abundance by a factor $>10^4$. It is followed by Ga, Y, Pd, Xe, Yb III, and Au, which have abundances larger than the solar ones by factors of the order of 10^3. Mn, Br, Yb II, and Pt are overabundant by factors larger than 10^2, while Cr and Ti are overabundant by factors of the order of 10. Elements overabundant in a lesser degree are Cu ([+0.95]), Sr ([+0.66)], Zr ([0.77]), Ba ([+0.64]), and Nd ([+0.97]). The most underabundant elements are N, Al and V, which could not be identified in the spectrum, so that their underabundances of [−1.7], [−1.9] and [−1.0], respectively, are only upper limits. Other underabundant elements are He ([−0.62]), C ([−0.55]) and Co ([−0.96]). The abundances of the remaining elements lie within the limits of ±0.5 dex.

Only a few observational studies have been carried out to test the vertical abundance stratification of certain elements in HgMn stars (Alecian 1982; Lanz et al. 1993; Savanov & Hubrig 2003). Our study of HD 175640 revealed different abundances of singly ionized ions lying on either side of the Balmer jump. The differences are within the limits of the standard deviations for Ca II, Cr I, Cr II, Mn I, Ni II, Zr II. They are larger than the standard deviations for Sc II, Ti II, Fe I, Y II, and Yb II. In the near UV, these elements give abundances larger than those derived from the visual lines, except for Fe I for which the opposite is true.

Possible signs of an ionization anomaly have been found from the study of Cr I, Cr II and Yb II, Yb III lines. The average abundance obtained from lines of Cr II is lower by 0.2 dex than from lines of Cr I. For the REE Yb, we find that the average abundance from the Yb III lines is 0.8 dex higher than that from the Yb II lines. The 0.2 dex abundance difference from Cr I and Cr II lines seems to confirm the vertical Cr stratification inferred by Savanov & Hubrig (2003) from Cr II lines lying on the wings of H_β at different distances from the core, although they found the larger abundance difference of 0.6 dex. No sign of vertical Cr abundance stratification comes from the abundances of Cr I and Cr II lines lying on either side of the Balmer jump.

Finally, the synthetic spectrum analysis has shown some deficiencies of the UVES spectrum reduction procedures related to small uncertainties in the wavelength calibrations as well as to large jumps and undulations of the échelle spectra. All these shortcomings contribute to reducing the agreement of the computed spectra with the observed spectra in certain wavelength regions.

Acknowledgements. We would like to express our gratitude to M. Schöller for his help with the layout of the paper and the website.

References

Albayrak, B., Gulliver, A. F., Adelman, S. J., Aydin, C., & Kocer, D. 2003, A&A, 400, 1043
Alecian, G. 1982, A&A, 107, 61
Anders, E., & Grevesse, N. 1989, Geochim. Cosmochim. Acta, 53, 197
Barnard, A. J., Cooper, J., & Smith, E. W. 1974, J. Quant. Spect. Rad. Transfer, 14, 1025
Barnard, A. J., Cooper, J., & Smith, E. W. 1975, J. Quant. Spect. Rad. Transfer, 15, 429
Becker, W., & Werth, G. 1983, Z. Physik A, 311, 41
Becker, W., Fisher, W., & Huhnermann, H. 1968, Z. Phys., 216, 142
Benck, E. C., Lawler, J. E., & Dakin, J. T. 1989, J. Opt. Soc. Am. B, 6, 11
Berry, H. G., Bromander, J., Curtis, L. J., & Buchta, R. 1971, Phys. Scr., 3, 125
Biémont, E. 1977, A&AS, 27, 489
Biémont, E., Dutrieux, J.-F., Martin, I., & Quintet, P. 1998, J. Phys. B.: At. Mol. Opt. Phys., 31, 3321
Biémont, E., Garnir, H. P., Lokhnygin, V., et al. 2001a, J. Phys. B: At. Mol. Opt. Phys., 34, 1869
Biémont, E., Garnir, H. P., Palmieri, P., et al. 2001b, Phys. Rev. A, 64, 022503
Biémont, E., Grevesse, N., Kwiatkovski, M., & Zimmermann, P. 1981, A&A, 108, 127
Biémont, E., Palmieri, P., & Quintet, P. 1999, Ap&SS, 269, 635
Black, J. H., Wisheit, J. C., & Laviana, E. 1972, ApJ, 177, 567
Bord, D. J., Cowley, C. C., & Norquist, P. L. 1997, MNRAS, 284, 869
Bord, D. J., Cowley, C. R., Hubrig, S., & Bidelman, W. P. 2003, AAS, 202, 3210B
Castelli, F., & Hubrig, S. 2004, A&A, 421, L1
Corliss, C. H., & Bozman, W. R. 1962, NBS Monograph, 53
Cowley, C. R., & Corliss, C. H. 1983, MNRAS, 203, 651
Cowley, C., Wiese, W. L., Fuhr, J., & Kuznetsova, L. A. 2000, Allen's astrophysical quantities, ed. A. N. Cox, 53
Dimitrijević, M. S., & Sahal-Bréchot, S. 1990, A&AS, 82, 519
Dolk, L., Wahlgren, G. M., Lumdberg, H., et al. 2002, A&A, 385, 111
Dolk, L., Wahlgren, G. M., & Hubrig, S. 2003, A&A, 402, 299
Dworetsky, M. M., & Budaj, J. 2000, MNRAS, 318, 1264
Dworetsky, M. M., Storey, P. J., & Jacobs, J. M. 1984, Phys. Scr., T8, 39
Dworetsky, Men. M., Jomaron, C. M., & Smith, C. A. 1998, A&A, 333, 665
Engleman, R., Jr. 1989, ApJ, 340, 1140
Fuhr, J. R., Martin, G. A., & Wiese, W. L. 1988, J. Phys. Chem. Ref. Data, 17, Suppl. 4
Grevesse, N., & Sauval, A. J. 1998, Space Sci. Rev., 85, 161
Griem, H. R. 1974, Spectral Line Broadening by Plasmas (Academic Press)
Gulliver, A. F., Adelman, S. J., & Friesen, T. P. 2004, A&A, 413, 285
Hannaford, P., Lowe, R. M., Grevesse, N., Biémont, E., & Whaling, W. 1982, ApJ, 261, 736
Hansen, J. E., & Persson, W. 1987, Phys. Scr., 36, 602
Heise, H. 1974, A&A, 34, 275
Hempel, M., & Holweger, H. 2003, A&A, 408, 1065
Hibbert, A. 1988, Phys. Scr., 38, 37
Holt, R. A., Scholl, T. J., & Rosner, S. D. 1999, MNRAS, 306, 107
Hubrig, S., & Castelli, F. 2001, A&A, 375, 963
Hubrig, S., Castelli, F., & Wahlgren, G. M. 1999, A&A, 346, 139
Hubrig, S., & Mathys, G. 1995, Comments Astrophys., 18, 167
Isberg, B., & Lizèn, U. 1985, Phys. Scr., 31, 533
Johansson, S., Wallerstein, G., Gilroy, K. K., & Joueizadeh, A. 1995, A&A, 300, 521
Jomaron, C. M., Dworetsky, M. M., & Allen, C. S. 1999, MNRAS, 303, 555
Karlsson, H., & Litzèn, U. 2000, J. Phys. B: At. Mol. Opt. Phys., 33, 2929
Kostyk, R. I., & Orlova, T. V. 1983, Astrometrya Astrofiz., 49, 39
Kurucz, R. L. 1988, Trans. IAU, XXB, ed. M. McNally (Dordrecht: Kluwer), 168

Kurucz, R. L. 1992, Rev. Mex. Astron. Astrofis., 23, 45
Kurucz, R. L. 1993a, ATLAS9 Stellar Atmosphere Programs and 2 km s^{-1} grid, CD-ROM, No. 13
Kurucz, R. L. 1993b, SYNTHE Spectrum Synthesis Programs and Line Data, CD-ROM, No. 18
Kurucz, R. L. 1997, in The 3rd Conf. on Faint Blue Stars, ed. A. G. D. Philip, J. Liebert, & R. A. Saffer (Schenectady: L. Davis Press), 33
Kurucz, R. L. 2003, private communication
Kurucz, R. L., & Avrett, E. H. 1981, Solar Spectrum Synthesis. I. A sample atlas from 224 to 300 nm, SAO Spec. Rep., 391
Kurucz, R. L., & Bell, B. 1995, Atomic Line List, CD-ROM, No. 23
Kurucz, R. L., & Peytremann, E. 1975, SAO Special Report, 362
Lanz, T., & Artru, M.-C. 1985, Phys. Scr., 32, 115
Lanz, T., Artru, M. C., Didelon, P., & Mathys, G. 1993, A&A, 272, 465
Lanz, T., Dimitrijević, & Artru, M. C. 1988, A&A, 192, 249
Leckrone, D. S., Proffitt, C. R., Wahlgren, G. M., et al. 1999, AJ, 117, 1454
Martin, G. A., Fuhr, J. R., & Wiese, W. L. 1988, J. Phys. Chem. Ref. Data, 17, Suppl. 3
Miles, B. M., & Wiese, W. L. 1969, NBS Technical Note, 474
Moore, C. E. 1965, Selected Tables of Atomic Spectra, NSRDS-NBS, 3
Moore, C. E. 1972, A Multiplet Table of Astrophysical Interest, NSRDS-NBS, 40
Nielsen, H., Karlsson, H., & Wahlgren, G. M. 2000, A&A, 363, 815
Nilsson, A. E., Johansson, S., & Kurucz, R. L. 1991, Phys. Scr., 44, 226
Norris, J. 1971, ApJS, 23, 213
Pickering, J. C., Thorne, A. P., & Perez, R. 2002, ApJS, 138, 247
Proffitt, C. R., Brage, T., Leckrone, D. S., et al. 1999, ApJ, 512, 942
Raassen, A. J. J., & Uylings, P. H. M. 1998, A&A, 340, 300 http://www.science.uva.nl/pub/orth/iron/FeII.E1
Rosberg, M., & Wyart, J.-F. 1997, Phys. Scr., 55, 690
Ryabchikova, T. A., & Smirnov, YU. M. 1994, Astron. Rep., 38, 70
Sadakane, K., Jugaku, J., & Takada-Hidai, M. 1985, ApJ, 297, 240
Sadakane, K., Jugaku, J., & Takada-Hidai, M. 1988, ApJ, 325, 776
Sadakane, K., Takada-Hidai, M., Takeda, Y., et al. 2001, PASJ, 53, 1223
Sansonetti, C. J., & Reader, J. 2001, Phys. Scr., 63, 219
Savanov, I., & Hubrig, S. 2003, A&A, 410, 299
Shamey, L. J. 1969, unpublished Ph.D. Thesis, University of Colorado
Schulz-Gulde, E. 1969, JQRST, 9, 13
Sigut, T. A. A. 2001, A&A, 377, L27
Sigut, T. A. A., Landstreet, J. D., & Shorlin, S. L. S. 2000, ApJ, 530, L89
Sigut, T. A. A., & Landstreet, J. D. 1990, MNRAS, 247, 611
Smith, K. C. 1993, A&A, 276, 393
Smith, K. C. 1994, A&A, 291, 521
Smith, K. C. 1996, A&A, 305, 902
Smith, K. C. 1997, A&A, 319, 928
Smith, K. C., & Dworetsky, M. M. 1993, A&A, 274, 335
Wahlgren, G. M., & Hubrig, S. 2000, A&A, 362, L13
Wahlgren, G. M., Dolk, L., Kalus, G., et al. 2000, ApJ, 539, 908
Wiese, W. L., Fuhr, J. R., & Deters, T. M. 1996, J. Phys. Chem. Ref. Data, Monograph, 7
Wiese, W. L., & Martin, G. A. 1980, NSRDS-NBS, 68
Wiese, W. L., Smith, M. W., & Glennon, B. M. 1966, NSRDS-NSB, 4
Wujec, T., & Weniger, J. 1981, J. Quant. Spectrosc. Radiat. Transfer, 25, 167
Zhang, Z. G., Svanberg, S., Palmieri, P., Quintet, P., & Biémont, E. 2002, A&A, 385, 724

Online Material

Appendix A: The element by element analysis

All the elements which contribute to the spectrum of HD 175640 are individually considered here. Tables A.1–A.3 list respectively the lines of the light elements, of the iron group elements and of the elements with atomic number $Z \geq 30$ which were analyzed for abundance purposes. In all three tables the lines of each element are arranged in increasing wavelength order. Multiplet numbers are mostly taken from Moore (1972), except for He I. In this case multiplet numbers from NIST and from Wiese et al. (1966) (the ones in parenthesis) are given. For each line, the log gf value, its reference, and the lower excitation potential are listed. In Table A.1 the Stark damping constant $\log(\gamma_S/N_e)$ for $T = 20\,000$ K and its reference are added. There are no damping constants for He I in Table A.1 because they were obtained by interpolating for temperature and, for a few lines, also for electron and ion density, in tables of Stark broadening parameters or Stark profiles (Sect. 4), whose reference can be found in Col. 7. In Table A.3, the excitation potential of the upper level is added. In all the tables the last three columns show the measured equivalent width, the corresponding abundance, and the remarks, if any needed. When no equivalent width is given, the abundance was derived from the comparison of observed and computed profiles. This kind of determination was mostly performed when different transitions belonging to the same multiplet are observed as a single profile. The average abundance and its standard deviation (when more lines were measured) are given at the top of the subtable relative to the given ion.

Helium (2)-He I: By varying the He abundance in steps of 0.01 dex we obtained $\log(N(\mathrm{He})/N_{\mathrm{tot}}) = -1.73$ (i.e. $[-0.62]$) from the comparison of the computed and observed profiles of the lines listed in Table A.1. All the weak lines are fully consistent with the adopted abundance, while some differences between observations and computations occur for the strongest lines. Figure A.1 shows that the blue wing of λ 4026 Å is not well reproduced, while the computed cores of $\lambda\lambda$ 4471 and 6678 Å are slightly too strong. We did not find any trace of the ^{3}He isotope for the line at 6678 Å, so that we assumed that the He isotopic ratio is the terrestrial one.

The weakness of all the He I lines observed in HD 175640 may justify the LTE assumption.

Beryllium (4)-Be II: The only unblended line observed in the spectrum is the Be II resonance line at 3130.420 Å, mult. 1. The abundance $\log(N(\mathrm{Be})/N_{\mathrm{tot}}) = -10.64$ derived from the equivalent width is solar. Sadakane et al. (1985) found $\log(N(\mathrm{Be})/N(\mathrm{H})) < -9.7$ from IUE spectra. The other Be II line of mult. 1 at 3131.065 Å is predicted weak for the above abundance and is heavy blended with Mn II. A weak unidentified absorption at 5270.3 Å can hardly be due to Be II 5270.28 Å mult. 3 as the other, stronger line of the same multiplet at 5270.815 Å is not observed.

The log gf values of the Kurucz line list, which were taken from Biémont et al. (1977), were used for the lines examined here. They do not differ by more than 0.005 dex from those available in the NIST database.

Boron (5)-Not observed: There are no observed absorptions at the position of B II 3451.287 Å, mult. 1. An absorption at 3451.32 Å identified as Fe II 3451.318 Å is much stronger than predicted both when $\log gf = -1.519$ from the Kurucz database and $\log gf = -1.651$ from Raassen & Uylings (1998) are used. We could speculate that boron contributes to the observed absorption, provided that its wavelength is 3451.320 Å and that it is highly overabundant. However, Sadakane et al. (1985) derived from IUE spectra a boron underabundance of the order of $[-1.4]$. Therefore we assume that no boron lines are observable in our spectra.

Carbon (6)-C I,C II: The most striking characteristic of carbon is the presence of the two strong emission lines of C I mult. 10 at 8335.148 Å and C I mult. 9 at 9405.730 Å. They are shown in Fig. A.2, where the observed spectrum, the computed spectrum and the telluric spectrum are superimposed.

There is no doubt that the carbon abundance is subsolar, but it is difficult to fix its exact value owing to the position of the strongest C I and C II lines in the red part of the spectrum where they are either embedded in strong telluric absorptions or heavily blended with them. Examples are C I mult. 3 at 9061.431 Å, 7231.33 Å and 7236.42 Å and C I mult. 2 at 9620.777 Å and 9658.430 Å. In addition, the spectrum is of bad quality in the 9074–9098 Å region, just where three C I lines of mult. 3 ($\lambda\lambda$ 9078.288, 9088.513 and 9094.830 Å) could have been measured.

The few C I and C II lines that have measurable equivalent widths are listed in Table A.1. We remark that C II mult. 4 at 3918.968 Å seems to blueshifted relatively to the wavelength taken from Wiese et al. (1996). If the shift is not real it could be blended with an unknown component. The average abundance from C I is -4.11 ± 0.23 dex, that from C II is -4.05 ± 0.16 dex, while the average abundance from all C I and C II lines is -4.08 ± 0.20 dex. After comparison of the synthetic spectrum with the observed spectrum we assumed $\log(N(\mathrm{C})/N_{\mathrm{tot}}) = -4.00$.

According to Hempel & Holweger (2003) no NLTE corrections are needed for the carbon lines examined in HD 175640 because no negligible NLTE effects are predicted in late B-type stars for lines with equivalent widths larger than 100 mÅ.

Nitrogen (7)-Not observed: There are no nitrogen lines observed in the spectrum. The computed N I lines of mult. 1 at 8680–8728 Å disappear for $\log(N(\mathrm{N})/N_{\mathrm{tot}}) = -5.78$. We adopted this value as upper limit for the nitrogen abundance. It corresponds to an underabundance of $[-1.66]$.

Oxygen (8)-O I,O II: We identified a large number of O I lines, and two O II lines of mult. 1 (4641.82 Å and 4649.14 Å) that were so weak that no measuraments of their equivalent widths were performed. All the O I lines analyzed in the spectrum are listed in Table A.1.

Table A.1. Abundances of the light elements.

Mult.	λ(Å)	log gf	Ref.[a]	χ_{low}(cm^{-1})	log(γ_S/N_e)	Ref.[b]	W(mÅ)	log(N_Z/N_{tot})	Notes
		He I	log N(He I)/N_{tot} = −1.73						
88 (22)	3819.6020	−2.968	NIST	169 086.87		DS90		−1.73	
88 (22)	3819.6028	−1.045	NIST	169 086.87		DS90		−1.73	
88 (22)	3819.6028	−1.794	NIST	169 086.87		DS90		−1.73	
88 (22)	3819.6131	−1.794	NIST	169 086.95		DS90		−1.73	
88 (22)	3819.6139	−1.315	NIST	169 086.95		DS90		−1.73	
88 (22)	3819.7573	−1.668	NIST	169 087.93		DS90		−1.73	
82 (20)	3867.4723	−2.055	NIST	169 086.87		DS90		−1.73	
82 (20)	3867.4837	−2.276	NIST	169 086.95		DS90		−1.73	
82 (20)	3867.6315	−2.754	NIST	169 087.93		DS90		−1.73	
32 (58)	3926.5443	−1.647	NIST	171 155.00		DS90		−1.73	Not observed
31 (55)	4009.2565	−1.473	NIST	171 135.00		DS90		−1.73	Not observed
25 (54)	4023.9798	−2.577	NIST	171 135.00		DS90		−1.73	On the wing of He I 4026
87 (18)	4026.1844	−2.625	NIST	169 086.87		SM69		−1.73	Bad fit for the blue wing
87 (18)	4026.1859	−1.448	NIST	169 086.87		SM69		−1.73	
87 (18)	4026.1860	−0.701	NIST	168 086.87		SM69		−1.73	
87 (18)	4026.1968	−1.449	NIST	169 086.95		SM69		−1.73	
87 (18)	4026.1983	−0.972	NIST	169 086.95		SM69		−1.73	
87 (18)	4026.3570	−1.324	NIST	169 087.93		SM69		−1.73	
81 (16)	4120.8108	−1.738	NIST	169 086.87		G74		−1.73	On the red wing of Hδ
81 (16)	4120.8237	−1.961	NIST	169 086.95		G74		−1.73	
81 (16)	4120.9916	−2.437	NIST	169 087.93		G74		−1.73	
30 (53)	4143.7590	−1.196	NIST	171 135.00		DS90		−1.73	Not observed
24 (52)	4168.9716	−2.338	NIST	171 135.00		DS90		−1.73	Not observed
29 (51)	4387.9291	−0.883	NIST	171 135.00		SM69		−1.73	
23 (50)	4437.5536	−2.034	NIST	171 135.00		G74		−1.73	
86 (14)	4471.4704	−2.203	NIST	169 086.87		BCS1		−1.73	
86 (14)	4471.4741	−1.026	NIST	169 086.87		BCS1		−1.73	
86 (14)	4471.4743	−0.278	NIST	169 086.87		BCS1		−1.73	
86 (14)	4471.4856	−1.025	NIST	169 086.95		BCS1		−1.73	
86 (14)	4471.4893	−0.550	NIST	169 086.95		BCS1		−1.73	
86 (14)	4471.6832	−0.903	NIST	169 087.93		BCS1		−1.73	
80 (12)	4713.1392	−1.230	NIST	169 086.87		G74		−1.73	Blend with Cr II, Fe II
80 (12)	4713.1562	−1.452	NIST	169 086.94		G74		−1.73	
80 (12)	4713.3757	−1.928	NIST	169 087.93		G74		−1.73	
28 (48)	4921.9310	−0.435	NIST	171 135.00		BCS2		−1.73	
13 (4)	5015.6776	−0.820	NIST	166 277.54		G74		−1.73	Blend with Fe II
22 (47)	5047.7384	−1.601	NIST	171 135.00		G74		−1.73	Blend with Fe II
85 (11)	5875.5987	−1.516	NIST	169 086.87		G74		−1.73	
85 (11)	5875.6139	−0.341	NIST	169 086.87		G74		−1.73	
85 (11)	5875.6148	+0.408	NIST	169 086.87		G74		−1.73	
85 (11)	5875.6251	−0.340	NIST	169 086.95		G74		−1.73	
85 (11)	5875.6403	+0.137	NIST	169 086.95		G74		−1.73	
85 (11)	5875.9663	−0.215	NIST	169 087.93		G74		−1.73	
27 (46)	6678.1517	+0.329	NIST	171 135.00		G74		−1.73	
79 (10)	7065.179	−0.461	NIST	169 086.87		G74		−1.73	
79 (10)	7065.217	−0.682	NIST	169 086.95		G74		−1.73	
79 (10)	7065.710	−1.160	NIST	169 087.93		G74		−1.73	
		Be II	log N(Be II)/N_{tot} = −10.64						
1	3130.420	−0.168	K,BIE	0.00	−5.80	G74 (K)	7.12	−10.64	
		C I	log N(C I)/N_{tot} = −4.11 ± 0.23						
6	4771.747	−1.866	CNO	60 393.14	−4.59	G74	1.58	−3.82	
13	4932.049	−1.658	CNO	61 981.82	−4.32	G74	1.19	−4.05	
3	9062.487	−0.456	CNO	60 333.43	−5.32	G74	24.41	−3.98	
3	9111.807	−0.298	CNO	60 393.14	−5.32	G74	21.88	−4.19	
2	9603.034	−0.896	CNO	60 333.43	−5.40	G74	3.05:	−4.49	
		C II	log N(C II)/N_{tot} = −4.05 ± 0.16						
4	3918.968	−0.533	CNO	131 724.37	−4.93	G74	12.23	−3.95	
6	4267.261	+0.717	CNO	145 550.70	−4.76	G74	22.57	−3.87	
2	6578.052	−0.026	CNO	116 537.65	−5.35	G74	8.68	−4.31	On the wing of H$_\alpha$
2	6582.882	−0.328	CNO	116 537.65	−5.35	G74	7.60	−4.08	On the wing of H$_\alpha$

Table A.1. continued.

Mult.	λ(Å)	log gf	Ref.[a]	χ_{low}(cm^{-1})	log(γ_S/N_e)	Ref.[b]	W(mÅ)	log(N_Z/N_{tot})	Notes
		O I log N(O I)/N_{tot} = −3.18 ± 0.11							
3	3947.295	−2.096	CNO	73 768.20	−4.70	G74	6.54	−3.40	
3	3947.481	−2.244	CNO	73 768.20	−4.70	G74		−3.40	
3	3947.586	−2.467	CNO	73 768.20	−4.70	G74		−3.40	
5	4368.190	−2.665	CNO	76 794.98	−4.68	G74		−3.20	
5	4368.242	−1.964	CNO	76 794.98	−4.68	G74		−3.20	
5	4368.258	−2.818	CNO	76 794.98	−4.68	G74		−3.20	
14	4967.380	−2.086	CNO	86 625.76	–	–			No fit
14	4967.380	−1.997	CNO	86 625.76	–	–			No fit
14	4967.380	−2.329	CNO	86 625.76	–	–			No fit
14	4967.880	−1.660	CNO	86 627.78	–	–			No fit
14	4967.880	−1.865	CNO	86 627.78	–	–			No fit
14	4967.880	−2.454	CNO	86 627.78	–	–			No fit
14	4968.790	−1.375	CNO	86 631.45	–	–			No fit
14	4968.790	−1.961	CNO	86 631.45	–	–			No fit
14	4968.790	−2.087	CNO	86 631.45	–	–			No fit
13	5020.218	−1.725	CNO	86 631.45	–	–	2.87	−3.35	
12	5329.096	−1.938	CNO	86 625.76	−3.43	G74		−3.27	
12	5329.099	−1.586	CNO	86 625.76	−3.43	G74		−3.27	
12	5329.107	−1.695	CNO	86 625.76	−3.43	G74		−3.27	
12	5329.673	−2.063	CNO	86 627.78	−3.43	G74		≤−3.27	Blend with Mn II
12	5329.681	−1.473	CNO	86 627.78	−3.43	G74		≤−3.27	Blend with Mn II
12	5329.690	−1.269	CNO	86 627.78	−3.43	G74		≤−3.27	Blend with Mn II
12	5330.735	−1.570	CNO	86 631.45	−3.43	G74		−3.27	
12	5330.741	−0.984	CNO	86 631.45	−3.43	G74		−3.27	
11	5435.178	−1.766	CNO	86 625.76	−3.82	G74	4.20	−3.20	
11	5435.775	−1.544	CNO	86 627.78	−3.82	G74	5.99	−3.16	
11	5436.862	−1.398	CNO	86 631.45	−3.82	G74	7.49	−3.20	
10	6155.961	−1.363	CNO	86 625.76	−3.96	G74		−3.17	
10	6155.971	−1.011	CNO	86 625.76	−3.96	G74		−3.17	
10	6155.989	−1.120	CNO	86 625.76	−3.96	G74		−3.17	
10	6156.737	−1.488	CNO	86 627.78	−3.96	G74		−3.17	
10	6156.755	−0.899	CNO	86 627.78	−3.96	G74		−3.17	
10	6156.778	−0.694	CNO	86 627.78	−3.96	G74		−3.17	
10	6158.149	−1.841	CNO	86 631.45	−3.96	G74		−3.17	Blend with Cr II, Cr II
10	6158.172	−0.996	CNO	86 631.45	−3.96	G74		−3.17	Blend with Cr II, Cr II
10	6158.187	−0.409	CNO	86 631.45	−3.96	G74		−3.17	Blend with Cr II, Cr II
9	6453.602	−1.288	CNO	86 625.76	−4.28	G74	7.34	−3.24	
9	6454.444	−1.066	CNO	86 627.78	−4.28	G74	11.95	−3.23	
9	6455.977	−0.920	CNO	86 631.45	−4.28	G74		(−3.27)	Blend with Ga II
21	7001.899	−1.489	CNO	88 630.59	−3.93	G74		−3.27	Blend with Mn II
21	7001.922	−1.012	CNO	88 630.59	−3.93	G74		−3.27	Blend with Mn II
21	7002.173	−2.644	CNO	88 631.15	−3.93	G74		−3.22	
21	7002.196	−1.489	CNO	88 631.15	−3.93	G74		−3.22	
21	7002.230	−0.741	CNO	88 631.15	−3.93	G74		−3.22	
21	7002.250	−1.364	CNO	88 631.30	−3.93	G74		−3.22	
38	7156.701	+0.288	CNO	102 662.03	−5.35	G74	23.70	−3.11	
1	7771.944	+0.369	CNO	73 768.20	−5.55	G74	190.78	−2.04	No fit
1	7774.166	+0.223	CNO	73 768.20	−5.55	G74	174.48	−2.08	No fit
1	7775.388	+0.001	CNO	73 768.20	−5.55	G74	148.12	−2.20	No fit
35	7947.548	+0.500	K, NBS	101 135.41	−5.54	G74	32.22	−3.02	
35	7950.803	+0.340	K, NBS	101 147.53	−5.54	G74	25.98	−3.09	
35	7952.159	+0.170	K, NBS	101 155.42	−5.54	G74	21.46	−3.14	
34	8221.824	+0.313	CNO	101 135.41	−5.40	G74		−3.10	
4	8446.247	−0.463	CNO	76 794.98	−5.44	G74			No fit
4	8446.359	+0.236	CNO	76 794.98	−5.44	G74			No fit
4	8446.758	+0.014	CNO	76 794.98	−5.44	G74			No fit
37	8820.423	+0.379	CNO	102 662.03	−5.51	G74	43.43	−3.04	
8	9260.806	−0.242	CNO	86 625.76	−4.95	G74			No fit
8	9260.848	+0.110	CNO	86 625.76	−4.95	G74			No fit
8	9260.848	+0.001	CNO	86 625.76	−4.95	G74			No fit

Table A.1. continued.

Mult.	λ(Å)	log gf	Ref.[a]	$\chi_{\rm low}$(cm^{-1})	log($\gamma_{\rm S}/N_{\rm e}$)	Ref.[b]	W(mÅ)	log($N_Z/N_{\rm tot}$)	Notes
			O I cont.						
8	9262.582	−0.367	CNO	86 627.78	−4.95	G74			No fit
8	9262.670	+0.223	CNO	86 627.78	−4.95	G74			No fit
8	9262.776	+0.427	CNO	86 627.78	−4.95	G74			No fit
8	9265.826	−0.719	CNO	86 631.45	−4.95	G74			No fit
8	9265.932	+0.126	CNO	86 631.45	−4.95	G74			No fit
8	9266.006	+0.712	CNO	86 631.45	−4.95	G74			No fit
			Ne I log N(Ne I)/$N_{\rm tot}$ = −4.35						
1	7032.413	−0.294	NIST	134 041.840	−6.32	G74	2.23	−4.35	
			Na I log N(Na I)/$N_{\rm tot}$ = −5.47						
6	5688.205	−0.450	K, KP	16 973.37	−5.68	G74		−5.47:	Blend with telluric lines
1	5889.950	+0.112	NIST	0.00	−5.64	G74		−5.47:	Blend interstell./circumstell. line
1	5895.924	−0.191	NIST	0.00	−5.64	G74		−5.47:	Blend interstell./ circumstell. line
4	8183.255	+0.260	NIST	16 956.17	−5.52	G74		≥−5.47:	Blend with telluric line
4	8194.790	−0.441	NIST	16 973.37	−5.52	G74		−5.47	
4	8194.824	+0.514	NIST	16 973.37	−5.52	G74		−5.47	
			Mg I log N(Mg I)/$N_{\rm tot}$ = −4.64 ± 0.06						
40	4702.991	−0.374	NIST	35 051.26	−3.98	G74	2.09	−4.72	
2	5167.321	−0.856	NIST	21 850.41	−5.27	G74	5.80	−4.57	
2	5172.684	−0.380	NIST	21 870.46	−5.27	G74	13.74	−4.63	
2	5183.604	−0.158	NIST	21 911.18	−5.27	G74		−4.58	Blend with Fe II,Ti II
			Mg II log N(Mg II)/$N_{\rm tot}$ = −4.71 ± 0.07						
10	4384.637	−0.792	NIST	80 619.50	−4.02	G74	24.11	−4.81	
10	4390.514	−1.706	NIST	80 650.02	−4.02	G74	39.57	−4.76	
10	4390.572	−0.530	NIST	80 650.02	−4.02	G74	39.57	−4.76	
9	4427.994	−1.201	NIST	80 619.50	−4.40	G74	13.44	−4.70	
4	4481.126	+0.730	NIST	71 490.19	−4.68	G74		−4.69	Bad fit for the core
4	4481.150	−0.570	NIST	71 490.19	−4.68	G74		−4.69	Bad fit for the core
4	4481.325	+0.575	NIST	71 490.06	−4.68	G74		−4.69	Bad fit for the core
8	7877.054	+0.390	NIST	80 619.50	−4.54	G74	64.50	−4.68	
8	7896.042	−0.303	NIST	80 650.02	−4.54	G74	28.14	−4.77	
8	7896.366	+0.647	NIST	80 650.02	−4.54	G74	85.58	−4.56	Blend with telluric line
–	8213.987	−0.279	NIST	80 619.50	−4.77	G74		−4.81	At the Paschen limit
–	8234.636	+0.024	NIST	80 650.02	−4.77	G74		−4.81	Blend with telluric line
–	9631.891	+0.663	NIST	93 310.59	–	–	57.42	−4.69	
–	9631.95	−0.639	NIST	93 310.59	–	–		−4.69	
–	9632.430	+0.507	NIST	93 311.11	–	–	47.05	−4.72	
			Si II log N(Si II)/$N_{\rm tot}$ = −4.72 ± 0.08						
1	3853.665	−1.517	K, BBCB	55 309.35	−4.91	G74	60.94	−4.77	
1	3856.018	−0.557	K, BBCB	55 325.18	−4.91	G74	108.86	−4.81	
1	3862.595	−0.817	K, BBCB	55 309.35	−4.91	G74	98.75	−4.71	
3.01	4072.709	−2.367	K, SG	79 338.50	−4.51	LDA	1.95	−4.75	
3.01	4075.452	−1.403	K, SG	79 355.02	−4.51	LDA	15.18	−4.72	
7.26	4190.724	−0.351	LA	108 820.60	−5.07	LDA	7.52	−4.66	
7.26	4198.133	−0.611	LA	108 778.70	−5.07	LDA	4.99	−4.59	
5	5041.024	+0.174	NIST	81 191.34	−4.70	G74	73.40	−4.65	
5	5055.984	+0.441	NIST	81 251.32	−4.70	G74	90.48	−4.65	
5	5056.317	−0.535	NIST	81 251.32	−4.70	G74	38.52	−4.63	
7.03	5466.432	−0.190	NIST	101 023.05	−3.85	G74	11.11	−4.74	
7.33	5669.563	+0.266	LA	114 529.14	–	–	5.68	−4.75	
7.33	5688.817	+0.106	LA	114 414.58	–	–	3.22	−4.87	
4	5957.559	−0.349	NIST	81 191.34	−4.91	G74	37.52	−4.65	
4	5978.930	−0.061	NIST	81 251.32	−4.91	G74	49.34	−4.65	
7.02	7848.816	+0.335	NIST	101 023.05	−4.25	G74	11.81	−4.81	
7.02	7849.722	+0.492	NIST	101 024.35	−4.25	G74	13.41	−4.89	
			Si III log N(Si III)/$N_{\rm tot}$ = −4.58 ± 0.04						
2	4552.622	+0.292	NIST	153 377.05	–	–	4.01	−4.62	
2	4567.840	+0.069	NIST	153 377.05	–	–	3.15	−4.54	

Owing to the triplet and quintet nature of most of the transitions, the oxygen abundance was estimated both from the profiles and from the equivalent widths. The adopted final value log(N(O)/$N_{\rm tot}$) = −3.18 ± 0.11 is the average abun-

Table A.1. continued.

Mult.	λ(Å)	log gf	Ref.[a]	$\chi_{\rm low}$(cm^1)	$\gamma_{\rm S}$	Ref.[b]	W(mÅ)	log($N_Z/N_{\rm tot}$)	Notes
		P II	log N(P II)/$N_{\rm tot}$ = −6.28 ± 0.08						
7	5296.077	−0.134	K, HI	87 124.60	–	–	2.20	−6.33	
6	5316.055	−0.341	K, HI	86 743.96	−4.09	G74	1.66	−6.28	
6	5344.729	−0.329	K, HI	86 597.55	−4.09	G74	1.88	−6.24	
6	5386.895	−0.305	K, HI	86 743.96	−4.09	G74	1.72	−6.29	
6	5425.880	+0.241	K, HI	87 124.60	−4.09	G74	4.20	−6.39	
5	6024.178	+0.137	K, HI	87 124.60	−4.40	G74	1.37	−6.20	
5	6034.039	−0.209	K, HI	86 597.55	−4.40	G74	2.15	−6.15	
5	6043.084	+0.384	K, HI	87 124.60	−4.40	G74	4.09	−6.41	
5	6034.039	−0.209	K, HI	86 597.55	−4.40	G74	2.15		
		S II	log N(S II)/$N_{\rm tot}$ = −5.12 ± 0.03						
44	4153.068	+0.617	NIST	128 233.20	–	–	8.25	−5.09	
44	4162.665	+0.777	NIST	128 599.16	–	–	9.53	−5.13	
1	5027.203	−0.705	NIST	105 599.06	–	–	3.05	−5.08	
1	5142.322	−0.822	NIST	106 044.24	–	–	1.92	−5.13	
39	5212.620	+0.318	NIST	121 530.02	–	–	3.64	−5.17	
6	5453.855	+0.482	NIST	110 268.60	–	–	11.70	−5.10	
		Ca I	log N(Ca I)/$N_{\rm tot}$ = −5.26						
2	4226.728	+0.244	NIST	0.00	−5.74	G74	2.4	−5.26	
		Ca II	log N(Ca II)/$N_{\rm tot}$ = −5.67 ± 0.25						
4	3158.869	+0.252	K, BWL	25 191.51	−5.07	G74	46.4	−5.90	
4	3179.331	+0.512	K, BWL	25 414.40	−5.07	G74	57.4	−5.76	
4	3181.275	−0.448	K, BWL	25 414.40	−5.07	G74	29.7	−5.83	
3	3706.024	−0.447	K, BWL	25 191.51	−5.09	G74		−5.54	Wings of H_{15}, H_{16}
3	3736.902	−0.147	K, BWL	25 414.40	−5.09	G74		−5.60	Red wing of H_{13}
1	3933.664	+0.134	K, BWL	0.00	−5.52	G74		−5.54	Bump on the red wing
1	3968.469	−0.179	K, BWL	0.00	−5.52	G74		−5.54	Blue wing of H_ϵ, red component
15	5001.479	−0.517	K, BWL	60 533.53	−4.24	G74		−5.64	Blend with Fe II
15	5019.971	−0.257	K, BWL	60 611.28	−4.24	G74		−5.64	Blend with Fe II
15	5021.138	−1.217	K, BWL	60 611.28	−4.24	G74		−5.54:	Weak
14	5285.266	−1.153	K, BWL	60 533.02	−4.30	G74		−5.54:	Weak
14	5307.224	−0.853	K, BWL	60 611.28	−4.30	G74		–	Blend with an unknown component
13	8201.720	+0.315	K, BWL	60 533.02	−4.62	G74		–	Telluric line
13	8248.796	+0.572	NIST	60 611.28	−4.62	G74		−6.40	At the Paschen limit
13	8254.721	−0.388	NIST	60 611.28	−4.62	G74		−5.8??	Weak, at the Paschen limit
2	8498.023	−1.312	K, BWL	13 650.19	−5.55	G74		−5.54	Shifted by +0.2 Å, blue wing of P_{15}
2	8542.091	−0.362	K, BWL	13 710.88	−5.55	G74			No observations
2	8662.141	−0.623	K, BWL	13 650.19	−5.55	G74		−5.20	Shifted by +0.2 Å, blue wing of P_{13}
12	9854.759	−0.228	K, BWL	60 533.02	−4.66	G74		≤−5.54	Bad spectrum, low S/N
12	9931.374	+0.072	K, BWL	60 611.28	−4.66	G74		≤−5.54	Bad spectrum, low S/N

[a] "K" before another log gf source means that the log gf is from Kurucz files available at `http://kurucz.harvard.edu/linelists/gf100` (BBCB) Berry et al. (1971); (BIE) Biémont (1977); (BWL) Black et al. (1972); (CNO) Wiese et al. (1996); (HI) Hibbert (1988); (KP) Kurucz & Peytremann (1975); (LA) Lanz & Artru (1985); (NBS) Wiese et al. (1966); (NIST) `http://physics.nist.gov/cgi-bin/AtData/lines_form`; (SG) Schulz-Gulde (1969).
[b] (BCS1) Barnard et al. (1974); (BCS2) Barnard et al. (1975); (DS90) Dimitrijevic & Sahal-Bréchot (1990); (G74) Griem (1974); (LDA) Lanz et al. (1988); (SM69) Shamey (1969).

dance derived only from the equivalent widths, provided that the lines of multiplets 1, 4 and 8 and all the lines with Stark broadening parameter not available from the literature are excluded from the mean. In fact, lines computed with the approximate Stark profiles of the SYNTHE code are too strong, as are the lines of mult. 14 at 4967–4968 Å. Furthermore, the comparison of the LTE computed spectrum with the observed spectrum has shown the inadequacy of the LTE models for reproducing the infrared strong O I lines, in particular those of mult. 1, 4 and 8 at 7773.4 Å, 8446.5 Å and 9263.9 Å, respectively. Numerous papers deal with the NLTE corrections for these lines in B-type stars. The most recent one is Hempel & Holweger (2003). We point out that the observed profiles of these lines cannot be reproduced in LTE even when

Table A.2. Abundances of the iron group elements.

Mult.	λ(Å)	log gf	Ref.[a]	$\chi_{\rm low}$	W(mÅ)	log(N_Z)/$N_{\rm tot}$)	Notes
			Sc II log N(Sc II)/$N_{\rm tot}$ = −9.08 ± 0.15				
3	3580.925	−0.070	K, MFW	0.00	2.02	−8.89	
2	3613.829	+0.520	K, MFW	177.76	5.81	−8.96	
2	3630.742	+0.340	K, MFW	67.76	4.28	−8.94	
2	3642.784	+0.180	K, MFW	0.00	2.73	−8.99	
7	4246.822	+0.320	K, MFW	2540.95	4.44	−9.37	
15	4314.083	−0.100	K, MFW	4987.79	1.96	−9.17	
14	4374.457	−0.440	K, MFW	4987.79	1.07	−9.10	
31	5526.790	+0.130	K, MFW	14261.32	0.86	−9.19	
			Ti II log N(Ti II)/$N_{\rm tot}$ = −5.67 ± 0.11				
5	3072.107	−0.620	PTP	225.73	61.34	−5.43	
4	3121.598	−2.360	PTP	0.00	16.36	−5.51	
4	3130.798	−1.190	PTP	94.10	44.49	−5.54	
10	3145.396	−2.600	PTP	983.89	7.31	−5.69	
4	3157.393	−2.170	PTP	94.10	18.33	−5.61	
10	3161.201	−0.690	PTP	908.02	54.92	−5.57	
10	3161.769	−0.550	PTP	983.89	59.71	−5.52	
10	3162.566	−0.380	PTP	1087.32	60.63	−5.65	
10	3168.518	−0.200	PTP	1215.84	66.26	−5.61	
3	3214.767	−1.400	PTP	393.44	38.79	−5.53	
2	3222.841	−0.420	PTP	94.10	63.99	−5.55	
3	3226.769	−1.840	PTP	225.73	26.00	−5.61	
2	3234.514	+0.430	PTP	393.44	86.84	−5.67	
23	3236.119	−0.430	PTP	8710.44	48.44	−5.53	
2	3236.572	+0.240	PTP	225.73	79.21	−5.70	
2	3239.036	+0.070	PTP	94.10	76.96	−5.60	
23	3239.661	−0.200	PTP	8744.25	76.96	−5.53	
2	3241.983	−0.030	PTP	0.00	76.81	−5.51	
23	3249.366	−1.360	PTP	8710.44	24.74	−5.57	
2	3251.908	−0.590	PTP	94.10	59.53	−5.55	
2	3254.245	−0.560	PTP	393.44	58.86	−5.58	
7	3308.803	−1.140	PTP	1087.32	41.01	−5.64	
7	3318.023	−1.040	PTP	983.89	46.15	−5.55	
7	3343.761	−1.150	PTP	1215.84	40.92	−5.63	
7	3346.741	−1.060	PTP	1087.42	45.59	−5.54	
1	3361.212	+0.430	PTP	225.73	84.33	−5.69	
1	3372.793	+0.280	PTP	94.10	79.51	−5.69	
1	3380.279	−0.570	K, MFW	393.44	61.97	−5.44	
1	3383.759	+0.160	PTP	0.00	87.01	−5.36	
6	3477.180	−0.960	PTP	983.89	46.13	−5.61	
6	3489.736	−1.980	PTP	1087.32	17.60	−5.71	
6	3500.330	−2.100	PTP	983.89	18.55	−5.56	
15	3561.575	−1.940	PTP	4268.58	11.65	−5.81	
15	3573.731	−1.490	PTP	4628.58	24.62	−5.66	
15	3587.131	−1.590	PTP	4897.65	22.00	−5.65	
15	3596.047	−1.030	PTP	4897.65	37.79	−5.58	
34	3900.539	−0.200	PTP	9118.26	76.60	−5.96	
34	3913.461	−0.420	PTP	8997.71	77.23	−5.73	
11	4012.383	−1.840	PTP	4628.58	41.10	−5.67	
87	4053.821	−1.130	PTP	15265.62	40.03	−5.76	
21	4161.529	−2.360	K, MFW	8744.25	17.44	−5.55	
105	4163.644	−0.130	PTP	20891.66	62.40	−5.77	
20	4287.873	−1.790	PTP	8710.44	27.82	−5.82	
41	4290.215	−0.850	PTP	9395.71	65.27	−5.71	
20	4294.094	−0.930	PTP	8744.25	63.27	−5.72	
41	4300.042	−0.440	PTP	9518.06	78.06	−5.74	
41	4301.922	−1.150	PTP	9363.62	54.33	−5.73	
41	4312.860	−1.100	PTP	9518.05	57.56	−5.68	
41	4314.971	−1.100	PTP	9363.62	55.37	−5.75	
41	4320.950	−1.800	PTP	9395.71	24.78	−5.85	

Table A.2. continued.

Mult.	λ(Å)	log gf	Ref.[a]	$\chi_{\rm low}$	W(mÅ)	log(N_Z)/$N_{\rm tot}$)	Notes
			Ti II cont.				
104	4367.652	−0.860	PTP	20 891.66	35.88	−5.80	
93	4374.816	−1.610	PTP	16 625.11	21.38	−5.70	
104	4386.847	−0.960	PTP	20 951.62	31.82	−5.80	
51	4394.059	−1.780	PTP	9850.90	30.58	−5.69	
19	4395.031	−0.540	PTP	8744.25	79.02	−5.64	
51	4399.765	−1.190	PTP	9975.92	54.35	−5.66	
115	4411.072	−0.670	PTP	24 961.03	31.84	−5.84	
40	4417.714	−1.190	PTP	9395.71	55.39	−5.66	
51	4418.331	−1.970	PTP	9395.71	19.61	−5.80	
40	4441.729	−2.330	PTP	9518.06	11.70	−5.76	
19	4443.801	−0.720	PTP	8710.44	72.95	−5.65	
19	4450.482	−1.520	PTP	8744.25	42.66	−5.72	
40	4464.448	−1.810	PTP	9363.62	28.90	−5.74	
31	4468.492	−0.600	K, MFW	9118.26	75.93	−5.65	
115	4488.325	−0.510	PTP	25 192.79	37.27	−5.84	
31	4501.270	−0.770	PTP	8997.71	71.44	−5.63	
50	4533.960	−0.530	PTP	9975.92	77.23	−5.64	
60	4544.016	−2.580	PTP	10 024.73	6.49	−5.77	
50	4563.757	−0.690	PTP	9850.90	68.15	−5.76	
82	4571.971	−0.320	PTP	12 676.97	81.77	−5.56	
59	4657.206	−2.240	PTP	10 024.73	12.39	−5.79	
49	4708.662	−2.340	PTP	9975.92	10.08	−5.80	
92	4779.985	−1.370	K, MFW	16 515.86	32.07	−5.65	
17	4798.532	−2.680	PTP	8710.44	7.48	−5.69	
92	4805.085	−1.100	K, MFW	16 625.11	45.57	−5.57	
114	4911.195	−0.610	PTP	25 192.79	36.40	−5.76	
113	5069.092	−1.820	PTP	25 192.79	5.75	−5.66	
113	5072.287	−1.060	PTP	25 192.79	20.15	−5.75	
–	5154.070	−1.750	PTP	12 628.73	22.57	−5.77	
86	5185.902	−1.490	PTP	15 265.62	32.05	−5.61	
–	5188.687	−1.050	PTP	12 758.11	50.88	−5.72	
–	5226.538	−1.260	PTP	12 628.73	44.34	−5.69	
103	5268.615	−1.620	K, MFW	20 951.62	11.80	−5.76	
–	5336.786	−1.590	PTP	12 758.11	29.32	−5.73	
–	5381.021	−1.920	PTP	12 628.73	16.59	−5.78	
			Cr I log N(Cr I)/$N_{\rm tot}$ = −5.22 ± 0.09				
4	3578.686	+0.409	K, MFW	0.00	6.26	−5.17	
4	3593.485	+0.307	K, MFW	0.00	4.52	−5.24	
4	3605.329	+0.197	K, MFW	0.00	4.41	−5.14	
1	4254.336	−0.114	K, MFW	0.00	6.40	−5.27	
1	4274.797	−0.231	K, MFW	0.00	4.23	−5.35	
1	4289.717	−0.361	K, MFW	0.00	3.28	−5.34	
7	5204.511	−0.208	K, MFW	7593.15	2.54	−5.16	
7	5206.037	+0.019	K, MFW	7593.15	4.93	−5.08	
7	5208.425	+0.158	K, MFW	7593.15	4.62	−5.25	
			Cr II log N(Cr II)/$N_{\rm tot}$ = −5.41 ± 0.07				
5	3118.646	−0.000	K, MFW	19 528.25	74.61	−5.38	
5	3120.359	+0.120	K, MFW	19 631.17	78.48	−5.38	
54	3122.596	−0.110	K, MFW	33 694.15	49.42	−5.25	
39	4539.595	−2.280	SL	32 603.40	13.96	−5.42	
44	4558.650	−0.410	SL	32 854.31	79.21	−5.34	
39	4565.770	−1.860	SL	32 603.40	27.00	−5.43	
–	4587.264	−1.648	K, MFW	52 321.01	3.77	−5.53	
44	4588.199	−0.643	K, MFW	32 836.68	71.39	−5.35	
44	4592.049	−1.217	K, MFW	32 854.95	44.53	−5.58	
44	4616.629	−1.291	K, MFW	32 844.76	44.28	−5.51	
44	4618.803	−0.860	SL	32 854.95	64.13	−5.35	
44	4634.070	−0.990	SL	32 844.76	57.91	−5.41	

Table A.2. continued.

Mult.	λ(Å)	log gf	Ref.[a]	$\chi_{\rm low}$	W(mÅ)	log(N_Z)/$N_{\rm tot}$)	Notes
			Cr II cont.				
–	4697.598	−1.882	K, MFW	45 730.58	6.36	−5.44	
30	4812.337	−1.995	K, K88	31 168.58	24.44	−5.44	
30	4824.127	−0.970	SL	31 219.35	65.81	−5.28	
30	4836.229	−2.000	SL	31 117.39	25.57	−5.38	
43	5237.329	−1.160	K, MFW	32 854.31	53.12	−5.38	
23	5246.768	−2.450	K, MFW	29 951.88	14.55	−5.39	
43	5279.880	−2.100	K, MFW	32 854.31	21.07	−5.33	
24	5305.860	−2.080	K, MFW	30 864.76	24.27	−5.38	
43	5308.440	−1.810	K, MFW	32 836.68	24.04	−5.53	
43	5310.700	−2.280	K, MFW	32 844.76	14.54	−5.38	
43	5313.590	−1.650	K, MFW	32 854.95	34.42	−5.40	
23	5420.922	−2.360	K, MFW	30 307.44	13.80	−5.48	
50	5502.067	−1.990	K, MFW	33 618.94	20.73	−5.40	
50	5508.606	−2.110	K, MFW	33 521.11	16.35	−5.43	
105	6053.466	−2.160	K, MFW	38 269.59	8.21	−5.44	
			Mn I log N(Mn I)/$N_{\rm tot}$ = −4.20 ± 0.08				
8	3577.868	+0.160	K, MFW	17 052.29	6.54	−4.29	
8	3595.107	−0.860	K, MFW	17 451.52	0.75	−4.27	
8	3607.526	−0.440	K, MFW	17 282.00	2.21	−4.21	
8	3608.481	−0.370	K, MFW	17 451.52	3.18	−4.09	
5	4018.100	−0.309	K, MFW	17 052.29	12.27	−4.18	
2	4030.753	−0.470	K, MFW	0.00	40.68	−4.18	(W, log($N/N_{\rm tot}$)$_{\rm JDA}$) = (41.0,−4.35)[b]
2	4034.483	−0.811	K, MFW	0.00	23.85	−4.32	(W, log($N/N_{\rm tot}$)$_{\rm JDA}$) = (23.0,−4.50)[b]
5	4041.355	+0.258	K, MFW	17 052.29	36.24	−4.02	
5	4055.544	−0.070	K, MFW	17 282.00	17.59	−4.20	
5	4070.278	−0.950	K, MFW	17 637.15	2.81	−4.22	
5	4082.939	−0.354	K, MFW	17 568.48	10.33	−4.20	
22	4453.012	−0.490	K, MFW	23 719.52	3.39	−4.24	
28	4457.044	−0.555	K, MFW	24 788.05	1.66	−4.43	
28	4458.254	+0.042	K, MFW	24 788.05	7.42	−4.33	
28	4461.079	−0.380	K, MFW	24 802.25	4.22	−4.18	
28	4462.031	+0.320	K, MFW	24 802.25	14.74	−4.25	
22	4464.682	−0.104	K, MFW	23 549.20	6.79	−4.31	
–	4479.393	+0.010	K, MFW	41 230.30	1.74	−3.99	
22	4490.080	−0.522	K, MFW	23 818.87	3.30	−4.21	
22	4502.213	−0.345	K, MFW	23 549.20	4.60	−4.26	
–	4626.530	+0.210	K, MFW	38 008.70	4.76	−3.92	
21	4727.461	−0.470	K, MFW	23 549.20	3.96	−4.20	
21	4739.110	−0.490	K, MFW	23 719.52	3.46	−4.23	
21	4762.367	+0.425	K, MFW	23 296.67	20.45	−4.24	
21	4765.846	−0.080	K, MFW	23 719.52	9.77	−4.14	
21	4766.418	+0.100	K, MFW	23 549.20	13.73	−4.14	
16	4783.427	+0.042	K, MFW	18 531.64	21.56	−4.12	
16	4823.524	+0.144	K, MFW	18 705.37	23.71	−4.14	
27	6013.480	−0.251	K, MFW	25 779.32	5.92	−4.13	
27	6021.790	+0.034	K, MFW	24 802.25	9.24	−4.19	
			Mn II log N(Mn II)/$N_{\rm tot}$ = −4.25 ± 0.04				
3	3441.988	−0.272	K, MFW	14 325.86	176.9	−4.27	
3	3460.316	−0.542	K, MFW	14 593.82	140.3	−4.25	
3	3482.905	−0.740	K, MFW	14 781.19	117.2	−4.28	
3	3488.677	−0.864	K, MFW	14 910.18	108.8	−4.26	
3	3495.833	−1.218	K, MFW	14 959.84	92.87	−4.15	
3	3496.809	−1.687	K, MFW	14 781.19	69.99	−4.27	
3	3497.526	−1.330	K, MFW	14 901.18	82.89	−4.26	
			The Mn II lines used by Jomaron et al. (1999) (JDA)				
–	3917.318	−1.147	K, K88	55 759.27	39.59	−4.55	(W, log($N/N_{\rm tot}$)$_{\rm JDA}$) = (43.5,−4.52)[b]
–	4363.258	−1.909	K, K88	44 899.82	39.35	−4.43	(W, log($N/N_{\rm tot}$)$_{\rm JDA}$) = (37.5,−4.54)[b]
–	4365.219	−1.350	K, K88	53 017.16	40.60	−4.46	(W, log($N/N_{\rm tot}$)$_{\rm JDA}$) = (40.5,−4.59)[b]
–	4478.635	−0.950	K, K88	53 597.13	54.37	−4.39	(W, log($N/N_{\rm tot}$)$_{\rm JDA}$) = (55.0,−4.66)[b]

Table A.2. continued.

Mult.	λ(Å)	log gf	Ref.[a]	χ_{low}	W(mÅ)	log(N_Z)/N_{tot})	Notes
			Fe I log N(Fe I)/N_{tot} = −4.78 ± 0.08				
23	3581.193	+0.406	K, FMW	6928.27	6.90	−4.84	
23	3618.768	+0.000	K, FMW	7985.78	2.06	−4.97	
43	4005.242	−0.610	K, FMW	12 560.93	1.96	−4.75	
43	4045.812	+0.280	K, FMW	11 976.24	12.67	−4.78	
43	4071.738	−0.022	K, FMW	12 698.55	6.26	−4.78	
42	4202.029	−0.708	K, FMW	11 976.24	1.94	−4.70	
419	4219.360	+0.120	K, FMW	28 819.95	1.02	−4.81	
152	4235.936	−0.341	K, FMW	19 562.44	1.12	−4.86	
42	4271.760	−0.164	K, FMW	11 976.24	6.74	−4.67	
41	4383.545	+0.200	K, FMW	11 976.24	12.06	−4.74	
41	4404.750	−0.142	K, FMW	12 560.93	6.09	−4.71	
41	4415.122	−0.615	K, FMW	12 968.55	2.00	−4.72	
			Fe II log N(Fe II)/N_{tot} = −4.84 ± 0.13				
173	3906.035	−1.830	K, FMW	44 929.55	15.01	−4.80	
3	3914.503	−4.050	K, FMW	13 473.41	4.38	−5.04	
173	3935.962	−1.860	K, FMW	44 915.05	16.00	−4.73	
3	3938.290	−3.890	K, FMW	13 471.41	8.55	−4.88	
3	3945.210	−4.250	K, FMW	13 673.18	3.84	−4.89	
28	4122.668	−3.380	K, FMW	20 830.58	10.98	−4.83	
27	4128.748	−3.770	K, FMW	20 830.58	6.90	−4.67	
28	4178.862	−2.480	K, FMW	20 830.58	34.36	−4.96	
28	4258.154	−3.400	K, FMW	21 812.05	7.57	−4.94	
27	4273.326	−3.258	K, FMW	21 812.05	10.74	−4.90	
28	4296.572	−3.010	K, FMW	21 812.05	19.75	−4.80	
27	4303.176	−2.490	K, FMW	21 812.05	34.78	−4.88	
28	4369.411	−3.670	K, FMW	22 409.85	5.04	−4.83	
27	4385.387	−2.570	K, FMW	22 409.85	24.50	−5.06	
32	4413.601	−3.870	K, FMW	21 581.64	2.06	−5.09	
27	4416.830	−2.600	K, FMW	22 409.85	30.13	−4.86	
37	4491.405	−2.700	K, FMW	23 031.30	24.60	−4.88	
38	4508.288	−2.210	K, FMW	23 031.30	37.25	−5.01	
37	4515.339	−2.480	K, FMW	23 939.36	31.54	−4.85	
37	4520.224	−2.600	K, FMW	22 637.21	29.09	−4.88	
38	4522.634	−2.030	K, FMW	22 939.36	44.78	−4.98	
38	4541.524	−3.050	K, FMW	23 031.30	17.41	−4.76	
186	4549.192	−1.870	K, FMW	47 674.72	15.09	−4.57	
38	4549.474	−1.750	K, FMW	22 810.36	53.65	−5.01	
37	4555.893	−2.290	K, FMW	22 810.36	34.65	−5.02	
38	4576.340	−3.040	K, FMW	22 939.36	18.15	−4.75	
37	4582.835	−3.100	K, FMW	22 939.36	12.89	−4.89	
38	4583.837	−2.020	K, FMW	22 637.21	55.43	−4.69	
38	4620.521	−3.280	K, FMW	22 810.36	10.08	−4.85	
186	4635.316	−1.650	K, FMW	47 674.72	18.70	−4.65	
43	4656.981	−3.630	K, FMW	23 317.63	5.90	−4.74	
37	4666.758	−3.330	K, FMW	22 810.36	9.50	−4.83	
25	4670.182	−4.100	K, FMW	20 830.58	2.12	−4.89	
43	4731.453	−3.360	K, FMW	23 317.63	13.19	−4.59	
42	4923.927	−1.320	K, FMW	23 317.63	75.84	−4.73	
36	4993.358	−3.650	K, FMW	22 637.20	4.71	−4.86	
42	5018.440	−1.220	K, FMW	23 317.63	83.50	−4.64	
35	5132.669	−4.180	K, FMW	22 637.20	2.35	−4.65	
42	5169.033	−0.870	K, FMW	23 317.63	88.23	−4.86	
49	5197.577	−2.100	K, FMW	26 055.42	36.50	−4.93	
49	5234.625	−2.050	K, FMW	25 981.63	37.62	−4.95	
–	5247.952	+0.630	K, FMW	84 938.18	11.82	−5.02	

Table A.2. continued.

Mult.	λ(Å)	log gf	Ref.[a]	$\chi_{\rm low}$	W(mÅ)	log(N_Z)/$N_{\rm tot}$)	Notes
			Fe II cont.				
185	5272.397	−2.030	K, FMW	48 039.09	9.61	−4.60	
49	5276.002	−1.940	K, FMW	25 805.33	39.99	−5.00	
41	5284.109	−3.190	K, FMW	23 317.63	13.28	−4.74	
49	5316.615	−1.850	K, FMW	25 428.78	47.28	−4.90	
49	5425.257	−3.360	K, FMW	25 805.33	3.74	−5.05	
–	5506.195	+0.950	K, FMW	84 863.35	21.48	−4.90	
55	5534.847	−2.930	K, FMW	26 170.18	16.85	−4.68	
–	5961.705	+0.699	K, FMW	86 124.30	13.10	−4.88	
46	6084.110	−3.980	K, FMW	25 805.33	1.95	−4.70	
74	6149.258	−2.724	K, K88	31 368.45	10.38	−4.81	
–	6383.722	−2.271	K, FMW	44 784.76	3.01	−5.05	
74	6416.919	−2.850	K, FMW	31 387.95	8.55	−4.78	
74	6456.383	−2.300	K, FMW	31 483.176	25.58	−4.64	
			Ni II log N(Ni II)/$N_{\rm tot}$ = −6.09 ± 0.16				
1	3274.916	−2.805	K03	23 108.28	2.20	−6.03	
5	3290.534	−2.755	K03	25 036.38	1.67	−6.08	
1	3290.683	−3.016	K03	23 796.18	2.28	−5.76	
1	3350.419	−2.355	K03	23 796.18	5.77	−5.94	
1	3373.969	−2.006	K03	23 108.28	10.27	−5.99	
4	3401.766	−2.682	K03	24 788.20	1.58	−6.17	
4	3407.300	−1.855	K03	24 835.93	9.51	−6.07	
1	3454.164	−2.146	K03	23 796.18	6.73	−6.04	
4	3471.386	−1.902	K03	24 835.93	8.71	−6.06	
1	3513.987	−1.507	K03	23 108.28	19.35	−5.97	
4	3576.764	−1.676	K03	24 788.20	11.65	−6.08	
12	4015.474	−2.410	K03	32 523.54	3.79	−6.35	
11	4067.031	−1.834	K03	32 499.53	10.74	−6.41	
10	4192.065	−3.270	K03	32 523.54	1.12	−6.04	
9	4244.779	−3.095	K03	32 523.54	0.89	−6.31	

[a] "K" before another log gf source means that the log gf is from Kurucz files available at `http://kurucz.harvard.edu/linelists/gf100` (FMW) Fuhr et al. (1988); (K88) Kurucz (1988); (K03) Kurucz (2003); (MFW) Martin et al. (1988); (PTP) Pickering et al. (2002); (SL) Sigut & Landstreet (1990).
[b] Equivalent widths W and abundances from Jomaron et al. (1999) (JDA).

the LTE overabundance derived from the measured equivalent widths is adopted. Figure A.3 compares the observed profiles of the O I triplet at 7773.4 Å with profiles computed with two different abundances, −3.18 dex and −2.10 dex. The first abundance is the one we adopted for oxygen in HD 175640 while the second abundance is the one we derived from the equivalent widths of the lines of O I triplet mult. 1. In the first case the computed cores are much weaker than the observed ones, in the second case the increased abundance increases not only the cores but also the wings, so that the profiles become broader and broader and will never agree with the observed ones.

The −3.18 dex oxygen abundance is only +0.3 dex larger than the solar one (Grevesse & Sauval 1998). However, a detailed NLTE analysis of O I lines is required before drawing any conclusion on the oxygen abundance in HD 175640.

Neon (10)-Ne I: Only very weak lines of Ne I were identified. The equivalent width of Ne I at 7032.4131 Å, mult. 1 gives log(N(Ne)/$N_{\rm tot}$) = −4.35. All the weak observed lines agree with the lines predicted by this abundance. An example is Ne I at 6506.528 Å. Neon is therefore underabundant by about 0.4 dex with respect to the solar abundance. Dworetsky & Buday (2000) assign an upper limit log(N(Ne)/N(H)) ≤ −4.9 to the neon abundance obtained from an NLTE analysis.

Sodium (11)-Na I: All the Na I lines observed in the spectrum (Table A.1) are either blended with telluric lines or are affected by a red component of interstellar or circumstellar origin, as are the lines of mult. 1 at 5889.95 Å and 5895.92 Å. For this reason, the abundance log(N(Na)/$N_{\rm tot}$) = −5.47, corresponding to an overabundance of +0.2 dex, is only a rough estimate.

Magnesium (12)-Mg I,Mg II: Several Mg I and Mg II lines can be observed in the spectrum, but only a few of them are unblended. Almost all the lines in the red part of the spectrum are affected by telluric absorptions, as for instance the two strong lines of Mg II mult. 1 at 9218.25 Å and 9244.26 Å, so that they

Table A.3. Abundances of elements with $Z \geq 31$.

Mult	λ(Å)	log gf	Ref.[a]	χ_{low}(cm^{-1})	χ_{up}(cm^{-1})	W(mÅ)	log N/N_{tot}	Notes
		Ga II	log N(Ga II)/N_{tot} = −5.43 ± 0.04					
–	4251.149	+0.35	RS94	113 815.92	137 332.35		−5.20	
–	4254.075	−0.23	RS94	113 842.19	137 342.44		−5.20	
–	4255.722	+0.634	NKW, RS94	113 842.19	137 333.33		−5.45	Bad fit, missing components
–	4255.937	−0.32	NKW, RS94	113 842.19	137 332.35		−5.45:	Blend with (wrong?) Mn II
–	4262.014	+0.98	RS94	113 883.19	137 339.64		−5.45	Blend with Cr II+Cr II
–	5338.240	+0.43	RS94	118 430.20	137 157.48		−5.65:	Bad fit
–	5360.402	+0.42	RS94	118 518.47	137 168.47		−5.45	
–	5363.585	+0.06	NKW	118 518.47	137 157.48		−5.45	Blend with (wrong?) Cr II
–	5416.318	+0.64	RS94	118 727.89	137 185.30		−5.25	
–	5421.275	−0.05	NKW	118 727.89	137 168.47		−5.45	
–	6334.069	+1.00	RS94	102 944.55	118 727.89		−5.65	
–	6419.239	+0.57	RS94	102 944.55	118 518.47		−5.55	Blend with (wrong?) Cr II
–	6455.923	−0.08	RS94	102 944.55	118 430.02		−5.45	Blend with O I
			guessed log gfs for Ga II					
–	4261.478	−1.10	GUESS	113 883.19	137 342.44			
–	4263.136	−0.50	GUESS	113 883.19	137 333.33			
–	5219.658	+0.35	GUESS	120 550.27	139 703.28			
–	7198.450	+0.25	GUESS	106 662.21	120 550.27			
–	7792.260	+0.00	GUESS	107 720.56	120 550.27			
		Br II	log N(Br II)/N_{tot} = −7.12 ± 0.04					
–	4704.850	+0.408	NIST	93 921.34	115 176.00	1.09	−7.16	
–	4785.500	+0.208	NIST	93 921.54	114 818.00	0.85	−7.07	
		Sr II	log N(Sr II)/N_{tot} = −8.41					
1	4077.709	+0.151	NIST	0.00	24 516.65	26.66	−8.41	
		Y II	log N(Y II)/N_{tot} = −6.66 ± 0.20					
10	3195.616	−0.420	K, HL	840.21	32 124.04	28.64	−6.35	
10	3200.272	−0.430	K, HL	1045.08	32 283.40	26.37	−6.45	
10	3203.322	−0.370	K, HL	840.21	32 048.78	27.86	−6.44	
10	3216.682	−0.020	K, HL	1045.08	32 124.04	35.67	−6.35	
10	3242.280	+0.210	K, HL	1449.81	32 283.40	40.16	−6.32	
18	3327.878	+0.130	K, CC	3296.18	33 336.72	32.32	−6.51	
3	3496.081	−0.720	K, HL	0.00	28 595.27	20.64	−6.48	
9	3549.005	−0.280	K, HL	1045.08	29 213.95	27.34	−6.48	
9	3584.514	−0.410	K, HL	840.21	28 730.01	24.78	−6.49	
9	3600.741	+0.280	K, HL	1044.81	29 213.95	42.41	−6.24	
9	3601.919	−0.180	K, HL	840.21	28 595.27	32.75	−6.30	
9	3611.044	+0.110	K, HL	1045.08	28 730.07	33.79	−6.52	
2	3633.122	−0.100	K, HL	1045.08	27 516.69	30.44	−6.54	
7	3818.341	−0.980	K, HL	1045.08	27 227.04	23.35	−6.90	
16	3930.660	−1.610	K, HL	3296.18	28 730.01	8.63	−6.76	
6	3950.352	−0.490	K, HL	840.21	26 147.25	39.01	−6.84	
16	3951.593	−1.980	K, HL	3296.18	28 595.27	3.22	−6.88	
6	3982.594	−0.490	K, HL	1045.08	26 147.25	36.23	−6.94	
5	4199.277	−2.150	K, HL	840.21	24 647.13	3.55	−6.82	
1	4204.695	−1.760	K, HL	0.00	23 776.24	7.89	−6.87	
5	4235.729	−1.500	K, HL	1045.08	24 647.13	10.66	−6.91	
5	4309.631	−0.750	K, HL	1449.81	24 647.13	30.09	−6.89	
5	4358.728	−1.329	K, HL	840.21	23 776.24	14.58	−6.91	
22	4883.684	+0.070	K, HL	8743.32	29 213.94	46.51	−6.64	
22	4900.120	−0.090	K, HL	8328.04	28 730.01	42.70	−6.66	
20	4982.129	−1.290	K, HL	8328.04	28 394.18	7.22	−6.88	
20	5087.416	−0.170	K, HL	8743.32	28 394.18	38.33	−6.72	
20	5119.112	−1.360	K, HL	8003.12	27 532.32	7.41	−6.82	

Table A.3. continued.

Mult.	λ(Å)	log gf	Ref.[a]	$\chi_{\rm low}$(cm^{-1})	$\chi_{\rm up}$(cm^{-1})	W(mÅ)	log(N_Z)/$N_{\rm tot}$)	Notes
			Y II cont.					
20	5200.406	−0.570	K, HL	8003.12	27 227.04	25.20	−6.83	
20	5205.724	−0.342	K, HL	8328.04	27 532.32	35.39	−6.68	
27	5473.388	−1.020	K, HL	14 081.26	32 283.40	7.68	−6.76	
27	5480.732	−0.990	K, HL	13 833.38	32 124.04	7.38	−6.82	
27	5497.408	−0.580	K, HL	14 098.07	32 283.40	18.31	−6.68	
27	5546.009	−1.100	K, HL	14 098.07	32 124.04	7.44	−6.69	
38	5662.925	+0.160	K, CC	15 682.90	33 336.72	40.07	−6.51	
34	5728.890	−1.120	K, HL	14 832.85	32 283.40	5.61	−6.76	
32	7881.881	−0.572	K, HL	14 832.85	27 516.69	11.95	−6.82	
			Zr II log N(Zr II)/$N_{\rm tot}$ = −8.67 ± 0.17					
3	3279.266	−0.230	K, CC'	736.44	31 249.28	2.47	−8.35	
1	3391.982	+0.463	K, CC'	1322.91	30 795.74	5.15	−8.63	
46	3479.383	+0.170	K, BG	5752.92	34 485.42	1.00	−8.83	
10	3496.192	+0.189	K, CC	314.67	28 909.04	2.60	−8.78	
41	4149.217	−0.030	K, CC	6467.61	30 561.75	2.34	−8.78	
			Rh II log N(Rh II)/$N_{\rm tot}$ = −8.50:					
1	3162.284	+0.000	K, GUESS	28 834.60	60 448.40			
5	3187.875	+0.000	K, GUESS	27 801.40	59 161.50			
1	3207.285	+0.000	K, GUESS	25 376.90	56 547.30			
2	3233.314	+0.000	K, GUESS	27 439.40	58 358.50			
6	3267.480	+0.000	K, GUESS	31 730.50	62 326.10			
5	3307.348	+0.000	K, GUESS	28 131.40	58 358.50			
4	3477.823?	+0.000	K, GUESS	27 801.40	56 547.30			
			Pd I log N(Pd I)/$N_{\rm tot}$ = −6.41 ± 0.30					
3	3242.700	−0.070	K, BG	6564.11	37 393.71	3.63	−5.96	
2	3404.579	+0.320	K, BG	6564.11	35 927.89	2.67	−6.47	
9	3553.080	+0.540	K, CB	11 721.77	39 858.33	0.82	−6.89	
2	3609.547	+0.050	K, BG	7754.40	35 451.40	1.39	−6.40	
1	3634.690	+0.090	K, CB	6564.11	34 068.93	2.02	−6.33	
			Xe II log N(Xe II)/$N_{\rm tot}$ = −5.96 ± 0.20					
–	4603.01	0.018	WM80	95 064.00	116 783.00	3.62	−6.32	
–	4844.33	0.491	WM80	93 068.00	113 705.00	11.33	−6.04	
–	5292.22	0.351	WM80	93 068.00	111 959.00	10.80	−5.81	
–	5372.39	−0.211	WM80	95 064.00	113 673.00	3.12	−5.96	
–	5419.15	0.215	WM80	95 064.00	113 512.00	7.75	−5.80	
–	5719.60	−0.746	WM80	96 033.00	113 512.00	1.79	−5.58	
–	5976.46	−0.222	WM80	95 054.00	111 782.00	1.60	−6.12	
–	6051.15	−0.252	WM80	95 438.00	111 959.00	1.46	−6.12	
–	6097.59	−0.237	WM80	95 397.00	111 792.00	1.94	−5.99	
–	6990.88	+0.200	WM80	99 405.00	113 705.00	2.52	−5.86	$\lambda_{\rm obs}$ = 6990.82 Å
			Other identified weak Xe II lines					
–	5260.44	−0.437	WM80	104 250.00	123 255.00			
–	5261.95	+0.150	WM80	112 925.00	131 924.00			
–	5438.96	−0.183	WM80	102 799.00	121 180.00			
–	5472.61	−0.449	WM80	95 437.00	113 705.00			Blend Cr II
–	5531.07	−0.616	WM80	95 437.00	113 512.00			
–	6036.20	−0.609	WM80	95 397.00	111 959.00			

can not be used for any abundance determination. Furthermore, there are some lines for which the Stark broadening parameters are lacking, like Mg II at 5401.52 Å and at 5401.56 Å, so that their computed profiles are very different from the observed ones.

The average abundance from Mg I lines with measurable equivalent widths is −4.64 ± 0.06 dex, that from Mg II is −4.71 ± 0.07 dex, while the average abundance from all the Mg I and Mg II lines is log(N(Mg)/$N_{\rm tot}$) = −4.69 ± 0.07, corresponding to an underabundance of [−0.23]. The average

Table A.3. continued.

Mult.	λ(Å)	log gf	Ref.[a]	$\chi_{\rm low}$(cm^{-1})	$\chi_{\rm up}$(cm^{-1})	W(mÅ)	log(N_Z)/$N_{\rm tot}$)	Notes
identified Xe II lines with no available log gf								
–	4448.13	0.00	GUESS	123 112.54	145 587.61			
–	4921.48	0.00	GUESS	102 799.07	123 112.54			
–	5339.33	0.00	GUESS	93 068.44	111 792.17			
–	5368.07	0.00	GUESS	105 947.55	124 571.09			
–	5525.53	0.00	GUESS	124 289.45	142 382.13			
–	5667.56	0.00	GUESS	96 033.48	113 679.89			
Ba II log N(Ba II)/$N_{\rm tot}$ = −9.27								
–	4554.029	+0.163	K, NBS	0.00	21 952.42		−9.27	
–	4934.076	−0.150	K, NBS	0.00	20 261.56	1.041	−9.35	
Pr III log N(Pr III)/$N_{\rm tot}$ = −9.62								
–	5299.969	−0.530	DREAM	2893.14	21 755.84		−9.62	
Nd III log N(Nd III)/$N_{\rm tot}$ = −9.57 ± 0.08								
–	5127.044	−1.080	DREAM	2388.00	21 887.00	1.08	−9.50	
–	5203.924	−1.190	DREAM	0.00	19 211.00	0.82	−9.65	
Yb II log N(Yb II)/$N_{\rm tot}$ = −8.10 ± 0.19								
–	3478.834	+0.460	DREAM	30 224.33	58 961.37	3.457	−7.82	
–	4180.810	−0.290	DREAM	30 392.23	54 304.30	1.064	−8.33	
–	5335.159	−0.260	DREAM	30 562.79	49 301.16	1.865	−8.08	
–	5352.954	−0.340	DREAM	30 224.33	48 900.41	1.280	−8.19	
Yb III log N(Yb III)/$N_{\rm tot}$ = −7.31 ± 0.01								
–	3325.514	−1.35	DREAM	42 425.00	72 487.00	3.24	−7.31	
–	3384.013	−0.58	DREAM	53 365.00	82 907.00	3.63	−7.32	
Pt II log N(Pt II)/$N_{\rm tot}$ = −7.63								
–	4514.124	−1.48	DSJ	29 261.97	51 408.37		−7.63	
Au II log N(Au II)/$N_{\rm tot}$ = −7.51 ± 0.06								
–	4016.672	−1.88	RW	48 510.89	73 403.84	1.06	−7.58	
–	4052.790	−1.69	RW	48 510.89	73 178.29	2.09	−7.45	
Hg I log N(Hg I)/$N_{\rm tot}$ = −6.19 ± 0.18								
–	4046.599	−0.818	BLD	37 645.08	62 350.46	0.89	−6.37	
–	5460.731	−0.185	BLD	44 042.98	62 350.46	3.05	−6.01	
Hg II log N(Hg II)/$N_{\rm tot}$ = −6.53 ± 0.23								
–	3983.890	−1.520	PS,SR	35 514.00	60 608.00		−6.30	
–	6149.470	+0.150	SR	95 714.41	111 971.46	1.95	−6.58	

[a] "K" before another log gf source means that the log gf is from Kurucz files available at `http://kurucz.harvard.edu/linelists/gf100` (BLD) Benck et al. (1989); (BG) Biémont et al. (1981); (CB) Corliss & Bozman (1962); (CC) Cowley & Corliss (1983); (CC') Cowley & Corliss (1983), out the fitting range; (DJS) Dworetsky et al. (1984); (DREAM) Biémont et al. (1999), `http://www.umh.ac.be/ astro/dream.shtml`; (GUESS) guessed values; (HL) Hannaford et al. (1982); (NBS) Miles & Wiese (1969); (NIST) `http://physics.nist.gov/cgi-bin/AtData/lines_form`; (NKW) Nielsen et al. (2000); (PS) Proffitt et al. (1999); (SR) Sansonetti & Reader (2001); (RS94) Ryabchikova & Smirnov (1994); (RW) Rosberg & Wyart (1997); (WM80) Wiese & Martin (1980).

Mg abundance gives an excellent agreement between the observed and computed wings of the Mg II lines at 4481 Å, but the computed cores are less deep than the observed ones.

Smith (1993) derived log(N(Mg)/N(H)) = −5.00 ± 0.18 from IUE spectra.

Aluminium (13)-Not observed: There are no aluminium lines observed in the spectrum, except for a feature at 4663.05 Å, which could be identified as Al II mult. 2 at 4663.046 Å. However, the abundance log(N(Al)/$N_{\rm tot}$) = −6.75 from the measured equivalent width 4.51 mA is too high when used to predict all the other unobserved Al I and Al II lines. We therefore assumed that this line is due to some other unidentified element. The computed lines of Al I mult. 1 at 3944.009 Å and 3961.523 Å disappear for the abundance −7.50 dex, which corresponds to an underabundance [−1.93]. We adopted this value as upper limit for the aluminium abundance.

From IUE spectra Smith (1993) derived log(N(Al)/N(H)) = −7.02 ± 0.31.

Silicon (14)-Si II,Si III: Numerous Si II lines and two weak Si III lines of mult. 2 at 4552.6 Å and 4567.8 Å were observed in the spectrum. The intense Si I line of mult. 3 at 3905.52 Å is

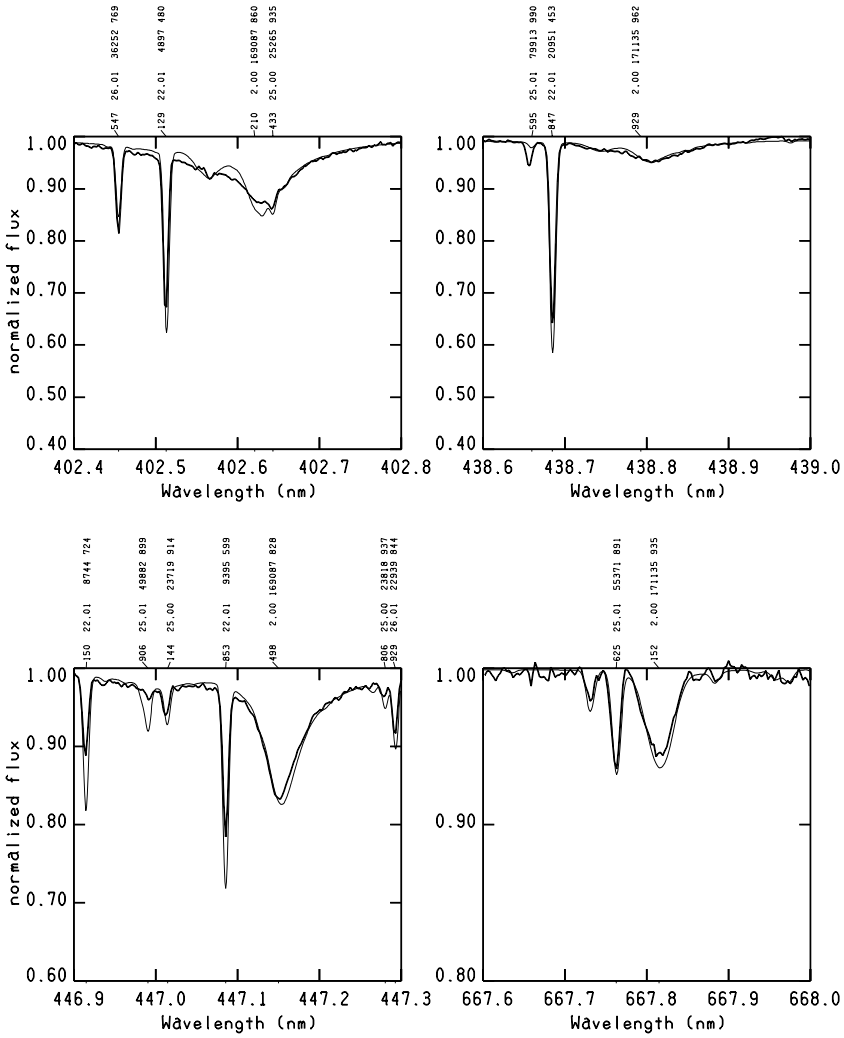

Fig. A.1. Comparison of observed (thick line) and computed (thin line) profiles of He I 402.6, 438.7, 447.1 and 667.8 nm. The meaning of the line identification labels like 547 26.01 36252 769 is: 547, last 3 digits of wavelength in nm (402.4547); 26.01, element (26) and charge (01), i.e. Fe II; 36252, lower energy level in cm^{-1}; 769, per mil residual flux of isolated line before rotation.

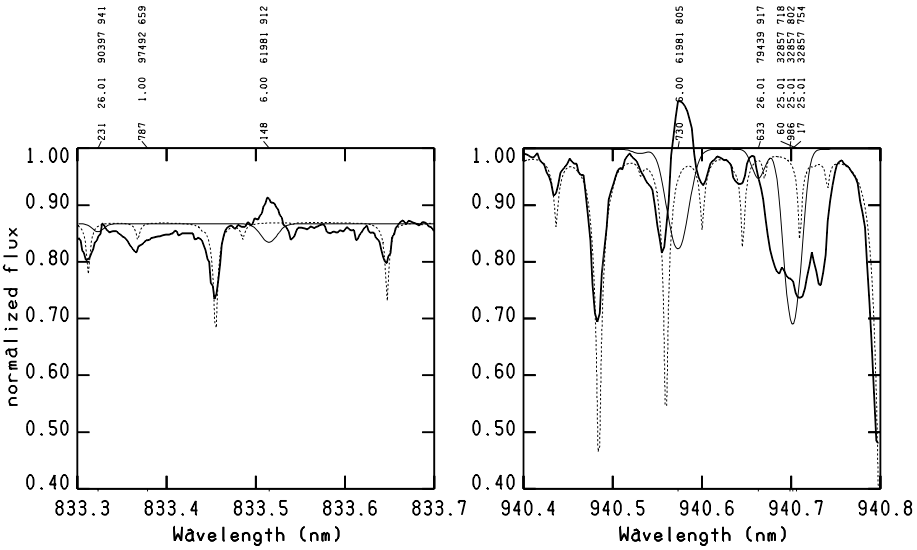

Fig. A.2. Observed emissions at the position of C I 833.5148 nm and C I 940.5730 nm. Observed spectrum (thick line), stellar synthetic spectrum (thin line), and telluric synthetic spectrum (dotted line) are superimposed. The meaning of the identification labels is the same as that given in the caption of Fig. A.1.

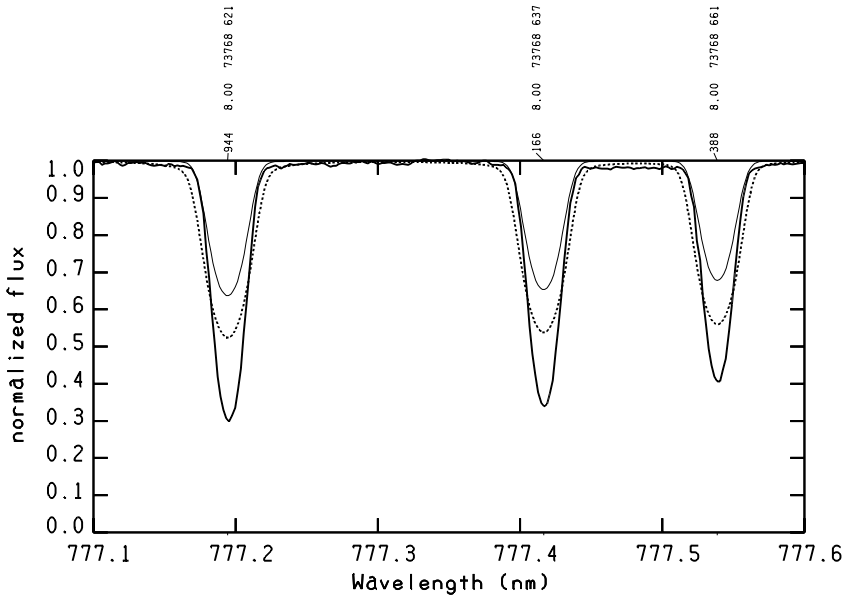

Fig. A.3. Synthetic LTE profiles of O I triplet mult. 1 at 777.2–777.5 nm computed with two different oxygen abundances, −3.18 dex (thin line) and −2.10 dex (dotted line), are compared with the observed profiles (thick line). The first abundance is the average abundance from selected equivalent widths (see text) the second abundance is that derived from the equivalent widths of the O I triplet mult. 1 lines. Increasing the O I abundance does not reduce the disgreement between the observed and computed profiles. The meaning of the identification labels is the same as that given in the caption of Fig. A.1.

heavily blended with a strong unidentified component, which is very probably a too weak predicted Mn II line at 3905.452 Å.

It was not easy to fix the Si abundance from the Si II lines on the basis of the Kurucz line lists only. In fact, they include all the Si II lines of the Moore (1965) multiplet tables, but missing Stark broadening parameters for some lines and the use of guessed oscillator strengths in several cases produced discordant abundances from the different lines. We implemented the silicon atomic data in the Kurucz line lists by replacing numerous guessed log gfs with those we derived from the multiplet oscillator strengths available in Lanz & Artru (1985) (LA) and by adding the radiative and Stark broadening parameters from Lanz et al. (1988) for a few lines.

We compared a few Si II oscillator strengths of the Kurucz line lists taken from Kurucz & Peytremann (1975)(KP) with log gfs from LA. They agree for almost all the lines. However, the KP log gfs of a few lines not studied by LA produced profiles much stronger than the observed ones. These lines are Si II mult. 20 at 3997.926 Å and Si II at 4002.592 Å, 4028.465 Å and 4035.278 Å due to the $3p^2\,{}^2P–3d'{}^2D$ transition. The KP log gfs of the last three lines, −0.610, −0.360 and −1.300 were replaced by −2.75, −3.10 and −2.60 derived from the comparison of observed and computed profiles when the Si II average abundance −4.72 dex from Table A.1 is adopted. Also the guessed log gfs of the Si II lines at 3991.780 Å and 4016.188 Å produce profiles which do not fit the observed spectrum.

We measured the equivalent widths of the Si II and Si III lines listed in Table A.1. The average abundances are −4.72 ± 0.08 dex and −4.58 ± 0.04 dex, respectively. The average abundance from all Si II and Si III lines is −4.71 ± 0.09 dex, which was adopted as final silicon abundance.

The LTE synthetic spectrum does not correctly predict the strong Si II lines of mult. 2 at 6347.11 Å and 6371.37 Å. The behaviour is analogous to that we showed in Fig. A.3 for the O I lines of mult. 1. The cores of the observed profiles are stronger than those computed for the average abundance −4.71 dex, while the observed wings are narrower than the computed ones. An increase of the abundance increases both the cores and the wings of the computed profiles, so that their shape is always different from that observed in the spectrum.

From IUE spectra Smith (1993) derived $\log(N(\mathrm{Si})/N(\mathrm{H})) = -4.60 \pm 0.10$.

Phosphorus (15)-P II: Only weak P II lines can be observed in the spectrum. We did not any change in the Kurucz line lists, except for the log gf of the lines at 3505.995 Å, 3786.581 Å and 6301.933 Å which yield computed lines which are not observed. In spite of Hibbert (1988) being the source quoted by Kurucz for these lines, a check of the log gfs derived from the transition probabilities A_l listed by Hibbert (1988) has shown that they are different from those of the Kurucz line lists. We derived −4.540, −2.719 and −2.455, respectively. The measured equivalent widths of the lines listed in Table A.1 give $\log(N(\mathrm{P})/N_{\mathrm{tot}}) = -6.28 \pm 0.08$, corresponding to an overabundance of [+0.3].

Sulfur (16)-S I,S II: Several weak S II lines can be observed in the spectrum. The average abundance from the measured equivalent widths (Table A.1) is −5.12 ± 0.3 dex, corresponding to the underabundance [−0.41].

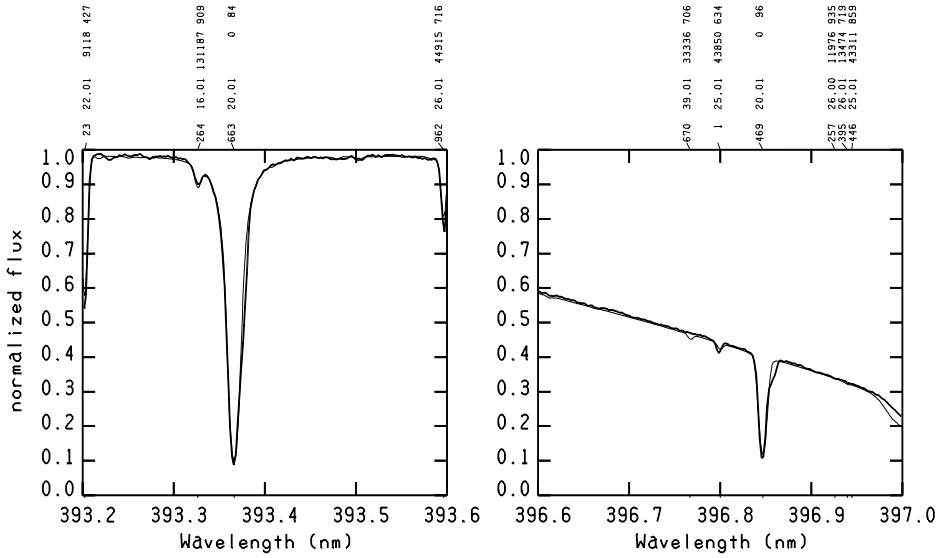

Fig. A.4. Comparison of the observed Ca II K and H profiles (thick line) with the computed ones (thin line). A bump can be observed on the red side of Ca II K while an unidentified red component is well detectable on the red wing of Ca II H. The meaning of the identification labels is the same as that given in the caption of Fig. A.1.

For this abundance, the lines of S I mult. 1 at 9212.863 Å and 9237.538 Å are predicted to be much weaker than what is observed. Possibly, NLTE computations could explain the discrepancy. We did not use them for the abundance determination.

Calcium (20)-Ca I,Ca II: There is a large scatter in the abundances derived from Ca I and Ca II and also from the different Ca II lines.

Only Ca I mult. 2 at 4226.728 Å is observed. The abundance from the equivalent width is $\log(N(\mathrm{Ca})/N_{\mathrm{tot}}) = -5.26$.

Most of the relevant Ca II lines lie on the wings of hydrogen profiles, except Ca II mult. 4 at 3158.8 Å, 3179.3 Å and 3181.2 Å. The average abundance from the equivalent widths of the three lines is $\log(N(\mathrm{Ca})/N_{\mathrm{tot}}) = -5.83 \pm 0.06$. Abundances from other lines were derived by comparing observed and computed profiles. Both lines of Ca II mult. 1 at 3933.663 Å (K-line) and 3968.469 Å (H-line) are affected by a red component of unknown origin (Fig. A.4). While a small bump is detectable on the red side of the K-line core, a component is well detectable on the red wing of the H-line. If the red components are neglected, the abundance from the H and K profiles is $\log(N(\mathrm{Ca})/N_{\mathrm{tot}}) = -5.54$, in agreement with the abundances from other Ca II lines observed in the 3700–6000 Å region, which range from −5.54 to −5.64 dex.

There are only two lines of the infrared Ca II triplet that can be observed in the spectrum. They are $\lambda\lambda$ 8498.023 Å and 8662.141 Å; the third line at 8542.091 Å is lost in the gap between the UVES èchelle orders. The two Ca II lines are redshifted by 0.2 Å from the expected position of the laboratory wavelength. This shift was explained by Castelli & Hubrig (2004) as due to an anomalous Ca isotopic mixture, in which the heaviest stable isotope ^{48}Ca is more abundant than the isotope ^{40}Ca, which is instead the predominant one in the terrestrial mixture. While the abundance from the first profile is −5.54 dex in agreement with the determinations from most Ca II lines, the abundance from the second profile is more than 0.3 dex larger, indicating possible NLTE effects.

Also the Ca II doublet at 8912.07 Å and 8927.36 Å is observable, but the lines predicted by the abundance of −5.54 dex are much stronger than what is observed. We did not use them for the average abundance determination owing to the unknown accuracy of their log gfs taken from Kurucz & Peytremann (1975). No other log gf sources for these lines were found. Both profiles are redshifted by about 0.03 Å, but this value is close to the uncertainties in the wavelength scale.

The line at 8248.796 Å, Ca II mult. 13, is a weak observed feature reproduced by an abundance of −6.40 dex.

We adopted as final abundance for computing the synthetic spectrum $\log(N(\mathrm{Ca})/N_{\mathrm{tot}}) = -5.54$.

Scandium (21)-Sc II: The abundance from the near-ultraviolet Sc II lines is solar and is 0.3 dex higher than that from the visual lines. We adopted as final value the average abundance from all the Sc II lines, $\log(N(\mathrm{Sc})/N_{\mathrm{tot}}) = -9.08 \pm 0.15$ dex.

Titanium (22)-Ti II: We identified numerous Ti II lines. All the lines with high excitation potential ($\chi_{\mathrm{low}} \gtrsim 62\,000$ cm^{-1}, i.e. 7.7 eV) and large transition probabilities (log $gf > -1.00$) are in emission. They can be observed starting from Ti II at 5846.579 Å. All the identified Ti II emission lines are listed in Table A.4. The columns R_{c}(obs) and R_{c}(calc) give the flux normalised to the continuum at the center of the line in the observed and synthetic spectra, respectively. R_{c}(obs) is a measure of the intensity of the observed emission. We assumed that some lines listed in Table A.4, although observed as absorptions, are affected by an emission reducing their intensity. They are all the lines with $R_{\mathrm{c}}(\mathrm{obs}) \leq 1.0$. Owing to the uncertainties

Table A.4. The Ti II emission lines. The line data are from Kurucz & Bell (1995).

λ_{calc}(Å)	Elem.	log gf	E_{low}(cm^{-1})	Conf.	E_{up}(cm^{-1})	Conf.	R_c(obs)	R_c(calc)	Notes[a]
5846.579	Ti II	−0.689	64 979.150	(3F)4d e4G	82 078.430	(3F)4f 4G	1.006	0.993	
5921.937	Ti II	−0.024	64 979.150	(3F)4d e4G	81 860.840	(3F)4f 4G	1.013	0.971	
5928.521	Ti II	−0.045	64 979.150	(3F)4d e4G	81 842.090	(3F)4f 2G	1.005	0.973	
5929.696	Ti II	+0.376	65 243.460	(3F)4d e4G	82 103.060	(3F)4f 4G	1.006	0.936	
5937.320	Ti II	−0.061	65 446.270	(3F)4d e4H	82 284.220	(3F)4f 2I	1.000	0.975	
5937.412	Ti II	+0.152	64 886.480	(3F)4d e4G	81 724.170	(3F)4f 4G	1.008	0.958	
5940.344	Ti II	+0.464	65 243.460	(3F)4d e4G	82 072.840	(3F)4f 4H	1.007	0.924	
5940.764	Ti II	−0.004	65 095.800	(3F)4d e4G	81 923.990	(3F)4f 2H	1.011	0.971	
5944.674	Ti II	−0.591	65 095.800	(3F)4d e4G	81 912.920	(3F)4f 4F	1.006	0.992	
5961.332	Ti II	−0.317	65 308.300	(3F)4d e4H	82 086.430	(3F)4f 4G	1.009	0.986	
5965.298	Ti II	−0.220	64 979.150	(3F)4d e4G	81 738.130	(3F)4f 4I	1.009	0.982	
5969.800	Ti II	−0.529	65 274.600	(3F)4d 4D	82 020.940	(3F)4f 4D	1.005	0.991	
5969.818	Ti II	−0.534	65 095.800	(3F)4d e4G	81 842.090	(3F)4f 2G	1.005	0.991	
5971.648	Ti II	+0.634	64 866.480	(3F)4d e4G	81 627.640	(3F)4f 4H	1.037	0.893	
5979.141	Ti II	−0.326	65 598.730	(3F)4d 4D	82 318.910	(3F)4f 2D	1.016	0.987	?
5983.979	Ti II	−0.182	64 979.150	(3F)4d e4G	81 685.810	(3F)4f 2G	1.000	0.979	
5987.388	Ti II	+0.673	64 979.150	(3F)4d e4G	81 676.300	(3F)4f 4H	1.046	0.886	
5988.980	Ti II	+0.012	65 308.300	(3F)4d e4H	82 001.010	(3F)4f 2I	1.016	0.971	
5989.486	Ti II	−0.205	65 460.010	(3F)4d f2F	82 151.310	(3F)4f 2F	1.004	0.982	
5990.839	Ti II	−0.105	65 460.010	(3F)4d f2F	82 147.540	(3F)4f 4F	1.002	0.978	
5994.938	Ti II	+0.808	65 243.460	(3F)4d e4G	81 919.580	(3F)4f 4I	1.013	0.861	
5995.668	Ti II	−0.348	65 186.750	(3F)4d e4H	81 860.840	(3F)4f 4G	1.000	0.987	
5995.708	Ti II	+0.184	65 460.010	(3F)4d f2F	82 133.990	(3F)4f 4D	1.000	0.959	
6001.395	Ti II	+0.751	65 095.800	(3F)4d e4G	81 753.980	(3F)4f 4H	1.051	0.872	
6001.895	Ti II	+0.193	65 446.270	(3F)4d e4H	82 103.060	(3F)4f 4G	1.004	0.959	
6002.418	Ti II	+0.280	65 186.750	(3F)4d e4H	81 842.090	(3F)4f 2G	1.022	0.948	
6005.194	Ti II	−0.202	65 598.730	(3F)4d 4D	82 246.370	(3F)4f 4D	1.000	0.983	
6005.786	Ti II	−0.217	65 243.460	(3F)4d e4G	81 889.460	(3F)4f 4I	1.000	0.983	
6012.750	Ti II	+1.103	65 590.190	(3F)4d e4H	82 216.910	(3F)4f 4I	0.995	0.792	
6012.804	Ti II	+0.743	65 446.270	(3F)4d e4H	82 072.840	(3F)4f 4H	0.993	0.879	
6015.753	Ti II	−0.040	65 460.010	(3F)4d f2F	82 078.430	(3F)4f 4G	1.000	0.975	
6022.697	Ti II	−0.367	65 397.570	(3F)4d 4D	81 966.830	(3F)4f 4P	1.000	0.988	
6024.933	Ti II*	−0.091	65 274.600	(3F)4d 4D	81 867.700	(3F)4f 4P	1.015	0.977	
6024.940	Ti II*	+0.152	65 213.800	(3F)4d 4D	81 806.880	(3F)4f 4F	1.015	0.961	
6029.271	Ti II	+0.670	65 308.300	(3F)4d e4H	81 889.460	(3F)4f 4I	1.053	0.892	
6039.682	Ti II	+0.264	65 598.730	(3F)4d 4D	82 151.310	(3F)4f 2F	1.012	0.953	
6040.120	Ti II	+0.650	65 186.750	(3F)4d e4H	81 738.130	(3F)4f 4I	1.036	0.896	
6041.058	Ti II	+0.288	65 598.730	(3F)4d 4D	82 147.540	(3F)4f 4F	1.000	0.951	
6042.201	Ti II	+0.169	65 397.570	(3F)4d 4D	81 943.250	(3F)4f 2F	1.035	0.961	
6046.008	Ti II	−0.278	65 598.730	(3F)4d 4D	82 133.990	(3F)4f 4D	1.021	0.986	
6046.546	Ti II	+0.126	65 308.300	(3F)4d e4H	81 842.090	(3F)4f 2G	1.000	0.964	
6053.297	Ti II	+0.169	65 397.570	(3F)4d 4D	81 912.920	(3F)4f 4F	1.014	0.961	
6059.156	Ti II	+0.143	65 274.600	(3F)4d 4D	81 773.980	(3F)4f 4F	1.024	0.963	
6065.306	Ti II	+0.379	65 590.190	(3F)4d e4H	82 072.840	(3F)4f 4H	1.000	0.941	
6066.392	Ti II	+0.121	65 598.730	(3F)4d 4D	82 078.430	(3F)4f 4G	1.024	0.966	
6068.745	Ti II	+0.558	65 446.270	(3F)4d e4H	81 919.580	(3F)4f 4I	1.000	0.915	
6072.446	Ti II	+0.141	65 397.570	(3F)4d 4D	81 860.840	(3F)4f 4G	1.009	0.963	
6073.760	Ti II	−0.139	65 314.270	(3F)4d f2F	81 773.980	(3F)4f 4F	1.022	0.980	
6076.270	Ti II	−0.037	65 460.010	(3F)4d 4D	81 724.170	(3F)4f 4G	1.008	0.975	
6078.941	Ti II	+0.206	65 308.300	(3F)4d e4H	81 753.980	(3F)4f 4H	1.011	0.958	
6079.862	Ti II	−0.009	65 446.270	(3F)4d e4H	81 889.460	(3F)4f 4I	1.007	0.974	
6080.712	Ti II	+0.003	65 186.750	(3F)4d e4H	81 627.640	(3F)4f 4H	1.000	0.972	
6102.542	Ti II	+0.178	65 460.010	(3F)4d f2F	81 842.090	(3F)4f 2G	1.011	0.961	
6106.471	Ti II	+0.416	65 314.270	(3F)4d f2F	81 685.810	(3F)4f 2G	1.042	0.936	
6107.791	Ti II	−0.371	65 308.300	(3F)4d e4H	81 676.300	(3F)4f 4H	1.004	0.988	
6123.782	Ti II	−0.325	65 598.730	(3F)4d 4D	81 923.990	(3F)4f 2H	1.006	0.987	
6128.245	Ti II	−0.629	65 314.270	(3F)4d f2F	81 627.640	(3F)4f 4H	1.008	0.993	

Table A.4. continued.

λ_{calc}(Å)	Elem.	log gf	E_{low}(cm^{-1})	Conf.	E_{up}(cm^{-1})	Conf.	R_c(obs)	R_c(calc)	Notes[a]
6141.516	Ti II	−0.325	65 460.010	(3F)4d f2F	81 738.130	(3F)4f 4I	1.000	0.987	
6418.376	Ti II	+0.001	66 794.010	(3F)4d 2P	82 369.970	(3F)4f 2P	1.007	0.980	
6431.383	Ti II	−0.366	66 521.010	(3F)4d 2P	82 043.850	(3F)4f 4P	1.009	0.991	
6439.486	Ti II	−0.071	66 794.010	(3F)4d 2P	82 318.910	(3F)4f 2D	1.008	0.983	
6445.572	Ti II	−0.947	66 794.010	(3F)4d 2P	82 304.250	(3F)4f 4S	1.023	0.998	Broad
6961.471	Ti II	+0.716	67 822.490	(3F)4d e2G	82 183.310	(3F)4f 2H	1.064	0.934	
6982.314	Ti II	+0.454	67 606.640	(3F)4d e2G	81 923.990	(3F)4f 2H	1.015	0.960	
7012.686	Ti II	+0.244	67 822.490	(3F)4d e2G	82 078.430	(3F)4f 4G	1.025	0.979	
7050.978	Ti II	+0.118	67 822.490	(3F)4d e2G	82 001.010	(3F)4f 2I	1.018	0.984	
7074.144	Ti II	+0.075	67 606.040	(3F)4d e2G	81 738.130	(3F)4f 4I	1.017	0.986	
7100.431	Ti II	−0.040	67 606.040	(3F)4d e2G	81 685.810	(3F)4f 2G	1.013	0.989	
7105.230	Ti II	−0.099	67 606.040	(3F)4d e2G	81 676.300	(3F)4f 4H	1.010	0.990	
7225.270	Ti II	+0.335	68 482.410	(3F)4d 2D	82 318.910	(3F)4f 2D	1.025	0.978	
7296.684	Ti II	−0.401	68 364.390	(3F)4d 2D	82 065.470	(3F)4f 2D	1.025	0.996	
7297.291	Ti II	+1.006	68 584.280	(3F)4d e2H	82 284.220	(3F)4f 2I	1.039	0.918	
7313.279	Ti II	+0.793	68 331.020	(3F)4d e2H	82 001.010	(3F)4f 2I	1.051	0.944	
7351.440	Ti II	+0.237	68 331.020	(3F)4d e2H	82 183.310	(3F)4f 2H	1.026	0.983	
7426.911	Ti II	−0.902	68 482.410	(3F)4d 2D	81 943.250	(3F)4f 2F	1.008	0.999	?
7443.684	Ti II	−0.580	68 482.410	(3F)4d 2D	81 912.920	(3F)4f 4F	1.005	0.997	?
7447.870	Ti II	+0.122	68 331.020	(3F)4d e2H	81 753.980	(3F)4f 4H	1.006	0.987	?
7574.057	Ti II	−0.703	68 951.980	(3F)4d f4F	82 151.310	(3F)4f 2F	1.012	0.998	
7653.044	Ti II	+0.606	69 084.440	(3F)4d f4F	82 147.540	(3F)4f 4F	1.016	0.969	
7679.192	Ti II	+0.661	69 084.440	(3F)4d f4F	82 103.060	(3F)4f 4G	1.013	0.965	
7681.729	Ti II	+0.194	68 846.520	(3F)4d f4F	81 860.840	(3F)4f 4G	1.012	0.987	
7706.784	Ti II	+0.346	68 951.980	(3F)4d f4F	81 923.990	(3F)4f 2H	1.020	0.982	
7713.367	Ti II	+0.273	68 951.980	(3F)4d f4F	81 912.920	(3F)4f 4F	1.011	0.985	
7716.915	Ti II	+0.429	68 769.190	(3F)4d f4F	81 724.170	(3F)4f 4G	1.010	0.978	
7733.343	Ti II	+0.035	68 846.520	(3F)4d f4F	81 773.980	(3F)4f 4F	1.013	0.991	
7786.450	Ti II	+0.251	68 846.520	(3F)4d f4F	81 685.810	(3F)4f 2G	1.011	0.986	
7805.972	Ti II	+0.128	71 461.590	(3F)5p 4G	84 268.770	(3F)5d 4G	1.006	0.991	?
7820.346	Ti II	+0.296	71 586.060	(3F)5p 4G	84 369.700	(3F)5d 4G	1.011	0.987	
7824.913	Ti II	+0.984	71 945.900	(3F)5p 4G	84 722.080	(3F)5d 4H	1.024	0.946	
7831.699	Ti II	+0.423	71 747.460	(3F)5p 4G	84 512.570	(3F)5d 4G	1.016	0.983	
7845.102	Ti II	+0.821	71 747.460	(3F)5p 4G	84 490.760	(3F)5d 4H	1.007	0.960	
7856.805	Ti II	+0.003	68 951.980	(3F)4d f4F	81 676.300	(3F)4f 4H	1.003	0.990	?
7869.297	Ti II	+0.616	71 461.590	(3F)5p 4G	84 165.710	(3F)5d 4H	1.000	0.973	?
7880.457	Ti II	+0.506	71 945.900	(3F)5p 4G	84 632.030	(3F)5d 4G	1.005	0.980	?
7994.391	Ti II	+0.566	72 126.700	(3F)5p 4F	84 632.030	(3F)5d 4G	1.017	0.979	
8838.415	Ti II	+0.517	71 945.900	(3F)5p 4G	83 257.040	(3F)6s 4F	1.016	0.973	?
8926.578	Ti II	+0.349	63 445.880	(3F)5s e2F	74 645.080	(3F)5p 2D	1.023	0.946	
9654.718	Ti II	+0.418	63 445.880	(3F)5s e2F	73 800.670	(2D)sp 2F	1.053	0.946	
9907.939	Ti II	−0.003	62 180.160	(3F)5s e4F	72 270.310	(3F)5p 4D	1.023	0.969	
9931.897	Ti II	+0.209	62 272.160	(3F)5s e4F	72 337.970	(3F)5p 4D	1.059	0.953	Bad spectrum
9956.695	Ti II	+0.397	62 410.780	(3F)5s e4F	72 451.520	(3F)5p 4D	1.012	0.934	Bad spectrum
9983.462	Ti II	+0.557	62 595.030	(3F)5s e4F	72 608.850	(3F)5p 4D	1.058	0.915	

[a] The symbol "*" indicates blended lines. The symbol "?" indicates doubtful emissions.

in the position of the continuum and in the log gf data, the only unquestionable emissions are those with R_c(obs) ≥ 1.01. Figure A.5 shows the Ti II emission at 6029.27 Å.

We adopted wavelengths and experimental log gfs from Pickering et al. (2002) for most of the Ti II lines with $\lambda <$ 5500 Å instead of the data from the Kurucz files, although several of them are from the Martin et al. (1988) critical compilation. We found that the Pickering et al. (2002) data improve the agreement between the observed and computed spectra considerably.

Abundances from equivalent widths are given in Table A.2. The average abundance is −5.67 ± 0.11 dex, so that Ti is over-

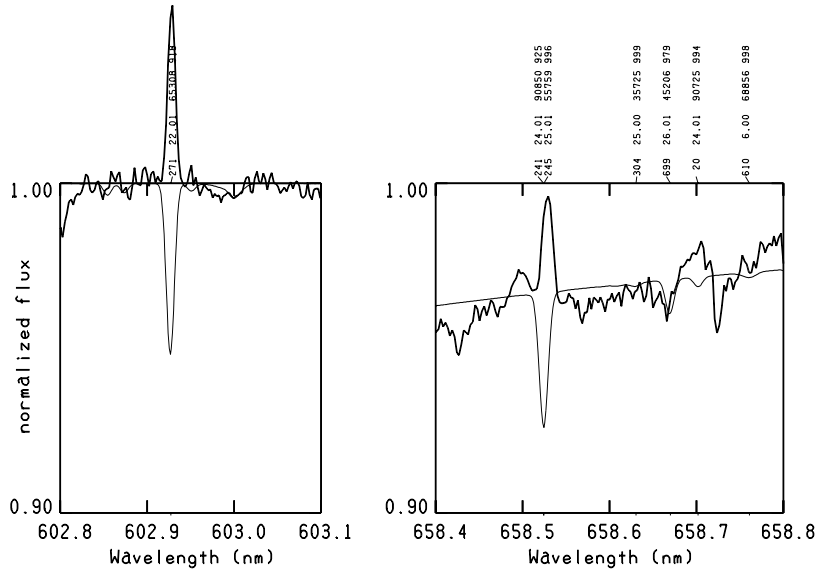

Fig. A.5. Observed emission lines at the position of Ti II 602.9271 nm (*left panel*, thick line) and of Cr II 658.5241 nm and Cr II 658.7020 nm (*right panel*, thick line). The thin line is the synthetic spectrum. The meaning of the identification labels is the same as that given in the caption of Fig. A.1.

abundant by 1.35 ± 0.11 dex. However, there is a small difference of 0.13 dex between the average abundance from lines shortward and longward of the Balmer discontinuity. The values are −5.59 ± 0.09 dex and −5.72 ± 0.08 dex, respectively.

Vanadium (23)-Not observed: No lines of vanadium were observed in the spectrum. We fixed an upper limit of −9.04 dex for the vanadium abundance from V II mult. 1 at 3100 Å. It corresponds to an underabundance [V/H] = −1.0,

Chromium (24)-Cr I,Cr II: We identified several Cr I and numerous Cr II lines. All the Cr II lines with high excitation potential ($\chi_{\rm low}$ larger than 89 000 cm^{-1}, i.e. 11 eV) and large transition probabilities (log $gf > -0.8$) are in emission. They can be observed starting from Cr II at 6121.434 Å. All the identified Cr II emission lines are listed in Table A.5. The meaning of the columns is the same as in Table A.4. Figure A.5 shows the Cr II emissions at 6285.241 Å and 6587.020 Å.

Sigut & Landstreet (1990) pointed out the large uncertainty affecting the Cr II log gfs. For the 4050–4650 Å interval, they reduced the discrepancies related to different sources by renormalising the Cr II oscillator strengths from Wujec & Weniger (1981) on a scale different from that adopted by Martin et al. (1988)(MFW). We adopted log gfs from MFW when the source is Kostyk & Orlova (1983) and from Sigut & Landstreet (1990) when the source is Wujec & Weniger (1981), except for Cr II $\lambda\lambda$ 4587.30, 4697.61 and 4715.12 Å. We kept log gfs from MFW for the three lines on the basis of the comparison of the observed and computed spectra. For Cr II at 4812.34 Å we adopted log $gf = -1.995$ from the Kurucz line lists in accordance with the discussion of Sigut & Landstreet (1990). For all the Cr II lines not considered by MFW we used log gfs from the Kurucz line lists without any renormalisation.

There are small wavelength differences in MFW and in the Kurucz line lists for a few Cr II lines. The wavelengths from Kurucz agree better with the observations. In several cases both the wavelengths from MFW and from the Kurucz line lists do not agree with the position of the observed lines. Examples are the Cr II lines at $\lambda\lambda$ 5308.46 Å, 5310.73 Å and 5313.61 Å, where the wavelengths are from MFW.

The average Cr I abundance is 0.2 dex larger than that from Cr II. The abundances are −5.22 ± 0.09 dex and −5.41 ± 0.07 dex, respectively. The average abundances from Cr II lines lying shortward and longward of the Balmer discontinuity are within the error limits. The average abundance from all the Cr I and Cr II lines is −5.36 ± 0.11 dex, corresponding to an overabundance of [+1.01].

Smith & Dworetsky (1993) obtained log(N(Cr)/N(H)) = −5.5 ± 0.1 from an IUE spectra analysis.

Manganese (25)-Mn I,Mn II: The spectrum is so rich in Mn I and Mn II lines that HD 175640 could be used as an ideal laboratory for studying the manganese spectrum.

The bulk of log gf data for Mn II lines comes from Kurucz (1992) computations, so that no spectral analyses of HgMn stars would be possible without the Kurucz data for this ion. Unfortunately, critical evaluations are unavailable for many of the Mn II lines, especially in the visible region.

There are numerous exceptionally broadened Mn II lines in the spectrum. This characteristic, which seems to be common to all HgMn stars, was first shown up by Jomaron et al. (1999), who explained it as due to hyperfine splitting. They were not fully able to reproduce the exceptionally broadened profiles owing to the lack of Mn II hyperfine structure experimental data. These measurements were made later on by Holt et al. (1999), who confirmed the findings of Jamaron et al. (1999).

Isotope 25 is the only isotope of manganese. We added in the line lists the hyperfine components of several Mn II lines

Table A.5. The Cr II emission lines. The line data are from Kurucz & Bell (1995).

λ_{calc}(Å)	Elem.	log gf	E_{low}(cm^{-1})	Conf.	E_{up}(cm^{-1})	Conf.	R_c(obs)	R_c(calc)	Notes[a]
6121.434	Cr II	−0.280	89 277.950	(5D)4d e4P	105 609.470	(5D)4f 6G	1.000	0.992	?
6128.189	Cr II	−0.492	89 325.320	(5D)4d e4G	105 638.840	(5D)4f 6F	1.007	0.995	
6158.621	Cr II	+0.718	89 174.080	(5D)4d e4G	105 406.990	(5D)4f 4H	0.990	0.928	
6161.031	Cr II	+0.573	89 056.020	(5D)4d e4G	105 282.580	(5D)4f 4H	1.002	0.945	
6172.927	Cr II	−0.239	89 336.890	(5D)4d e4P	105 532.180	(5D)4f 4D	1.012	0.991	
6179.226	Cr II	−0.055	89 724.270	(5D)4d f4D	105 903.050	(5D)4f 4F	1.007	0.987	
6181.354	Cr II	+0.189	89 812.420	(5D)4d f4D	105 985.630	(5D)4f 4F	1.017	0.978	
6182.340	Cr II	+0.452	89 336.890	(5D)4d e4P	105 507.520	(5D)4f 4D	1.023	0.960	
6186.315	Cr II	+0.336	89 885.080	(5D)4d f4D	106 045.320	(5D)4f 4G	1.009	0.971	
6193.551	Cr II	+0.012	89 056.020	(5D)4d e4G	105 197.380	(5D)4f 6H	1.000	0.984	
6209.250	Cr II	−0.169	89 885.080	(5D)4d f4D	105 985.630	(5D)4f 4F	1.009	0.990	
6213.078	Cr II	+0.037	89 812.420	(5D)4d f4D	105 903.050	(5D)4f 4F	1.008	0.985	
6213.538	Cr II	+0.143	89 174.080	(5D)4d e4G	105 263.520	(5D)4f 6H	1.000	0.979	
6231.676	Cr II	+0.061	89 325.320	(5D)4d e4G	105 367.930	(5D)4f 6H	1.000	0.983	
6237.002	Cr II	−0.104	89 254.560	(5D)4d e4P	105 283.470	(5D)4f 4P	1.003	0.988	
6285.601	Cr II	−0.229	89 885.080	(5D)4d f4D	105 790.060	(5D)4f 4F	1.028	0.992	
6299.534	Cr II	−0.679	89 336.890	(5D)4d e4P	105 206.690	(4F)sp p4D	1.015	1.000	
6301.413	Cr II	−0.162	89 812.420	(5D)4d f4D	105 677.490	(5D)4f 4G	1.009	0.990	
6309.669	Cr II	−0.013	89 277.950	(5D)4d e4P	105 122.260	(5D)4f 4P	1.013	0.986	
6311.509	Cr II	−0.190	89 885.080	(5D)4d f4D	105 724.770	(5D)4f 4G	1.008	0.991	
6324.198	Cr II	−0.121	89 724.270	(5D)4d f4D	105 532.180	(5D)4f 4D	1.015	0.990	
6369.654	Cr II	−0.692	89 812.420	(5D)4d f4D	105 507.520	(5D)4f 4D	1.008	0.997	
6399.280	Cr II	+0.004	89 885.080	(5D)4d f4D	105 507.520	(5D)4f 4D	1.004	0.987	
6501.575	Cr II	−0.310	90 608.990	(5D)4d e4F	105 985.630	(5D)4f 4F	1.011	0.994	
6526.302	Cr II	+0.173	89 885.080	(5D)4d f4D	105 203.460	(4F)sp r4F	1.003	0.982	
6536.680	Cr II	+0.026	90 680.990	(5D)4d e4F	105 903.050	(5D)4f 4F	1.016	0.988	
6551.373	Cr II	+0.229	90 725.870	(5D)4d e4F	105 985.630	(5D)4f 4F	1.025	0.982	
6579.572	Cr II	+0.215	90 850.960	(5D)4d e4F	106 045.320	(5D)4f 4G	1.019	0.983	
6585.241	Cr II	+0.829	90 850.960	(5D)4d e4F	106 032.240	(5D)4f 4G	1.030	0.939	
6592.341	Cr II	+0.217	90 512.560	(5D)4d e4F	105 677.490	(5D)4f 4G	1.021	0.982	
6613.776	Cr II	+0.485	90 608.990	(5D)4d e4F	105 724.770	(5D)4f 4G	1.007	0.968	
6636.427	Cr II	+0.573	90 725.870	(5D)4d e4F	105 790.060	(5D)4f 4F	1.029	0.963	
6656.120	Cr II	+0.066	90 512.560	(5D)4d e4F	105 532.180	(5D)4f 4D	1.005	0.987	
7211.765	Cr II	+0.656	93 143.880	(5D)5p 6F	107 006.290	(5D)5d 6G	1.000	0.963	
7226.064	Cr II	+0.791	93 276.860	(5D)5p 6F	107 111.840	(5D)5d 6G	1.011	0.953	
7242.963	Cr II	+0.904	93 444.170	(5D)5p 6F	107 246.870	(5D)5d 6G	1.000	0.943	
7394.889	Cr II	+0.451	94 177.180	(5D)5p 6D	107 696.310	(5D)5d 6D	1.000	0.980	
9448.293	Cr II	+0.179	84 495.700	(5D)5s e4D	95 076.720	(5D)5p 4D	1.048	0.956	
9951.294	Cr II	+0.126	84 209.880	(5D)5s e4D	94 256.070	(5D)5p 4F	1.042	0.971	
9952.493	Cr II	+0.318	84 320.210	(5D)5s e4D	94 365.190	(5D)5p 4F	1.024	0.957	
9970.727	Cr II	+0.477	84 495.700	(5D)5s e4D	94 522.310	(5D)5p 4F	1.048	0.943	
9974.826	Cr II	+0.535	84 726.710	(5D)6s e4D	94 749.200	(5D)5p 4F	1.024	0.938	

[a] The symbol "?" indicates doubtful emissions.

showing a large broadening in the spectrum. We adopted either the hyperfine log gfs taken from Holt et al. (1999) or we used the HYPERFINE code (Kurucz & Bell 1995) to compute hyperfine wavelengths and log gfs from the A and B hyperfine constants measured by Holt et al. (1999). Unfortunately, they cover only part of the Mn II levels.

The comparison of the wavelengths measured by Holt et al. (1999) with those from the Kurucz line lists has yielded non-negligible differences in some cases. The comparison of the observations with spectra computed with the two sets of wavelengths has favoured the Holt et al. (1999) data so that they were adopted in the line lists. Finally, in the Kurucz line lists the wavelengths of the lines of mult. 13 at 6122–6132 Å were replaced by the wavelengths measured by Johansson et al. (1995).

Table A.6 lists line data and (total or partial) hyperfine splitting for a large sample of Mn II lines. The multiplet number when available, the adopted wavelength, the adopted log gf, its source, the lower and upper excitation potentials in cm^{-1} and the total (or partial) hyperfine splitting hfs_{tot} are listed in successive columns. Here hfs_{tot} indicates the separation of the outermost components. Wavelengths marked with an asterisk were taken from Holt et al. (1999), while the others are from the Kurucz line lists. "hfs" just after the wavelength indicates that we added the hyperfine components of that line in the line lists. The hyperfine splitting hfs_{tot} listed in Col. 7 is total or partial according to whether the A and B constants are known for both levels or for only one of the levels involved in the transition. Some lines showing a large broadening in the observed spectrum, but lacking hyperfine data for computing the synthetic spectrum, are also listed in the table. Figure 3 in the main paper shows the extreme hyperfine broadening which affects the Mn II lines at 7353.549 Å and 7415.803 Å. Other lines much broader than the computed ones are those at 9407.0 Å(Fig. A.2), 9408.7 Å and 9446.8 Å, in spite of the hyperfine splitting of the upper level being considered in the computations. The hyperfine splitting of their lower level is unknown and this is probably the reason for the disagreement.

No Mn II emission lines are observed in the spectrum but there are some lines in the red part of the spectrum which are much weaker than the predicted ones. This disagreement could be explained either with an superimposed emission or with wrong line data. The most remarkable features are those predicted at $\lambda\lambda$ 9867.0, 9903.836, 9904.464, 9905.269, 9906.221 and 9907.212 Å.

The Mn abundance log $(N(\mathrm{Mn})/N_{\mathrm{tot}}) = -4.20$, corresponding to [Mn/H] = +2.4, was derived from the measured equivalent widths (Table A.2) of both Mn I and Mn II lines having critically evaluated log gfs available in Martin et al. (1988). Therefore, for Mn II, only the lines of Mn II mult. 3 at 3464.0 Å were used. Hyperfine structure has negligible effects on these lines.

We have added in Table A.2 the abundances from the Mn II lines at $\lambda\lambda$ 3917.318, 4363.25, 4365.220 and 4478.637 Å, which were used by Jomaron et al. (1999) to study the Mn abundance in a given sample of HgMn stars. We excluded them from the averaged abundance determination. The average abundance from the four lines is −4.46 ± 0.06 dex. The discrepancy with the average abundance from the other examined lines amounts to −0.26 dex, which could be interpreted as an indication of manganese stratification. However, the log gf uncertainties prevent us from drawing any firm conclusion about manganese stratification insomuch that the average abundances from Mn I (−4.19 ± 0.10 dex) and Mn II (−4.25 ± 0.04 dex) are within the error limits. Also the differences between the average abundances from Mn I lines lying shortward and longward of the Balmer discontinuity are well within the error limits.

For comparison, we recall that the average abundances $\log(N(\mathrm{Mn})/N(\mathrm{H}))$ from Jomaron et al. (1999) are −4.44 ± 0.05 for Mn I and −4.54 ± 0.05 for Mn II. Smith et al. (1993) derived $\log(N(\mathrm{Mn})/N(\mathrm{H})) = -4.35 \pm 0.05$ from the Mn II resonance lines at 2576 Å, 2593 Å, and 2605 Å measured in IUE spectra.

Iron (26)-Fe I,Fe II: The average Fe abundance from the equivalent widths of all the examined Fe I and Fe II lines (Table A.2) is $\log(N(\mathrm{Fe})/N_{\mathrm{tot}}) = -4.83 \pm 0.13$, corresponding to an underabundance of [−0.3]. The average abundance from Fe I lines, −4.78 ± 0.08 dex, agrees within the error limits with the average abundance from Fe II lines, −4.84 ± 0.13 dex, while the abundances from the Fe I lines shortward and longward of the Balmer discontinuity differ by 0.15 dex, which is more than the error limits. Lines lying in the near UV give the lower abundance value. The Fe II abundance from this study is the same as that derived by Hubrig & Castelli (2001) using only the equivalent width of the Fe II line at 6149.258 Å measured in a spectrum observed at CFHT.

Smith & Dworetsky (1993) found $\log(N(\mathrm{Fe})/N(\mathrm{H})) = -5.05 \pm 0.05$ from the analysis of IUE spectra.

Cobalt (27)-Co II (Not observed?): No cobalt lines were observed in the UVES spectra, except for Co II mult. 2 at 3501.717 Å, which could also be noise as well. The computed profile reproduces the observed spectrum for an abundance $\log(N(\mathrm{Co})/N_{\mathrm{tot}}) = -8.08$, which is about ten times lower than the solar abundance. We adopted the above value.

Smith & Dworetsky (1993) derived an upper limit $\log(N(\mathrm{Co})/N(\mathrm{H})) \leq -9.0 \pm 0.5$ from an IUE spectra analysis.

Nickel (28)-Ni II: The equivalent widths of the measured Ni II lines (Table A.2) give an underabundance [−0.3] if log gfs recomputed by Kurucz (2003) are used for all the lines examined (Table A.2). Instead, if log gfs from Heise (1974) are used, the nickel underabundance changes from [−0.3] to [−0.8]. There are no Ni II critically evaluated log gfs in the NIST database for the whole wavelength region studied by us. We adopted the abundance $\log(N(\mathrm{Ni})/N_{\mathrm{tot}}) = -6.09 \pm 0.16$, which is that based on the Kurucz (2003) log gfs. Smith & Dworetsky (1993) found $\log(N(\mathrm{Ni})/N(\mathrm{H})) = -6.2 \pm 0.3$ from their analysis of IUE spectra.

Copper (29)-Cu I: While no Cu II lines were observed, the Cu I line at 3247.540 Å was measured. It is probably blended with some unknown component, as it is asymmetric, with a more extended red wing. In fact, the abundance −6.52 dex from

Table A.6. Line data and total hyperfine splitting in a sample of Mn II lines.

Mult.	λ^a(Å)	log gf	Ref.^{b}	χ_{low}(cm^{-1})	χ_{up}(cm^{-1})	hfs$_{tot}$(Å)	Notes^c
–	3159.302,hfs	−1.720	K, K88	62 587.50	94 230.90	0.077	No fit, TWC
–	3330.778,hfs	−0.659	K, K88	37 851.47	67 865.85	0.031	
–	3364.213	−1.956	K, K88	52 383.72	82 099.82	no data	hfs
–	3366.028,hfs	−2.880	K, K88	43 696.19	73 396.26	0.045	No fit, TWC
–	3366.121,hfs	−2.181	K, K88	43 696.19	73 395.44	0.052	No fit, TWC
–	3418.232,hfs	−2.024	K, K88	44 138.96	73 385.46	0.031	
1	3438.974	−2.293	K, MFW	9472.97	38 543.08	no data	hfs
3	3441.988,hfs	−0.272	K, MFW	14 325.86	43 370.51	0.011	
–	3457.801,hfs	−2.338	K, K88	43 395.38	72 307.21	0.061	No fit, TWC
1	3460.030,hfs	−2.561	K, K88	9472.97	38 543.08	0.026	
3	3460.316,hfs	−0.542	K, MFW	14 593.82	43 484.64	0.015	
–	3461.458,hfs	−1.614	K, K88	44 899.82	73 781.11	0.044	
–	3462.341,hfs	−2.099	K, K88	44 521.52	73 395.44	0.013	No fit
3	3474.040,hfs	−0.999	K, MFW	14 593.82	43 370.51	0.011	
3	3474.129,hfs	−1.089	K, MFW	14 781.19	43 557.14	0.018	
3	3482.905,hfs	−0.740	K, MFW	14 781.19	43 484.64	0.014	
3	3488.677,hfs	−0.864	K, MFW	14 901.18	43 557.14	0.018	
3	3495.833,hfs	−1.218	K, MFW	14 959.84	43 557.14	0.018	
3	3496.809,hfs	−1.687	K, MFW	14 781.19	43 370.51	0.009	
3	3497.526,hfs	−1.330	K, MFW	14 901.18	43 484.64	0.014	
–	3509.939,hfs	−1.324	K, K88	43 528.64	72 011.02	0.096	
–	3685.051,hfs	−1.299	K, K88	43 528.64	70 657.58	0.106	Blend with Mn II 3685.042 Å
–	3695.917,hfs	−1.966	K, K88	43 696.19	70 745.38	0.072	
–	3763.730	−1.360	K, K88	41 182.53	67 744.37	no data	hfs
–	3812.239	−1.897	K, K88	44 521.52	70 745.38	no data	hfs
–	3844.161	−1.379	K, K88	44 521.52	70 527.62	no data	hfs
–	3848.574	−3.333	K, K88	44 521.52	70 497.80	no data	hfs
–	3897.604,hfs	−1.697	K, K88	43 395.38	69 044.90	0.078	No fit, TSC
–	3917.318,hfs	−1.147	K, K88	55 759.27	81 279.71	0.046	
–	3943.858,hfs	−2.464	K, K88	43 696.19	69 044.90	0.082	No fit, TWC
–	3995.317,hfs	−2.441	K, K88	43 395.38	68 417.61	0.096	No fit, TSC
–	4000.033,hfs	−1.212	K, K88	62 587.50	87 580.23	0.123	No fit, TSC
–	4039.681,hfs	−3.357	K, K88	43 537.18	68 284.62	0.097	
–	4136.902	−1.290	K, K88	49 517.58	73 683.44	no data	hfs
2	4174.318	−3.548	K, K88	14 593.820	38 543.08	0.001	
2	4205.375*	−3.376	K, K88	14 593.820	38 366.18	0.039	
7	4206.368*,hfs	−1.566	K, K88	43 528.64	67 295.43	0.129	
2	4207.234	−4.470	K, K88	14 781.190	38 543.08	0.002	No fit, TSC
–	4237.861*	−2.959	K, K88	43 311.30	66 901.44	0.002	
2	4238.785*	−3.626	K, K88	14 781.190	38 366.18	0.038	
–	4239.184*,hfs	−2.250	K, K88	43 311.30	66 894.09	0.050	
–	4240.385*	−2.066	K, K88	49 820.16	73 396.26	0.071	
–	4242.329*	−1.262	K, K88	49 820.16	73 385.46	0.057	Blend with Cr II
–	4242.920*	−2.992	K, K88	43 339.42	66 901.44	0.035	
7	4244.246*	−2.396	K, K88	43 339.42	66 894.09	0.038	
–	4247.954*	−3.379	K, K88	43 395.38	66 929.52	0.087	TWC, large disagreement
–	4251.727*	−1.058	K, K88	49 882.15	73 395.44	0.012	
–	4252.961*	−1.138	K, K88	49 889.86	73 396.26	0.018	Blend with Mn II
7	4253.018*	−2.403	K, K88	43 395.38	66 901.44	0.08	Blend with Mn II
–	4253.124*	−2.092	K, K88	49 889.86	73 395.44	0.018	Blend with Mn II
7	4259.191*,hfs	−1.589	K, K88	43 537.18	67 009.16	0.094	
2	4260.462*	−4.246	K, K88	14 901.180	38 366.180	0.038	TSC
–	4281.948*	−2.554	K, K88	43 339.42	66 686.70	0.029	Blend with Mn II
–	4282.490,hfs	−1.679	K, K88	44 521.52	67 865.85	0.052	
6	4283.766*,hfs	−2.204	K, K88	43 339.42	66 676.78	0.028	
6	4284.429	−2.265	K, K88	43 311.30	66 645.07	0.025	

Table A.6. continued.

Mult.	λ^a(Å)	log gf	Ref.^{b}	$\chi_{\rm low}$(cm^{-1})	$\chi_{\rm up}$(cm^{-1})	hfs$_{\rm tot}$(Å)	Notes^c
–	4288.067*	−1.890	K, K88	33 906.57	77 220.56	0.013	
–	4289.595*	−3.306	K, K88	43 339.42	66 645.07	0.027	TWC
6	4292.233*,hfs	−2.226	K, K88	43 395.38	66 686.70	0.077	No fit, TWC
6	4300.254*,hfs	−2.880	K, K88	43 395.38	66 643.31	0.079	No fit, TWC
–	4302.957*	−6.136	K, K88	43 696.19	66 929.52	0.093	Observed, not predicted
–	4308.153*	−1.723	K, K88	43 696.19	66 901.44	0.092	
–	4317.720*	−1.917	K, K88	55 759.27	78 913.17	0.032	
6	4325.047*,hfs	−2.299	K, K88	43 528.64	66 643.31	0.119	
6	4326.643*,hfs	−1.254	K, K88	43 537.18	66 643.31	0.091	
–	4336.959*	−2.551	K, K88	43 850.42	66 901.44	0.020	
–	4338.345*	−2.090	K, K88	43 850.42	66 894.09	0.039	
–	4382.579*	−1.977	K, K88	44 745.46	67 766.76	0.041	
6	4343.983*,hfs	−1.095	K, K88	43 528.64	66 542.53	0.118	
6	4345.593*	−2.164	K, K88	43 537.18	66 542.53	0.090	
–	4346.406*	−1.544	K, K88	52 718.80	75 719.93	0.004	
–	4348.396*,hfs	−1.500	K, K88	43 696.19	66 686.70	0.082	
–	4356.628*	−2.026	K, K88	43 696.19	66 643.31	0.084	
–	4363.254*	−1.909	K, K88	44 899.82	67 812.05	0.041	
–	4365.220*	−1.350	K, K88	53 017.16	75 919.09	0.006	
–	4377.744*,hfs	−2.144	K, K88	43 850.42	66 686.70	0.017	
–	4379.644*,hfs	−1.850	K, K88	43 850.42	66 676.78	0.018	
–	4385.738*	−3.029	K, K88	43 850.42	66 645.07	0.016	
–	4403.513*	−1.804	K, K88	53 017.16	75 719.93	0.004	
–	4434.062*	−1.514	K, K88	53 017.16	75 563.49	0.000	Blend with Mg II
–	4441.996*	−2.355	K, K88	44 138.96	66 645.07	0.026	
–	4478.635*	−0.950	K, K88	53 597.13	75 919.09	0.007	
–	4518.953*	−1.329	K, K88	53 597.13	75 719.93	0.007	
5	4727.841,hfs	−2.017	K, K88	43 311.30	64 456.69	0.015	No fit
5	4730.395,hfs	−2.147	K, K88	43 339.42	64 473.39	0.047	
5	4738.290,hfs	−2.244	K, K88	43 395.38	64 494.14	0.115	No fit
5	4755.727,hfs	−1.242	K, K88	43 528.64	64 550.04	0.176	Large disagreement
5	4764.728,hfs	−1.351	K, K88	43 537.18	64 518.87	0.136	Large disagreement
–	5102.517	−1.934	K, K88	48 317.85	67 910.56	no data	hfs
–	5177.648	−1.772	K, K88	48 435.96	67 744.37	no data	hfs
–	5294.315	−0.037	K, K88	79 540.87	98 423.80	no data	hfs
–	5295.384	+0.360	K, K88	79 544.68	98 423.80	no data	hfs
–	5295.412	+0.360	K, K88	79 544.68	98 423.70	no data	hfs
–	6008.190	−1.271	K, K88	83 255.79	99 895.13	no data	hfs
–	6009.205	−1.050	K, K88	83 255.79	99 892.32	no data	hfs
–	6009.858	−1.096	K, K88	83 255.79	99 890.51	no data	hfs
–	6411.004,hfs	−1.487	K, K88	66 452.53	82 136.40	0.105	
–	7083.538*	−3.089	K, K88	53 698.70	67 812.05	0.103	
–	7098.194*	−3.083	K, K88	53 781.71	67 865.85	0.076	
–	7106.329*	−2.171	K, K88	53 698.70	67 766.76	0.108	
–	7110.354*	−1.923	K, K88	53 805.80	67 865.85	0.077	
–	7125.441*	−2.059	K, K88	53 781.71	67 812.05	0.077	
–	7137.694*	−2.976	K, K88	53 805.80	67 812.05	0.073	
–	7148.506*	−3.016	K, K88	53 781.71	67 766.76	0.105	Blend with telluric lines
–	7323.762*	−3.210	K, K88	54 846.24	68 496.61	0.055	
–	7330.577*,hfs	−2.713	K, K88	29 919.43	43 557.14	0.359	
–	7347.813*,hfs	−3.814	K, K88	29 951.42	43 557.14	0.253	
–	7353.549*,hfs	−2.726	K, K88	29 889.52	43 484.64	0.385	
–	7369.763*,hfs	−3.174	K, K88	29 919.43	43 484.64	0.350	
–	7373.426*	−2.806	K, K88	54 938.19	68 496.61	0.068	
–	7387.184*,hfs	−2.553	K, K88	29 951.42	43 484.64	0.242	
–	7415.803*,hfs	−2.202	K, K88	29 889.52	43 370.51	0.373	

Table A.6. continued.

Mult.	λ^a(Å)	log gf	Ref.^{b}	χ_{low}(cm^{-1})	χ_{up}(cm^{-1})	hfs$_{tot}$(Å)	Notes^c
–	7416.637*	−3.703	K, K88	54 938.19	68 417.61	0.061	
–	7432.294*,hfs	−2.498	K, K88	29 919.43	43 370.51	0.337	
–	7471.581*	−2.877	K, K88	55 166.31	68 496.61	0.094	
–	7490.309*	−3.019	K, K88	62 572.20	75 919.09	0.196	
–	7490.752*	−2.779	K, K88	65 567.07	78 913.17	0.081	
–	7498.931*	−2.282	K, K88	62 587.50	75 919.09	0.416	Not observed
–	7515.955*	−2.917	K, K88	55 116.31	68 417.61	0.087	Blend with Fe II
–	7942.111*	−2.456	K, K88	55 696.99	68 284.62	0.148	
–	9407.015,hfs	−2.554	K, K88	32 857.19	43 484.64	0.109	TWC
–	9408.696,hfs	−2.951	K, K88	32 859.09	43 484.64	0.109	TWC
–	9446.846,hfs	−2.389	K, K88	32 787.87	43 370.51	0.079	TWC

[a] (hfs) the hyperfine components are included in the adopted line lists; (*) the wavelength is from Holt et al. (1999).
[b] "K" before another log gf source means that the log gf is from Kurucz files available at `http://kurucz.harvard.edu/linelists/gf100` K88: Kurucz (1988); MFW: Martin et al. (1988).
[c] (TWC) the computed profile is weaker than the observed one; (TSC) the computed profile is stronger than the observed one; (hfs) observed hyperfine broadening.

the equivalent width 5.96 mA gives a too strong computed profile. On the basis of the synthetic spectrum we adopted $\log(N(\mathrm{Cu})/N_{\mathrm{tot}}) = -6.88$, corresponding to an overabundance of [+0.95]. This value well reproduces also Cu I 3273.954 Å which is blended with Mn II 3274.044 Å.

Smith (1994) derived $\log(N(\mathrm{Cu})/N(\mathrm{H})) = -6.85 \pm 0.15$ from Cu II lines observed in IUE spectra.

Zinc (30)-Not observed: No zinc lines were observed. Smith (1994) found $\log(N(\mathrm{Zn})/N(\mathrm{H})) = -9.22 \pm 0.30$ from Zn II lines observed in IUE spectra. This corresponds to an underabundance [−1.8].

Gallium (31)-Ga I,Ga II: There are only two Ga I lines in the studied range with available log gfs in the NIST database. They are Ga I mult. 1 at 4032.990 Å and 4172.039 Å. Both lines were observed in the spectrum, but they were not measured owing to their blending with other lines. Other Ga I lines can be found in the Kurucz line lists with guessed log gf values. The line at 6396.560 Å, if present, is heavily blended with Mn II 6396.565 Å.

There are no Ga II lines in the Kurucz line lists and there are no Ga II log gfs in the NIST database for the studied region. We used the Isberg & Litzén (1985) Ga II line list to identify Ga II lines in the spectrum and we searched the literature for Ga II oscillator strengths. The most complete set of log gfs in the optical region is that from Ryabchikova & Smirnov (1994) who consider 12 Ga II lines. However, the log gf uncertainty can be estimated when different determinations are compared. For instance, for the line at 6334 Å there is the choice between log gf = +1.00 from Ryabchikova & Smirnov (1994) and log gf = +0.36 from Lanz et al. (1993), while for the line at 5421.275 Å the log gf value is +0.55 according to Ryabchikova & Smirnov (1994) and −0.05 according to Nielsen et al. (2000). The comparison of the observed and computed profiles has led us to adopt +1.00 in the first case and −0.05 in the second case. In general, we adopted the Nielsen et al. (2000) log gfs, which are the same as those given by Ryabchikova & Smirnov (1994) for almost all the analyzed lines. For the transitions at 4255 Å we separated the 4255.722 Å and 4255.937 Å contributions. We replaced the global log gf = +0.68 with log gf = +0.634 and log gf = −0.320, respectively (Nielsen et al. 2000).

Several Ga II profiles are affected by isotopic and hyperfine broadening. Ga II in HgMn stars was discussed by Nielsen et al. (2000) and by Dworetsky et al. (1998). Gallium has two stable isotopes Ga^{69} and Ga^{71} with relative terrestrial abundances 0.60108 and 0.39892 (Anders & Grevesse 1989). Lines from each isotope are affected by hyperfine splitting of the levels. Karlsson & Litzèn (2000) measured the isotopic and the hyperfine structure of 18 Ga II lines by means of Fourier transform spectroscopy. They obtained hyperfine A constants for 8 levels. The B constants were found to be close to zero. We used the A constants in the HYPERFINE code (Kurucz & Bell 1995) to compute hyperfine log gfs for 8 lines with $\lambda > 5000$ Å. Their hyperfine and isotopic wavelengths were taken from Karlsson & Litzèn (2000). For 7 Ga II lines at 4251–4263 Å, arising from the 4d–4f transition, Karlsson & Litzèn (2000) measured the wavelengths and the relative intensities of numerous components. We estimated the log gf of each component from the ratio of the intensity of the component to the total intensity of the components. We did not use the standard formulae of the LS coupling (Cowley et al. 2000) owing to the lack in Table 3 of Karlsson & Litzén (2000) of the F total angular momentum for the lower and upper level of the transitions.

The Ga II isotopic and hyperfine components that we derived from Karlsson & Litzèn (2000) for 15 Ga II lines are

Table A.7. The Ga II lines analysed. When the two isotopes Ga^{69} and Ga^{71} are considered separately, the oscillator strengths are log $gf(Ga^{69})$ = −0.222 and log $gf(Ga^{71})$ = −0.398.

Isot.	λ(Å)	log gf_{iso}	log gf_{hfs}	log gf_{comp}
	4251.149	log gf_{tot} = +0.35		
69+71	4251.112	0.0	−2.049	−1.699
69+71	4251.130	0.0	−0.766	−0.416
69+71	4251.167	0.0	−0.086	+0.264
	4254.075	log gf_{tot} = −0.23		
69+71	4254.047	0.0	−0.338	−0.568
69+71	4250.070	0.0	−0.599	−0.829
69+71	4254.092	0.0	−0.741	−0.971
69+71	4254.111	0.0	−0.970	−1.200
	4255.722	log gf_{tot} = +0.634		
69+71	4255.622	0.0	−1.385	−0.751
69+71	4255.642	0.0	−1.406	−0.772
69+71	4255.657	0.0	−1.534	−0.900
69+71	4255.672	0.0	−1.148	−0.514
69+71	4255.688	0.0	−1.746	−1.112
69+71	4255.716	0.0	−0.453	+0.181
69+71	4255.742	0.0	−1.200	−0.566
69+71	4255.774	0.0	−0.597	+0.037
69+71	4255.791	0.0	−0.876	−0.242
	4255.937	log gf_{tot} = −0.32		
69+71	4255.818	0.0	−1.631	−1.951
69+71	4255.839	0.0	−1.915	−2.235
69+71	4255.857	0.0	−1.330	−1.650
69+71	4255.904	0.0	−0.677	−0.997
69+71	4255.924	0.0	−0.839	−1.159
69+71	4255.949	0.0	−1.251	−1.571
69+71	4255.971	0.0	−1.100	−1.420
69+71	4255.994	0.0	−0.718	−1.038
69+71	4256.013	0.0	−0.899	−1.219
	4261.4780	log gf_{tot} = −1.10		
69+71	4261.432	0.0	−0.757	−1.857
69+71	4261.448	0.0	−0.699	−1.799
69+71	4261.477	0.0	−1.000	−2.100
69+71	4261.509	0.0	−0.280	−1.380
	4262.014	log gf_{tot} = +0.98		
69+71	4262.010	0.0	−0.016	+0.964
69+71	4262.051	0.0	−1.525	−0.545
69+71	4262.067	0.0	−2.228	−1.248
	4263.1361	log gf_{tot} = −0.50		
69+71	4262.983	0.0	−1.204	−1.704
69+71	4263.018	0.0	−1.169	−1.669
69+71	4263.050	0.0	−1.204	−1.704
69+71	4263.070	0.0	−1.137	−1.637
69+71	4263.097	0.0	−1.505	−2.005
69+71	4263.113	0.0	−1.584	−2.084
69+71	4263.144	0.0	−0.593	−1.093
69+71	4263.176	0.0	−1.505	−2.005
69+71	4263.239	0.0	−0.621	−1.121
69+71	4263.266	0.0	−0.821	−1.321
	5338.240	log gf_{tot} = +0.43		
71	5338.137	−0.398	−0.778	−0.746
69	5338.159	−0.222	−0.783	−0.575
71	5338.199	−0.398	−0.477	−0.445
69	5338.208	−0.222	−0.475	−0.267
69	5338.289	−0.222	−0.301	−0.093
71	5338.302	−0.398	−0.301	−0.269

Isot.	λ(Å)	log gf_{iso}	log gf_{hfs}	log gf_{comp}
	5360.4022	log gf_{tot} = +0.42		
71	5360.314	−0.398	−1.079	−1.057
69	5360.334	−0.222	−1.079	−0.881
71	5360.335	−0.398	−1.079	−1.057
69	5360.350	−0.222	−1.079	−0.881
71	5360.357	−0.398	−0.678	−0.656
69	5360.368	−0.222	−0.678	−0.480
71	5360.391	−0.398	−0.972	−0.950
71	5360.394	−0.222	−0.972	−0.774
69	5360.411	−0.222	−1.778	−1.580
71	5360.412	−0.398	−1.778	−1.756
69	5360.432	−0.222	−0.398	−0.200
71	5360.438	−0.398	−0.398	−0.376
69	5360.469	−0.222	−1.046	−0.848
71	5360.486	−0.398	−1.044	−1.022
69	5360.496	−0.222	−2.000	−1.802
71	5360.521	−0.398	−2.000	−1.978
	5363.5854	log gf_{tot} = +0.06		
71	5363.353	−0.398	−1.556	−1.894
69	5363.402	−0.222	−1.556	−1.718
71	5363.416	−0.398	−0.857	−1.195
71	5363.430	−0.398	−0.857	−1.195
69	5363.451	−0.222	−0.857	−1.019
69	5363.463	−0.222	−0.857	−1.019
71	5363.493	−0.398	−1.352	−1.690
69	5363.512	−0.222	−1.352	−1.514
69	5363.594	−0.222	−0.824	−0.986
71	5363.597	−0.398	−0.824	−1.162
69	5363.613	−0.222	−0.824	−0.986
71	5363.621	−0.398	−0.824	−1.162
69	5363.695	−0.222	−0.456	−0.618
71	5363.725	−0.398	−0.456	−0.794
	5416.3179	log gf_{tot} = +0.64		
71	5416.287	−0.398	−0.796	−0.554
71	5416.292	−0.398	−1.000	−0.758
69	5416.295	−0.222	−0.796	−0.378
71	5416.296	−0.398	−0.611	−0.369
69	5416.299	−0.222	−1.000	−0.582
69	5416.302	−0.222	−0.611	−0.193
71	5416.320	−0.398	−0.447	−0.205
69	5416.321	−0.222	−0.447	−0.029
69	5416.350	−0.222	−1.398	−0.980
71	5416.356	−0.398	−1.398	−1.156
69	5416.378	−0.222	−1.282	−0.864
71	5416.393	−0.398	−1.282	−1.040
69	5416.419	−0.222	−1.389	−0.971
69	5416.433	−0.222	−2.544	−2.126
71	5416.444	−0.398	−1.389	−1.147
71	5416.462	−0.398	−2.544	−2.302
69	5416.495	−0.222	−2.690	−2.272
71	5416.541	−0.398	−2.690	−2.448

Table A.7. continued.

Isot.	λ(Å)	log $gf_{\rm iso}$	log $gf_{\rm hfs}$	log $gf_{\rm comp}$
	5421.2746	log $gf_{\rm tot}$ = −0.05		
71	5421.122	−0.398	−1.301	−1.749
71	5421.143	−0.398	−1.301	−1.749
71	5421.152	−0.398	−1.155	−1.603
69	5421.156	−0.222	−1.301	−1.573
69	5421.172	−0.222	−1.301	−1.573
69	5421.179	−0.222	−1.155	−1.427
71	5421.186	−0.398	−1.097	−1.545
69	5421.206	−0.222	−1.097	−1.369
71	5421.207	−0.398	−1.301	−1.749
71	5421.211	−0.398	−1.243	−1.691
69	5421.223	−0.222	−1.301	−1.573
69	5421.226	−0.222	−1.243	−1.515
71	5421.259	−0.398	−0.762	−1.210
69	5421.264	−0.222	−0.762	−1.034
69	5421.291	−0.222	−1.155	−1.427
71	5421.294	−0.398	−1.155	−1.603
69	5421.344	−0.222	−0.465	−0.737
71	5421.361	−0.398	−0.465	−0.913
69	5421.382	−0.222	−1.243	−1.515
71	5421.409	−0.398	−1.243	−1.691
	6419.2391	log $gf_{\rm tot}$ = +0.57		
71	6418.970	−0.398	−0.859	−0.687
71	6418.991	−0.398	−0.824	−0.652
69	6419.030	−0.222	−0.857	−0.509
69	6419.047	−0.222	−0.824	−0.476
71	6419.080	−0.398	−1.556	−1.384
69	6419.117	−0.222	−1.556	−1.208
71	6419.175	−0.398	−1.352	−1.180
69	6419.191	−0.222	−1.352	−1.004
69	6419.278	−0.222	−0.857	−0.509
71	6419.284	−0.398	−0.857	−0.685
69	6419.315	−0.222	−0.456	−0.108
71	6419.332	−0.398	−0.456	−0.284
69	6419.459	−0.222	−0.824	−0.476
71	6419.516	−0.398	−0.824	−0.652

Isot.	λ(Å)	log $gf_{\rm iso}$	log $gf_{\rm hfs}$	log $gf_{\rm comp}$
	6334.0688	log $gf_{\rm tot}$ = +1.00		
71	6333.911	−0.398	−1.079	−0.477
69	6333.948	−0.222	−1.079	−0.301
71	6333.964	−0.398	−0.678	+0.076
69	6333.989	−0.222	−0.678	+0.100
71	6333.998	−0.398	−1.079	−0.477
69	6334.017	−0.222	−1.079	−0.301
69	6334.089	−0.222	−0.398	+0.380
71	6334.091	−0.398	−0.398	+0.204
69	6334.104	−0.222	−0.972	−0.194
71	6334.110	−0.398	−0.972	−0.370
69	6334.173	−0.222	−1.778	−1.000
71	6334.198	−0.398	−1.778	−1.176
69	6334.250	−0.222	−1.046	−0.268
71	6334.295	−0.398	−1.046	−0.444
69	6334.365	−0.222	−2.000	−1.222
71	6334.442	−0.398	−2.000	−1.398
	6455.9231	log $gf_{\rm tot}$ = −0.08		
71	6455.578	−0.398	−0.778	−1.256
69	6455.653	−0.222	−0.778	−1.080
71	6455.784	−0.398	−0.477	−0.955
69	6455.816	−0.222	−0.477	−0.779
69	6456.087	−0.222	−0.301	−0.603
71	6456.123	−0.398	−0.301	−0.779

listed in Table A.7. We included them in the Kurucz line lists. Table A.7 is formed by subtables, one for each line investigated. The wavelength and the log gf of the examined transition are given in italics at the top of each subtable. The wavelengths of the isotopic and hyperfine components follow. They are listed in Col. 2 in increasing wavelength order. Columns 3 and 4 show the oscillator strengths of the isotopic and hyperfine components, log $gf_{\rm iso}$ and log $gf_{\rm hfs}$, respectively. The total oscillator strength of each component, log $gf_{\rm comp}$, is given in the last column. It was obtained by summing the log gf of the whole transition with log $gf_{\rm iso}$ and log $gf_{\rm hfs}$.

The Ga II lines analyzed in HD 175640, their log gf, the source, and the abundances derived from the line profiles are shown in Table A.3. The average abundance is $\log(N({\rm Ga})/N_{\rm tot}) = -5.43 \pm 0.04$, corresponding to an overabundance [+3.73]. A few other Ga II lines not used for abundance purposes have been added to Table A.3. Their log gf is that which gives the best agreement between the observed and computed profiles for the adopted abundance.

The analysis of the individual Ga II lines shows that the observed Ga II profile at λ 4251 Å is slightly broader and stronger than that computed for the adopted −5.43 dex abundance. A similar behaviour was pointed out by Nielsen et al. (2000) in κ Cnc and in HR 7775. The line could be blended with an unknown blue absorption line. The observed Ga II profile at λ 4255.7–4255.9 would be better reproduced if the predicted

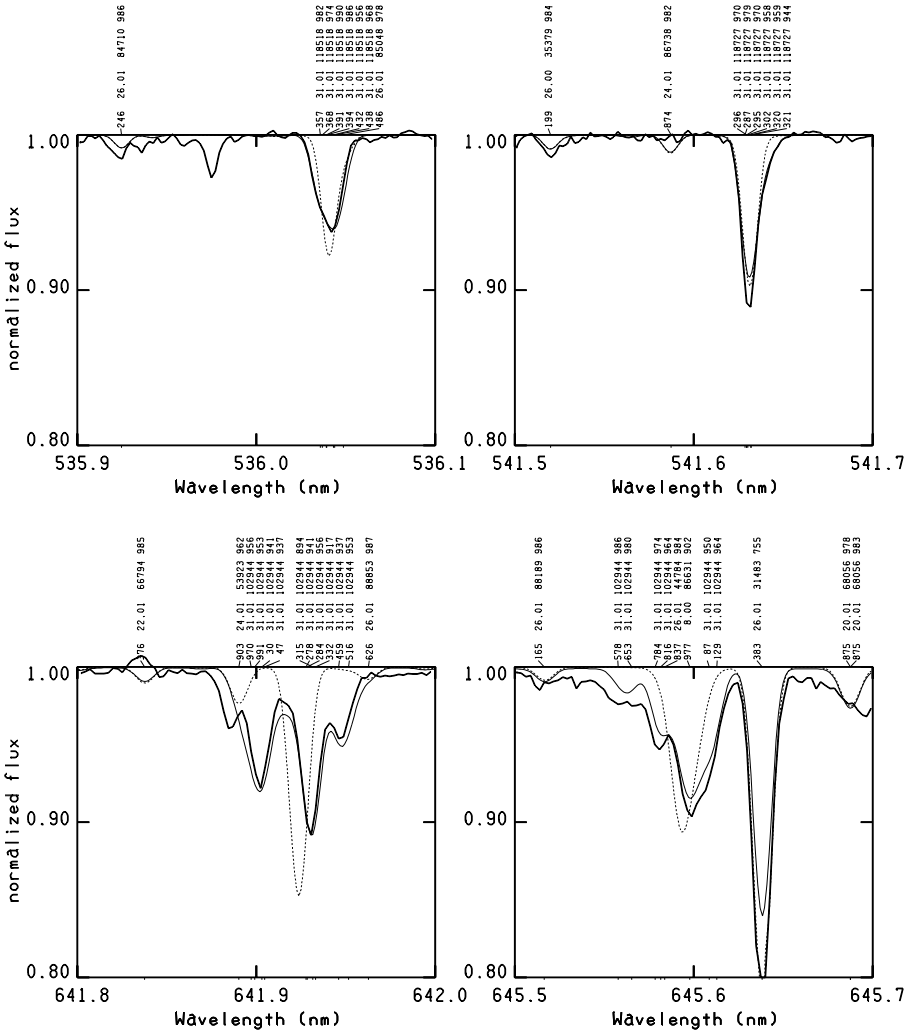

Fig. A.6. The observed profiles (thick full lines) of Ga II at $\lambda\lambda$ 536.03, 541.63, 641.89, 641.93, and 645.65–645.68 nm are compared with synthetic profiles computed once without any hyperfine structure (dotted lines) and once with hyperfine structure included in the computations (thin full lines) The meaning of the identification labels is the same as that given in the caption of Fig. A.1.

Mn II at 5256.014 Å is dropped. The observed and computed profiles of the blend Cr II 4261.9 Å, Ga II 4262.0 Å agree rather well. Although hfs and isotopic structures are not well evident in the Ga II lines observed at 5338.24 Å, 5360.40 Å, 5363.58 Å, 5416.31 Å and 5421.27 Å, the synthetic profiles reproduce well the observed ones only when the fine structures are considered in the computations. Large structures due to the isotopic and hyperfine splittings can be observed in the lines at 6334 Å, 6419 Å and 6456 Å. Figure A.6 compares each of the profiles observed at 5360.4 Å, 5421.3 Å, 6419.0 Å and 6456.0 Å with two synthetic profiles, one computed with isotopic and hyperfine structures, the other without them.

Dworetsky et al. (1998) obtained $\log(N(\mathrm{Ga})/N(\mathrm{H})) = -5.36 \pm 0.14$ for this star.

Arsenic (33)-As II (Not observed?): Sadakane et al. (2001) identified in the 5100–6400 Å region of the HgMn stars 46 Aquilae eight absorption features at 5105.58 Å, 5107.55 Å, 5231.38 Å, 5331.23 Å, 5497.73 Å, 5558.09 Å, 5651.32 Å and at 6110.07 Å as As II. We observed weak unidentified features in HD 175640 only at 5331.23 Å, 5497.73 Å, 5558.09 Å and 5651.32 Å. Other As II lines listed in the NIST database, even with stronger intensities, are not detectable in the spectrum. This suggests that other elements than As II may produce the four weak unidentified lines. We did not find in the literature any $\log gf$ for As II in the visible region.

Bromine (35)-Br II: Only the three Br II lines at 4704.85 Å, 4785.50 Å and 4816.70 Å have $\log gf$ values in the NIST database. We measured the equivalent widths of the first two lines, which yielded a Br overabundance of [+2.3].

Strontium (38)-Sr II: Only few Sr II lines were identified in the spectrum. The equivalent width of the unique Sr II unblended line at 4077.71 Å yields $\log(N(\mathrm{Sr})/N_{\mathrm{tot}}) = -8.41$, corresponding to an overabundance of [+0.7]. This value correctly reproduces the other observed Sr II blended lines, in particular the blend at 4215.5 Å having Sr II λ 4215.52 Å as main component.

Yttrium (39)-Y II: Although numerous Y II unblended lines were identified in the spectrum on the basis of the Kurucz line lists, only half of them could be used for abundance purposes, owing to the lack of log gf values for a large number of Y II transitions. Lines with unknown log gfs have guessed values in the Kurucz line lists so that the predicted lines in the synthetic spectrum have fictitious intensities.

The most reliable log gf source is Hannaford et al. (1982), who provided experimental values. Some other log gfs in the Kurucz line lists were obtained from a fitting procedure from Cowley & Corliss (1983). However, log gfs of lines with energy levels lying outside the validity range of the fitting procedure predict lines so much stronger than the observed ones that they should be considered unreliable values.

Nilsson et al. (1991) have measured Y II wavelengths in the region 1000–48 800 Å. We added a few lines from Nilsson et al. (1991) in the Kurucz line lists and assigned guessed log gfs to them. We also replaced a few wavelengths in the Kurucz database with wavelengths measured by Nilsson et al. (1991) as they agree better with the position of the observed lines.

The average abundance from the equivalent widths of the lines listed in Table A.3 is $\log(N(\mathrm{Y\,II})/N_{\rm tot}) = -6.66 \pm 0.20$, corresponding to [Y/H] = +3.14. However, there is a difference of 0.4 dex between the average abundances derived from lines lying shortward or longward of the Balmer discontinuity. These abundances are -6.42 ± 0.06 dex and -6.79 ± 0.10 dex, respectively.

Zirconium (40)-Zr II: Only a few weak Zr II lines were identified. From the equivalent widths listed in Table A.3 we derived an overabundance [Zr/H] = +0.77.

Rhodium (45)-Rh II: We identified all the Rh II lines listed in Table A.3. Owing to the lack of log gfs for them, we used the guessed oscillator strengths from the Kurucz line lists. Assuming log gf = 0.00 for Rh II at λ 3233.314 Å the abundance is −8.50 dex, viz. Rh II should be overabundant by about [+2.4]. The wavelengths in the Kurucz line lists are slightly different from those given in the Moore (1972) tables. The observed wavelengths correspond better with the Moore than to the Kurucz data. When needed, we modified the wavelengths in the Kurucz line lists to match the position of the observed lines. For the lines embedded in blends the wavelengths from Moore (1972) were adopted.

Palladium (46)-Pd I, Pd II: Several very weak Pd I lines included in the Kurucz line lists were identified in the spectrum. The measured equivalent widths (Table A.3) give an average overabundance [+3.94].

The log gf sources in the Kurucz database are Biémont et al. (1981) and Corliss & Bozman (1962).

We did not identify Pd II owing to the lack of these lines in our line lists. However, as pointed out by the referee Dr. C.R. Cowley, they were identified in HD 175640 by Bord et al. (2003)[8]. Two Pd II lines can be seen as unidentified features in our synthetic spectrum at 3243.1 Å and 3267.4 Å.

Table A.8. Isotopic and hyperfine structure of Ba II 4554 Å.

Isot.	λ(Å)	log $gf_{\rm iso}$	log $gf_{\rm hfs}$	log $gf_{\rm comp}$
	4554.029	log $gf_{\rm tot}$ = +0.163		
137	4553.995	−0.950	−0.806	−1.573
137	4553.997	−0.950	−0.806	−1.573
137	4553.998	−0.950	−1.204	−1.991
135	4553.999	−1.181	−0.806	−1.824
135	4554.001	−1.181	−0.806	−1.824
135	4554.001	−1.181	−1.204	−2.222
138	4554.029	−0.144	0.000	+0.019
134	4554.029	−1.617	0.000	−1.454
136	4554.029	−1.105	0.000	−0.942
135	4554.046	−1.181	−0.359	−1.377
135	4554.049	−1.181	−0.806	−1.824
137	4554.049	−0.950	−0.359	−1.146
135	4554.050	−1.181	−1.505	−2.523
137	4554.051	−0.950	−0.806	−1.573
137	4554.052	−0.950	−1.505	−2.291

Xenon (54)-Xe II: Numerous Xe II lines were identified in the spectrum. Because no Xe II lines are included in the Kurucz line lists, we added all the Xe II lines available in Wiese & Martin (1980). From lines with measurable equivalent widths (Table A.3) we obtained $\log(N(\mathrm{Xe})/N_{\rm tot}) = -5.96 \pm 0.20$, corresponding to an overabundance [Xe/H] = +3.87 dex. We added in Table A.3 some other weak Xe II lines with no measurable equivalent widths, but which are well reproduced in the synthetic spectrum by the above abundance. We also added in Table A.3 a few other Xe II lines observed in the spectrum. Their wavelengths and energy levels were taken from Hansen & Persson (1987). We assigned a fictitious log gf = 0.00 to them to be able to compute an approximate profile in the synthetic spectrum.

Barium (56)-Ba II: Only two very weak Ba II lines at 4554.03 Å and 4934.08 Å were identified in the spectrum.

Barium has seven isotopes, Ba^{130}, Ba^{132}, Ba^{134}, Ba^{135}, Ba^{136}, Ba^{137} and Ba^{138}. The stable ones are those with mass numbers 134 to 138. The lines of odd isotopes of Ba are affected by hyperfine structure. We considered all the isotopic and hyperfine components for computing the Ba II profile at 4554.03 Å. They are listed in Table A.8. The hfs components were computed with the HYPERFINE code (Kurucz & Bell 1995) using the hyperfine constants A and B taken from Becker & Werth (1983) and Becker et al. (1968). The isotopic intensi-

[8] http://www.astro.lsa.umich.edu/users/cowley/AAS0503Don/P7143.htm

ties are from Anders & Grevesse (1989). The wavelength and the log gf of the whole transition were taken from Miles & Wiese (1969). However, the line at λ 4554.03 Å is so weak in HD 175640 that hyperfine and isotopic broadenings do not contribute to the profile in a significant way. The abundance from this profile is $\log(N(\mathrm{Ba})/N_{\mathrm{tot}}) = -9.27$, which corresponds to an overabundance [+0.64].

Cerium (58)-Not observed?: Numerous Ce II lines are considered in the Kurucz line lists, but no Ce III lines. We added to the Kurucz line lists only those Ce III lines which were studied by Bord et al. (1997), but we adopted the log gf values available in the DREAM database.

No Ce III lines can be identified in the spectrum, although some weak Ce II lines could be present (i.e. λ 5079.682). The abundance $\log(N(\mathrm{Ce})/N_{\mathrm{tot}}) = -7.8$ derived from Ce II predicts very strong unobserved Ce III lines. We assumed Ce solar abundance for computing the synthetic spectrum although a large overabundance of Ce II compared to that of Ce III cannot be excluded.

Praseodymium (59)-Pr III: There are numerous Pr II lines in the Kurucz line lists, but none of Pr III. We added only those Pr III lines which were studied by Dolk et al. (2002), but we adopted the log gf values from Biémont et al. (2001b) for them.

No lines of Pr II were observed, but lines of Pr III may be present. With the aid of the synthetic spectrum we identified Pr III lines at 5264.433 Å, 5299.969 Å and 7781.985 Å. The abundance which fits the profile of the second unblended line is $\log(N(\mathrm{Pr})/N_{\mathrm{tot}}) = -9.62$, corresponding to an overabundance [Pr/H] = +1.7. This is not in conflict with the predicted intensity of the first line which is blended with Mg II and with that of the last line, which is at the level of the noise. However, other weak Pr III lines with no observed counterparts are predicted for this abundance.

Neodymium (60)-Nd III: There are numerous Nd II lines in the Kurucz line lists, but none of Nd III. We added only those Nd III lines which were studied by Dolk et al. (2002), but we adopted the log gf values from Zhang et al. (2002), available in the DREAM database.

We identified weak lines of Nd III at $\lambda\lambda$ 5102.455, 5127.044, 5203.902 and 5203.924 Å. They are rather well reproduced by the abundance $\log(N(\mathrm{Nd})/N_{\mathrm{tot}}) = -9.60$, corresponding to an overabundance [Nd/H] = +0.94. Weak Nd III absorption features not in conflict with the observations are predicted for this abundance at 4903.241 Å and 4927.488 Å.

Ytterbium (70)-Yb II,Yb III: Among the REE, only Yb II and Yb III have been identified without any doubt in this star (Bord et al. 2003).

There are numerous Yb II lines in the Kurucz line lists, but none of Yb III. We added Yb III lines from Biémont et al. (2001a) and replaced the Yb II log gfs of the Kurucz line lists with those from Biémont et al. (1998). All the Biémont et al. (2001a; 1998) log gfs were taken from the DREAM database.

The average abundance from the Yb II equivalent widths is $\log(N(\mathrm{Y})/N_{\mathrm{tot}}) = -8.10 \pm 0.19$ (Table A.3). If log gfs from the Kurucz database are used, the abundance is -8.31 ± 0.16. The average abundance from the Yb III equivalent widths is $\log(N(\mathrm{Yb})/N_{\mathrm{tot}}) = -7.3$, namely 0.7 dex higher than that from Yb II (Table A.3). The synthetic spectrum was computed with $\log(N(\mathrm{Yb})/N_{\mathrm{tot}}) = -8.10$.

Osmium (76)-Os II: Only four Os II lines are available in the Kurucz line lists for the studied region. They lie shortward of the Balmer discontinuity. The line at 3173.931 Å is predicted in the synthetic spectrum for solar abundance. It is a very weak line not in conflict with the observed spectrum.

Iridium (77)-Ir II: Only the line of Ir II at 3042.553 Å is available in the Kurucz line lists for the studied region. The line profile computed for a solar iridium abundance agrees well with the observed spectrum.

Platinum (78)-Pt II We investigated the presence in the spectrum of the Pt II lines listed by Engleman (1989). Two lines were identified, λ 4061.644 Å and λ 4514.124 Å. The first produces an asymmetric profile centered at the position of Fe II λ 4061.782 Å, the second can be unambigously observed.

There are no Pt II lines in the Kurucz line lists. We added the seven Pt II lines for which astrophysical log gfs from Dworetsky et al. (1984) are available. For the lines at 4046.443 Å, 4288.371 Å, and 4514.124 Å we also considered the isotopic and hyperfine wavelengths from Engleman (1989) together with the isotopic composition from Anders & Grevesse (1989). From the line profile at 4514.124 Å we obtained a Pt II abundance of −7.63 dex, corresponding to an overabundance [+2.57].

The line at λ 4061.644 Å computed for the above abundance contributes to the observed blend, but the line predicted at λ 4046.443 Å is not observed. There are also very weak predicted Pt II lines with no observable counterparts at $\lambda\lambda$ 4288.371 Å and 4034.181 Å.

Unfortunately, we did not find neither experimental nor theoretical log gfs for Pt II lines lying shortward of the Balmer discontinuity.

Gold (79)-Au II: There are no Au II lines in the Kurucz line lists. We added the Au II lines from Rosberg & Wyart (1997) for the range 3040–10 000 Å.

We identified and measured the equivalent widths of two lines at 4016.672 and 4052.790 Å, respectively. The average abundance is $\log(N(\mathrm{Au})/N_{\mathrm{tot}}) = -7.51 \pm 0.06$, corresponding to an overabundance [Au/H] = +3.52.

Mercury (80)-Hg I,Hg II: For $\lambda > 4000$ Å we replaced log gfs of the Kurucz line lists with the log gfs from Benck et al. (1989) for Hg I. We took wavelengths and log gfs from

Table A.9. Isotopic and hyperfine structure of H I at 4358 Å and Hg II at 3984 and 6149 Å.

Isot.	λ(Å)	log $gf_{\rm iso}$	log $gf_{\rm hfs}$	log $gf_{\rm comp}$
Hg I	*4358.3* Å	log $gf_{\rm tot}$ = −0.323		
199a	4358.175	−1.301	−0.959	−2.583
201a	4358.228	−1.301	−0.832	−2.456
201b	4358.341	−1.301	−0.862	−2.486
201c	4358.288	−1.301	−1.552	−3.176
199b	4358.314	−1.301	−0.259	−1.883
201d	4358.316	−1.301	−1.352	−2.976
204	4358.320	−1.523	0.000	−1.846
202	4358.326	−0.432	0.000	−0.755
200	4358.332	−0.456	0.000	−0.779
198	4358.337	−0.886	0.000	−1.209
196	4358.341	−50.000	0.000	−50.323
201e	4358.352	−1.301	−0.462	−2.086
201f	4358.362	−1.301	−0.862	−2.486
199c	4358.379	−1.301	−0.649	−2.273
201g	4358.442	−1.301	−0.832	−2.456
199d	4358.520	−1.301	−0.959	−2.583
Hg II	*3983.89* Å	log $gf_{\rm tot}$ = −1.520		
196	3983.771	0.000	−50.000	−51.520
198	3983.839	−0.886	0.000	−2.406
199a	3983.844	−1.301	−0.373	−3.194
199b	3983.853	−1.301	−0.240	−3.061
200	3983.912	−0.456	0.000	−1.976
201a	3983.932	−1.301	−0.438	−3.259
201b	3983.941	−1.301	−0.201	−3.022
202	3983.993	−0.432	0.000	−1.952
204	3984.072	−1.523	0.000	−3.043
Hg II	*6149.47* Å	log $gf_{\rm tot}$ = +0.150		
199a	6149.419	−1.301	−0.436	−1.587
201a	6149.451	−1.301	−0.239	−1.390
204	6149.461	−1.523	0.000	−1.373
202	6149.469	−0.432	0.000	−0.282
200	6149.477	−0.456	0.000	−0.306
198	6149.483	−0.886	0.000	−0.736
199b	6149.504	−1.301	−0.198	−1.349
201b	6149.513	−1.301	−0.373	−1.524

Sansonetti & Reader (2001) for Hg II. Only for the Hg II line at 3984 Å did we adopt log gf = −1.520, which is the mean value of −1.529 dex from Proffitt et al. (1999) and −1.510 dex from Sansonetti & Reader (2001).

Mercury has seven isotopes: 196, 198, 199, 200, 201, 202 and 204. The isotopes 199 and 201 are affected by hyperfine splitting. We considered all the isotopic and hyperfine components for computing Hg I at 4358 Å and Hg II at 3984 Å and 6149 Å. They are listed in Table A.9 The hyperfine oscillator strengths were taken from Dolk et al. (2003). The mercury isotopic composition of HD 175640 was derived from Hg II at 3984 Å by assuming log(N(Hg)/$N_{\rm tot}$) = −6.30. It is very different from the terrestrial one and very close to that found by Dolk et al. (2003). We recall that the terrestrial log $gf_{\rm iso}$ values of the isotopes 196, 198, 199, 200, 201, 202 and 204 are −2.814, −1.001, −0.773, −0.636, −0.880, −0.525 and −1.163, respectively (Anders & Grevesse 1989).

The abundance −6.30 dex that we derived from Hg II at λ 3984 Å was used to compute the synthetic spectrum. Four Hg I lines at 3125.665 Å, 4046.56 Å, 4358.3 Å, and 5460.73 Å and five Hg II lines at 3984 Å, 5425.253 Å 5677.105 Å, 6149 Å, and 7944.555 Å are predicted for this abundance. The computed profiles of the first three Hg I lines are slightly stronger than the observed ones, while Hg I at 5460.731 Å is predicted weaker than observed. The line of Hg II at 5425.253 Å is heavy blended with Fe II λ 5425.257 Å. The whole predicted blend is stronger than the observed one. Hg II at 5677.105 Å and 7944.555 Å are not observed but they are predicted in the synthetic spectrum. Finally, the computed line of Hg II at 6149.475 Å is slightly stronger than the observed one.

We could conclude that, except for Hg I at 5460.731 Å, the abundance derived from Hg II λ 3984 Å is too large in spite of its agreement with that found by Dolk et al. (2003), which is log(N(Hg)/$N_{\rm tot}$) = −6.35 ± 0.15 Furthermore, this abundance is lower than that. derived by Smith (1997) from Hg II at 1942 Å, which was estimated to lie between −6.25 and −6.15 dex.

Table A.10. Unidentified absorption lines.

λ_{calc}(Å)	Notes[a]
4735.55	Mn I 4635.542?
4753.20	Mn I 4753.226, Mn II 4753.179
4783.15	
4927.12	
4942.10	bl Fe II 4942.177
4977.53	
4991.60	
5031.28	
5036.30	
5037.87	
5038.30	
5038.87	Cr I 5038.87?
5040.12	
5043.65	
5044.55	
5057.00	Hf II 5057.03?
5058.15	Hf II 5058.15?
5073.45	
5084.30	
5090.60	
5091.60	Mn II 5091.608, strong
5098.28	Strong
5101.83	
5104.75	
5105.85	Mn II 5105.889, As II? strong
5121.87	
5122.05	
5126.00	
5126.20	
5126.83	
5127.20	
5127.33	
5128.48	
5128.60	
5130.00	
5130.17	
5130.63	
5131.70	
5132.00	
5134.06	
5134.16	
5135.27	
5136.15	
5136.30	
5138.60	
5139.07	
5139.25	Fe I 5139.251
5140.20	
5145.50	
5148.55	
5149.25	
5152.70	
5152.98	
5153.78	
5156.45	
5157.50	
5158.07	
5163.00	
5163.58	
5164.92	
5165.70	
5166.20	
5167.125	
5167.7	
5167.82	
5170.125	
5171.30	
5176.725	
5177.40	
5179.15	
5179.55	
5181.65	
5186.10	
5190.00	
5190.45	
5192.75	
5193.725	
5194.40	
5195.10	
5195.225	
5195.95	
5210.55	
5215.20	
5221.05	
5222.175	
5225.25	
5225.35	
5226.05	
5228.625	
5234.30	
5236.00	
5236.35	
5236.45	
5237.675	
5238.475	
5239.35	
5240.325	
5240.575	
5241.20	
5244.975	
5245.075	
5246.55	
5247.70	
5248.35	
5257.35	
5258.675	
5260.100	
5261.20	
5261.60	
5270.30	
5272.05	
5274.20	
5277.80	
5281.35	
5282.225	
5282.50	
5283.075	
5284.00	
5284.575	
5288.825	
5290.10	
5300.125	
5304.65	
5305.15	
5305.40	
5306.35	
5308.80	
5311.075	
5321.825	
5327.15	
5327.75	
5329.35	
5330.55	Br II
5331.23	As II?
5332.975	
5336.20	
5340.25	
5341.7	
5342.05	
5348.35	
5350.70	
5354.40	
5355.90	
5357.1	
5359.75	
5383.5	
5390.60	
5410.35	
5451.75	
5482.7	
5497.7	As II?
5505.75	
5506.35	
5513.425	
5515.20	
5516.00	
5518.075	
5518.20	
5518.525	
5521.875	
5533.1	
5533.4	
5536.575	
5537.075	
5537.45	
5558.075	As II?
5620.00	
5651.3	As II?
5660.5	
5706.35	Si II 5706.37?
5734.3	
5753.85	

[a] The symbol "?" indicates possible identifications.

Table A.11. Unidentified emission lines.

λ_{obs}(Å)	R_c(obs)	Notes[a]	λ_{obs}(Å)	R_c(obs)	Notes[a]	λ_{obs}(Å)	R_c(obs)	Notes[a]
6000.15	1.018		6745.32	1.013	Cr II 6745.239?	8732.65	1.016	
6037.93	1.020		6814.40	1.031		8761.60	1.022	Mn II 8761.644?
6146.07	1.013		6845.15	1.037		9032.95	1.035	
6177.50	1.027		6849.80	1.010		9036.12	1.086	
6255.37	1.018		7453.67	1.013		9208.45	1.041	Mn II 9208.604?
6312.25	1.021		7662.90	1.042		9242.65	1.033	Mn II 9242.744?
6344.80	1.019		8493.12	1.022		9394.00	1.055	
6447.10	1.018		8676.70	1.020		9497.465	1.021	Fe II?
6534.15	1.025		8706.30	1.007		9573.25	1.051	
6618.50	1.016		8721.55	1.013				

[a] The symbol "?" indicates possible identifications.